NASA Technical Paper 1306

Determination of Stability and Control Parameters of a Light Airplane From Flight Data Using Two Estimation Methods

Vladislav Klein

MARCH 1979

NASA

NASA Technical Paper 1306

Determination of Stability and Control Parameters of a Light Airplane From Flight Data Using Two Estimation Methods

Vladislav Klein
The George Washington University
Joint Institute for Advancement of Flight Sciences
Langley Research Center
Hampton, Virginia

National Aeronautics
and Space Administration

**Scientific and Technical
Information Office**

1979

SUMMARY

Values for stability and control parameters have been determined by use of the equation error method and the maximum likelihood method from maneuvering flight data for a low-wing, single-engine, general aviation airplane. The airplane responses were excited from steady flights at different airspeeds using the stabilator, aileron, and rudder deflections. The model of the airplane is based on the equations of motion with the linear aerodynamics. From the repeated measurements, the two standard-deviation confidence intervals for the estimated parameters were established. These bounds are used for the comparison of parameters determined by both methods and also for the assessment of an effect of different input forms and power settings. The static parameters are also compared with results from steady flights. Using these comparisons, the best values of estimated parameters were determined and their accuracies specified.

INTRODUCTION

The National Aeronautics and Space Administration is currently involved in extensive general aviation stall-spin studies. During the research program, several airplanes have been tested in the wind tunnel and in flight, and more tests with other airplanes are anticipated. In undertaking the stall-spin research, the airplane dynamics in prestall regimes must be understood. For that reason part of the overall program includes the measurement of airplane transient maneuvers for the extraction of a complete set of stability and control parameters. These parameters include aerodynamic derivatives and the values of aerodynamic coefficients corresponding to steady flight conditions.

There have been several previous attempts using systems identification to determine parameters of general aviation airplanes from unsteady measurements. These attempts differ in the amount of data available, estimation techniques, and verification of results obtained. In reference 1 the equation error method (regression analysis) is applied to measured longitudinal data corresponding to good excitation of the long- and short-period modes. The same technique is used in reference 2 for the determination of the lateral derivatives from flights with different values of thrust coefficients. The equation error method, based on a least-squares technique, is very attractive because of its simplicity. It can be easily applied to each of the equations of motion separately and provides direct estimates of the unknown parameters. The resulting estimates are, however, biased as a consequence of the measurement errors in the input and output variables.

A second procedure used in airplane parameter estimation is the output error method. Because it usually uses the maximum likelihood estimation, it is often called the maximum likelihood method. The airplane longitudinal and lateral aerodynamic parameters obtained by this method are presented in references 3 and 4 and are compared with aerodynamic derivatives obtained from wind-tunnel tests and theoretical predictions. The maximum likelihood estimates are theoretically

superior to those obtained from the equation error method. These estimates are asymptotically unbiased, consistent, and efficient, provided that the model of an airplane is correct and the input variables are measured without errors. However, the maximum likelihood method applied to the problem mentioned is time consuming because of its iterative nature and because all equations of motion considered enter the estimation algorithm. In some experiments, small variances of the measurement noise, unknown modeling errors, and a limited number of data points could substantially reduce the superiority of the maximum likelihood method to the equation error method. Under these conditions, both methods might provide identical values for the estimated parameters. Detailed description and comparison of both methods can be found in references 5 and 6.

The purpose of this report is to document estimates of the stability and control parameters for one of the general aviation airplanes involved in the stall-spin program. The parameters are extracted from longitudinal and lateral maneuvers initiated from steady flights at different airspeeds. The airspeed range extends from the minimum airspeed at which the airplane can still be maneuvered to the maximum airspeed in horizontal flight. The two methods already mentioned were applied to measured flight data in an attempt to obtain more accurate values of the stability and control parameters for the test airplane.

This report first describes the test airplane, instrumentation, flight tests, and data reduction. Then the mathematical model of the airplane is introduced, and the estimation methods are outlined. The results from both methods are then compared. The static parameters are also compared with the results obtained from steady flights. Last, the effect of input form and power setting in the estimated parameter values is demonstrated, the best values of parameters are determined, and their accuracies are specified.

SYMBOLS

A	wing aspect ratio
a_l	$= \partial C_{L,t}/\partial \alpha_t$
a_x, a_y, a_z	reading of longitudinal, lateral, and vertical accelerometer, respectively, g units
b	wing span, m
b_y	constant bias error in variable y
C_D	drag coefficient, $D/\bar{q}S$
C_L	lift coefficient, $L/\bar{q}S$
$C_{L,t}$	lift coefficient of tail, $L_t/\bar{q}S$
C_l	rolling-moment coefficient, $M_X/\bar{q}Sb$
C_m	pitching-moment coefficient, $M_Y/\bar{q}S\bar{c}$

C_n yawing-moment coefficient, $M_Z/\bar{q}Sb$

C_T thrust coefficient, $T/\bar{q}S$

C_X longitudinal-force coefficient, $F_X/\bar{q}S$

C_Y lateral-force coefficient, $F_Y/\bar{q}S$

C_Z vertical-force coefficient, $F_Z/\bar{q}S$

$\bar{c}$ wing mean aerodynamic chord, m

D drag, N

F $= \bar{c}h_{no}/l_n$

F_X, F_Y, F_Z forces along X, Y, and Z body axes, respectively, N

F_1, F_2 terms in equations of motion defined by equations (A19) and (A20)

f( ) function which represents state-equation model

g acceleration due to gravity, m/sec^2

g( ) function which represents output-equation model

H sensitivity matrix

H_n stick-fixed center-of-gravity margin

h distance of center of gravity aft of leading edge of wing mean chord expressed in percent of $\bar{c}$

h_{no} distance of aerodynamic center aft of leading edge of wing mean chord expressed in percent of $\bar{c}$

I_X, I_Y, I_Z moment of inertia about X, Y, and Z body axes, respectively, $kg\text{-}m^2$

I_{XZ} product of inertia, $kg\text{-}m^2$

J cost function

j $= \sqrt{-1}$

K_ϕ term defined by equation (B16)

$k_{\delta_a}, k_{\delta_r}, k_{l_n\beta}, k_{n_l\beta}$ terms defined by equations (B17) to (B19)

L lift, N

l distance of aerodynamic center of tail aft of aerodynamic center of airplane without tail, m

l_n	distance of aerodynamic center of tail aft of neutral point of airplane, m
l_t	distance of aerodynamic center of tail aft center of gravity, m
M	Fisher information matrix
M_X, M_Y, M_Z	rolling, pitching, and yawing moments, respectively, N-m
m	mass, kg
m_{jj}	main diagonal element of the M matrix
N	number of data points
$\vec{n}$	measurement noise vector
p	roll rate, rad/sec or deg/sec
$p(\vec{z}/\vec{\Theta})$	likelihood function
q	pitch rate, rad/sec or deg/sec
q_θ	number of unknown parameters
$\bar{q}$	dynamic pressure, $\frac{1}{2}\rho V^2$, N/m^2
R	measurement noise covariance matrix
r	yaw rate, rad/sec or deg/sec
S	wing area, m^2
S_t	tail area, m^2
s(y)	standard error of variable y
s_{jj}	main diagonal element of the M^{-1} matrix
T	thrust, N
t	time, sec
$\vec{u}$	input vector
u,v,w	velocity along X, Y, and Z body axes, respectively, m/sec
V	airplane total velocity, m/sec

V_i	indicated airspeed, knots
V_T	modified tail volume defined by equation (B3)
$\vec{x}$	state vector
x_α, y_α	x- and y-coordinates of angle-of-attack vane relative to airplane center of gravity, m
x_β, z_β	x- and z-coordinates of sideslip vane relative to airplane center of gravity, m
$\vec{y}$	output vector
$\vec{z}$	measurement vector
α	angle of attack, rad or deg
α_v	angle of attack measured by wind vane, rad or deg
β	sideslip angle, rad or deg
β_v	sideslip angle measured by wind vane, rad or deg
δ_a	aileron deflection (one-half of sum of left aileron deflection and right aileron deflection), rad
δ_e	stabilator deflection, rad or deg
δ_r	rudder deflection, rad or deg
δ_t	trim tab deflection, rad or deg
ε	downwash angle at tail, rad or deg
Θ	unknown parameter
Θ_p	predicted value of unknown parameter
$\vec{\Theta}$	vector of unknown parameters
θ	pitch angle, rad or deg
λ_y	scale factor error of variable y
ν_y	residual of variable y
ρ	air density, kg/m^3
σ	standard deviation

ϕ bank angle, rad or deg

ϕ_{yu} phase-angle characteristics relating y and u variables, deg

ω angular frequency, rad/sec

Aerodynamic derivatives (referenced to a system of body axes with the origin at the aircraft center of gravity, which is located at 20.6 percent of $\bar{c}$):

$$C_{L_q} = \frac{\partial C_L}{\partial \frac{q\bar{c}}{2V}} \qquad C_{L_\alpha} = \frac{\partial C_L}{\partial \alpha} \qquad C_{L_{\delta e}} = \frac{\partial C_L}{\partial \delta_e}$$

$$C_{l_p} = \frac{\partial C_l}{\partial \frac{pb}{2V}} \qquad C_{l_r} = \frac{\partial C_l}{\partial \frac{rb}{2V}} \qquad C_{l_\beta} = \frac{\partial C_l}{\partial \beta}$$

$$C_{l_{\delta a}} = \frac{\partial C_l}{\partial \delta_a} \qquad C_{l_{\delta r}} = \frac{\partial C_l}{\partial \delta_r} \qquad C_{m_q} = \frac{\partial C_m}{\partial \frac{q\bar{c}}{2V}}$$

$$C_{m_{q\alpha}} = \frac{\partial^2 C_m}{\partial \frac{q\bar{c}}{2V} \partial \alpha} \qquad C_{m_\alpha} = \frac{\partial C_m}{\partial \alpha} \qquad C_{m_{\dot{\alpha}}} = \frac{\partial C_m}{\partial \frac{\dot{\alpha}\bar{c}}{2V}}$$

$$C_{m_{\alpha 2}} = \frac{1}{2} \frac{\partial^2 C_m}{\partial \alpha^2} \qquad C_{m_{\delta e}} = \frac{\partial C_m}{\partial \delta_e} \qquad C_{n_p} = \frac{\partial C_n}{\partial \frac{pb}{2V}}$$

$$C_{n_r} = \frac{\partial C_n}{\partial \frac{rb}{2V}} \qquad C_{n_\beta} = \frac{\partial C_n}{\partial \beta} \qquad C_{n_{\delta a}} = \frac{\partial C_n}{\partial \delta_a}$$

$$C_{n_{\delta r}} = \frac{\partial C_n}{\partial \delta_r} \qquad C_{X_\alpha} = \frac{\partial C_X}{\partial \alpha} \qquad C_{Y_p} = \frac{\partial C_Y}{\partial \frac{pb}{2V}}$$

$$C_{Y_\beta} = \frac{\partial C_Y}{\partial \beta} \qquad C_{Y_{\delta r}} = \frac{\partial C_Y}{\partial \delta_r} \qquad C_{Z_q} = \frac{\partial C_Z}{\partial \frac{\bar{q}\bar{c}}{2V}}$$

$$C_{Z_\alpha} = \frac{\partial C_Z}{\partial \alpha} \qquad C_{Z_{\alpha 2}} = \frac{1}{2}\frac{\partial^2 C_Z}{\partial \alpha^2} \qquad C_{Z_{\delta e}} = \frac{\partial C_Z}{\partial \delta_e}$$

$C'_{m,o}$, C'_{m_α}, C'_{m_q}, and $C'_{m_{\delta e}}$ defined in appendix A (eqs. (A8) to (A11)).

Subscripts:

E	measured
o	trimmed condition
t	tail

Superscripts:

T	transpose matrix
-1	inverse matrix
^	estimated values
-	mean
·	derivative with respect to time
→	vector

Abbreviations:

c.g.	center of gravity
EE	equation error
ML	maximum likelihood
rms	root mean square

TEST AIRCRAFT AND INSTRUMENTATION SYSTEM

For this study, a four-place, low-wing, single-engine airplane was used. The control surfaces included conventional ailerons, rudder, and all-movable tail (stabilator). The basic geometric, mass, and inertia characteristics are

summarized in table I. The moments of inertia were measured for the airplane in its early test configuration. The airplane was later modified by the installation of an onboard rocket system which is used primarily for spin recovery. The resulting changes in the airplane configuration affected only its mass and inertia characteristics. New moments of inertia were calculated from those previously measured.

An analog measurement system was installed in the airplane for recording control surface deflections, stick and rudder forces, airplane response variables, and other quantities defining flight and engine conditions. Control position motions (input variables) were measured by rotary potentiometers directly attached to the control surfaces. An orthogonal triad of linear accelerometers was rigidly mounted on the center line of the cockpit floor at a location close to the allowable center-of-gravity range of the airplane (fig. 1). The sensitive axes of all accelerometers were alined to the reference axes of the airplane.

Incidence angles were measured by a swiveling vane mounted on booms ahead of each wing tip (fig. 1). Because the corrected readings of both vanes gave identical results, only the angle-of-attack and angle-of-sideslip data from the right vane were used for the analysis. The indicated airspeed was obtained from the airplane's air data system which consisted of a simple total pressure orifice located on each side of the fuselage. Total temperature was measured by a sensor located on the top of the fuselage. The remainder of the instrumentation system included three rate gyros, attitude gyros, signal conditioning, power supplies, and tape recorder. These components were mounted on a rack behind the front seats as shown in figure 1. A summary of measured quantities used in this study, transducers, and static characteristics of corresponding channels is presented in table II. The root-mean-square (rms) errors were estimated from recorded signals during the preflight and postflight ground operation of the instrumentation system with the airplane engine running. Both the resolution and the rms errors are referred to the digitized data.

Table III presents dynamic characteristics of transducers used for the measurement of airplane response. These characteristics were obtained from dynamic calibration. The equivalent time constants given in the last column of table III represent the approximation of the transducer dynamics by a first-order system.

FLIGHT TEST AND DATA REDUCTION

Airplane responses were measured in six flights. Table IV summarizes pertinent flight test conditions and the average mass and inertia characteristics of the airplane in these flights. Mass and inertia characteristics for each run analyzed were determined from the airplane take-off weight and estimated fuel consumption during the flight.

The longitudinal and lateral modes were excited separately, primarily from the trimmed level flights at the airspeeds listed in table IV. For the investigation of power effect, perturbations were initiated from a steady climb with full power and from a steady descent with idle power.

In longitudinal flights, the inputs used were stabilator deflections having the form of a pulse, a doublet, or a combination of both. In the lateral case, both the rudder and aileron were applied simultaneously. Various forms of these inputs are shown later. In all cases, the α- and β-traces were examined to determine that the atmospheric turbulence was negligible.

The measured flight data were filtered with a 6-Hz low-pass filter and sampled at the rate of 20 samples per second. The sampled data were used to produce automatic data tabulations, time history plots, and final tape for airplane parameter estimation. This tape included the following variables: time, true airspeed, incidence angles (right vane), angular velocities, attitude angles, linear accelerations, control surface deflections, and incidence angles (left vane).

True airspeed was obtained from the indicated airspeed by applying corrections for measured position error of the static pressure system and by using the air density values computed from the measured air temperature and static pressure. The angle-of-attack vane readings were corrected for air upwash by a multiplication constant. This constant was estimated from steady horizontal flights by comparing longitudinal accelerometer and wind vane readings. The recorded linear accelerations were converted into the acceleration of the airplane's center of gravity. The effective aileron deflection was computed as a mean value of the sum of the right and left aileron deflections.

The next step preliminary to airplane parameter estimation included a compatibility check of measured response variables in steady and maneuvering flights. The relationship between variables α_v, θ, a_z, and a_x, and ϕ, β_v, and a_y was examined from the initial steady parts of various test runs. These data showed very small scatter in values of the longitudinal and lateral accelerations and sideslip. It was, therefore, assumed that the measurements of a_x, a_y, and β_v were corrupted only by zero-mean random noise. Then the bias errors in α_v, θ, a_z, and ϕ in the form of constant offsets were determined. Similar bias errors in p, q, and r were found by assuming steady flight conditions. All these estimates were verified by the analysis of transient maneuvers. The compatibility check of aircraft response variables in maneuvering flights included the prediction of V, β_v, α_v, ϕ, and the estimation of constant bias errors in measured data. The technique used is based on airplane kinematic equations and an extended Kalman filter and is described in reference 7.

Typical results from the compatibility checks are given in figures 2 to 5 and in tables V and VI. In figure 2 the measured and predicted responses in V, α_v, and θ are compared. A similar comparison for the variables V, β_v, α_v, ϕ, and θ taken from one of the lateral maneuvers is presented in figure 4. The resulting residuals and the standard errors of the measured responses estimated from these residuals are included in figures 3 and 5. All the residuals, in general, indicate good agreement between measured and predicted data. The larger discrepancy in measured and predicted airspeed is still within the rms error of the measuring instrument, which was estimated to be equal to 0.89 m/sec. (See table II.)

Table V compares various estimates of bias errors in the longitudinal output variables. The error estimates from transient data were unaffected by the assumption that $b_{a_X} = 0$ and were close to those from the steady data. Because this pattern was observed in other maneuvers that were analyzed, only the estimates from steady-state data were used for corrections of the longitudinal responses.

For the lateral case presented in table VI, the estimated bias error in a_Y is significantly different from the initially assumed zero. The inclusion of b_{a_Y} as an unknown parameter in the model affected the estimate of b_ϕ only. This particular run and other similar runs analyzed indicated some differences between the bias errors estimated from steady-state and transient data. These differences had, however, no significant effect on the estimated stability and control parameters. The errors estimated from steady-state data were, therefore, used for corrections of measured time histories of p, r, and ϕ.

MATHEMATICAL MODEL OF AIRPLANE

A mathematical model of the airplane was formulated in the form of the state and output equations as

$$\dot{\vec{x}} = f(\vec{x},\vec{u},\vec{\Theta},t) \tag{1}$$

and

$$\vec{y} = g(\vec{x},\vec{u},\vec{\Theta},t) \tag{2}$$

where $\vec{x}$, $\vec{y}$, and $\vec{u}$ are the state, output, and input vectors, respectively, and $\vec{\Theta}$ is the vector of unknown parameters. For the longitudinal motion, the four vectors in equations (1) and (2) have the form

$$\vec{x}^T = [u,w,q,\theta]$$

$$\vec{y}^T = [V,\alpha_v,q,\theta,a_X,a_Z]$$

$$u^T = \delta_e$$

$$\Theta^T = [C_{X,o},C_{X_\alpha},C_{Z,o},C_{Z_\alpha},C_{Z_q},C_{Z_{\delta_e}},C'_{m,o},C'_{m_\alpha},C'_{m_q},C'_{m_{\delta_e}}]$$

and for the lateral motion

$$\vec{x}^T = [v, p, r, \phi]$$

$$\vec{y}^T = [\beta_v, p, r, \phi, a_Y]$$

$$u^T = [\delta_a, \delta_r]$$

$$\Theta^T = [C_{Y,o}, C_{Y_\beta}, C_{Y_p}, C_{Y_{\delta r}}, C_{l,o}, C_{l_\beta}, C_{l_p}, C_{l_r}, C_{l_{\delta a}}, C_{l_{\delta r}},$$
$$C_{n,o}, C_{n_\beta}, C_{n_p}, C_{n_r}, C_{n_{\delta a}}, C_{n_{\delta r}}]$$

The equations of motion are presented in detail in appendix A. Their form resulted from an examination of measured responses of the test airplane, and from wind-tunnel and flight-test results on similar airplanes. The coupling between the lateral and longitudinal motion during the measurement of lateral responses is included in the lateral equations by replacing the variables u, w, q, and θ with their measured values.

ESTIMATION METHODS

The equation error (EE) method represents an application of regression analysis to each state equation separately; it is a method which minimizes the sum of squared errors satisfying the equation. The cost function for the state equation has the form

$$J_r = \frac{1}{2} \sum_{i=1}^{N} \left[\dot{x}_{rEi} - f_{ri}\left(\vec{x}_E, \vec{u}, \vec{\theta}_r\right) \right]^2 \tag{3}$$

where N is the number of data points and E denotes the measured quantity. The least squares solution for $\vec{\theta}_r$ is obtained by finding the minimum of J_r. The standard errors of the parameters are obtained from the information matrix in the so-called normal equations and from the residuals $\dot{x}_{rEi} - f_{ri}\left(\vec{x}_E, \vec{u}, \vec{\theta}_r\right)$. (See ref. 2.)

In the airplane force equations the variables $\dot{x}_{rE}$ were replaced by measured linear accelerations as indicated by equations (A12), (A13), and (A23) to (A25). In the moment equations the angular accelerations were calculated from measured angular rates using splines.

Detailed descriptions of the maximum likelihood (ML) method and of the computing program can be found in references 8 and 9. The ML method is based

on the maximalization of the log-likelihood function $\log p(\vec{z}/\vec{\Theta})$. The computing starts with the approximate values for the unknown parameters in the state equations and then iterates until the minimum of the cost function

$$J = \frac{1}{2} \sum_{i=1}^{N} \left(\vec{z}_i - \hat{\vec{y}}_i \right)^T \hat{R}^{-1} \left(\vec{z}_i - \hat{\vec{y}}_i \right) \tag{4}$$

is found. In equation (4), $\vec{z}$ is the measured vector $\vec{z} = \vec{y} + \vec{n}$, where $\vec{n}$ is the measurement noise vector. The measurement noise covariance matrix R is estimated as

$$\hat{R} = \text{diag} \frac{1}{N} \sum_{i=1}^{N} \vec{v}_i \vec{v}_i^T \tag{5}$$

where $\vec{v}_i = \vec{z}_i - \hat{\vec{y}}_i$ are the residuals.

After the kth iteration the new estimates of unknown parameters are found as

$$\hat{\vec{\Theta}}_k = \hat{\vec{\Theta}}_{k-1} + \Delta\hat{\vec{\Theta}}_k \tag{6}$$

where the vector $\Delta\hat{\vec{\Theta}}_k$ is computed from the expression

$$\Delta\hat{\vec{\Theta}}_k = -M^{-1}(\Theta_{k-1}) \left(\frac{\partial J}{\partial \Theta} \right)^T_{\Theta=\Theta_{k-1}} \tag{7}$$

The matrix M is the Fisher information matrix. The inverse of the information matrix gives a lower bound on the error covariance matrix for the estimated parameters. Using the modified Newton-Raphson method, described in reference 6, this matrix is approximated as

$$M = \sum_{i=1}^{N} H_i^T \hat{R}^{-1} H_i$$

In this expression H is the sensitivity matrix whose elements are $\partial\vec{y}/\partial\Theta_j$, where $j = 1, 2, \ldots, q_\theta$ and where q_θ is the number of unknown parameters. The main diagonal term of the information matrix m_{jj} defines the sensitivity of measured output variables with respect to the parameter Θ_j. (See ref. 10.)

The main diagonal term of M^{-1}, s_{jj}, is, therefore, the Cramér-Rao lower bound on the variance of the parameter $\hat{\Theta}_j$. It can be shown that

$$\frac{1}{m_{jj}} \leq s_{jj}$$

where the equal sign holds for the uncorrelated parameters.

RESULTS AND DISCUSSION

Longitudinal Characteristics

The first part of the longitudinal data consists of 16 runs measured at different airspeeds. In these runs the transient motion of the airplane was excited from level flights by using the stabilator deflection in the form of a single pulse or doublet. Estimated parameters and their standard errors from one run at $C_L = 0.61$ are summarized in table VII. All parameters included in the model indicate satisfactory identifiability as expressed by their standard errors or lower bounds on these errors. Significant differences in the estimates using the EE method and ML method exist in the derivatives C_{Z_α} and C_{m_α}. From calculated parameter covariance matrices a strong correlation (the correlation coefficient about 0.94) was observed between the parameters C_{Z_q} and $C_{Z_{\delta e}}$ and between C_{m_q} and $C_{m_{\delta e}}$, regardless of the estimation method.

Measured time histories and those computed by using parameters obtained by the EE method are given in figure 6. Considerable disagreement is apparent only between measured and computed outputs V and a_χ. The bad fit in these variables is not important because their variations are small. Plots similar to those in figure 6 are presented in figure 7, where the parameters used were obtained by the ML method. The resulting residuals in the output variables are plotted in figure 8. In this figure the standard errors of the output variables estimated from the residuals are also given. If the model of the airplane were correct, the residuals would form a white random sequence. Examination of their time histories in figure 8 indicates, however, the influence of certain modeling errors (incorrect form of aerodynamic model equations, uncorrected bias errors in measurement data, external disturbances). The incorrect model resulted in bias errors in the estimated stability and control parameters and in an increase of the Cramér-Rao lower bound.

The parameters obtained from all 16 runs mentioned are presented in figures 9 and 10. Figure 9 includes the estimates by the EE method plotted against lift coefficient. The range of C_L corresponds to the change in the angle of attack from approximately 0^o to 11^o. A distinction has been made between the resulting points where a pulse or doublet input was used. Each plot of a parameter against C_Z was fitted by a first- or second-order polynomial, or by a combination of both. The change in the functional relationship from linear to quadratic was based on results from steady-state data as is shown later.

In figure 10 the results from both estimation techniques were compared. The 2σ bounds on the EE estimates were computed from the differences between the estimates and the fitted curves. The 2σ bounds can be used for an assessment of significant differences in results from both methods. As in table VII, the most pronounced difference exists in the estimates of C_{Z_α}. The large differences in C_{Z_q} and $C_{Z_{\delta e}}$ at higher values of C_L are not important because these parameters have small effect only on the resulting motion of the airplane. For the remaining parameters, both techniques provide, in general, equivalent estimates. Estimates of the parameters $C_{X,o}$ and C_{X_α} are consistent even if the airspeed changes in the maneuvers analyzed were small. This is a promising indication of a possibility to estimate the performance characteristics of the airplane provided the necessary thrust information is available.

Effect of nonlinear terms in aerodynamic model equations.- The examination of figures 9 and 10 shows variations of derivatives C_{Z_α}, C'_{m_α}, and C'_{m_q} with C_L at higher values of the lift coefficient. The effect of these variations is not included in the aerodynamic model equations used. Therefore, for the assessment of model adequacy at higher angles of attack, the estimated standard errors in the main output variables α_v, q, and a_z were plotted against C_L, as shown in figure 11. The estimates of measurement noise standard errors obtained from the compatibility check and instrumentation system characteristics, as presented in figure 3 and table II, have been added to these plots. The plots of figure 11 indicate the increase of the standard error in all three variables with increasing values of C_L. A possible modeling error in the aerodynamic model equations has been checked using the data from one run at $C_L = 1.26$. The data were analyzed by using the ML method and the modified aerodynamic model. The model included three additional nonlinear terms $C_{Z_{\alpha 2}}(\alpha - \alpha_o)^2$, $C'_{m_{\alpha 2}}(\alpha - \alpha_o)^2$, and $C_{m_{q\alpha}} \frac{\bar{qc}(\alpha - \alpha_o)}{2V}$.

The resulting estimates are compared in table VIII with those based on the linear aerodynamics. In this table, the main diagonal elements of the information and parameter covariance matrices m_{jj} and s_{jj} are also presented. The comparison shows that the extended model significantly influenced some of the parameters. The new estimates for C_{Z_q} and $C_{Z_{\delta e}}$ are closer to those expected. With the nonlinear aerodynamics, there was an improvement in terms of standard errors in parameters, correlation between parameters, sensitivities, and measure-

ment noise standard errors. The values of nonlinear terms agree well with those predicted from figures 9 and 10. The standard errors of the nonlinear parameters were reasonably low, and any strong correlation between the linear and nonlinear parameters was not observed, as indicated by values of the correlation coefficients given in table IX.

Comparison of parameters estimated from steady-state and transient flight data.- The accuracy of estimated parameters was checked by the comparison of their values with those obtained from steady measurements. Data needed for the estimation of static stability and control derivatives were measured in slow acceleration-deceleration horizontal flights and in steady climbs and descents ("saw-tooth" flights). In figure 12 the measured and fitted lift coefficient is plotted against the angle of attack. The same measured data from steady climbs with full power and steady descent with idle power are compared with the previous measurements in figure 13.

The measured and fitted stick-fixed trim curves (δ_e against C_L) are plotted in figure 14 for two airplane center-of-gravity positions. The effect of power setting on these data is demonstrated in figure 15. All measured steady-state data indicate changes in derivatives C_{Z_α} and C_{m_α} with increasing C_L and also with different power setting.

The data from figure 12 and figure 14 were used for computing aerodynamic derivatives from expressions developed for an airplane with a conventional horizontal tail in reference 11 and modified for an all-movable tail. The relationship between directly estimated quantities from measured steady-state data and aerodynamic derivatives are summarized in appendix B. The results obtained are presented in table X where they are compared with the estimates from transient data. These estimates are the mean values from the range of C_L within which the derivatives are assumed to have constant values.

The comparison shows that the estimates from steady flights agree very well with those obtained from transient data by using the ML method. Only the values for the derivative C'_{m_q} differ significantly. However, the value

for this derivative from steady-state data represents an approximation only. The results in table X can then be considered an indication of good confidence in the ML estimates for all parameters.

In addition to the comparison in table X, two derivatives C_{Z_α} and C'_{m_α}

estimated from steady-state and transient data were plotted against C_L in figure 16. All three estimates show the same trend with the increased value of C_L. However, the differences in values of C_{Z_α} remain.

Effect of different input forms and power settings on estimated parameters.- In addition to the 16 runs analyzed, runs with different input forms were used to estimate the parameters. Data from runs with full and idle power were also used. All of these additional runs were measured at $C_L \approx 0.57$. The examples of various stabilator-deflection time histories are given in figure 17. The input A consists of a series of pulses, the input B1 includes either sharp

pulses or double pulses, and the input B2 is a combination of sharp pulses with a slowly varying stabilator deflection used for better excitation of the airspeed changes.

The effect of pulse and doublet on the parameter estimates has already been shown in figures 9 and 10. Some differences are apparent in derivatives C_{Z_α}, C'_{m_α}, and C'_{m_q} at higher angles of attack. The effect of the remaining input forms is shown in figure 18, where the new sets of estimates are compared with previous results. The results indicate that the estimates from runs with input A are very similar to those based on measurements with pulse and doublet input form. However, for the input forms B1 and B2, some differences in the estimates of pitching-moment derivatives appeared. These differences are mainly visible in the results of the EE method. For all input forms used, the Cramér-Rao bound on the standard errors of the estimated parameters remained almost the same. Also, the strong correlation between C_{Z_q} and $C_{Z_{\delta e}}$ and between C_{m_q} and $C_{m_{\delta e}}$ was unchanged. These results agree with the investigation of effects of control inputs on the estimated parameters made in reference 7.

For a more detailed investigation of a possible effect of the sharp pulse or short doublet on the estimates, two sets of results were compared. The input forms used and their harmonic contents are given in figure 19; the parameter estimates, relative sensitivities, standard errors, and the measurement noise standard errors are presented in table XI.

The results from the run with sharp doublet show the incorrect sign in C_{Z_q}; significant differences in C_{Z_α}, C'_{m_α}, and C'_{m_q}; decreased sensitivities; and increased inaccuracy. There is also a large standard error in the pitching velocity. The time history of the residuals in q for this run included a dominant deterministic component whose form was similar to the expected time history of the angular acceleration in pitch. The degradation of results from the data with sharp doublet input can be attributed to modeling errors in the equations of motion and/or to the uncorrected errors in measured pitching velocity. The comparison of measured and predicted frequency response curves displayed in figure 20 shows this effect even more clearly. The predicted frequency response curves were computed from linearized equations (A2), (A3), and (A7) with the derivatives from table XI. The measured data were obtained by applying Fourier transforms to the measured time histories of δ_e, q, and a_Z.

The measured data with slow doublet agree well with the prediction. In the second run with a sharp doublet, the frequency response curves $a_Z(j\omega)/\delta_e(j\omega)$ again agree, but there are greater differences in the amplitude and phase characteristics of the frequency response function $q(j\omega)/\delta_e(j\omega)$. The change in phase angle in the measured data is greater than theoretically possible considering the form of transfer function developed from equations (A2) and (A3). To explain the differences mentioned, a new check and dynamic calibration of the pertinent rate gyro were made, and the measured pitch angle was compared with that pre-

dicted from the pitch rate gyro reading. Both checks indicated that the instrumentation was functioning correctly and that no time-delay correction in measured q(t) was needed. Another reason for the effect of the sharp doublet on the parameter estimates is in the modeling of the airplane. The confirmation of this conclusion, however, would need theoretical and experimental study which is beyond the scope of the present report.

The results in figure 18 concerning power effect indicate that there were no differences between the estimates with full power and power required for the level flights. The changes in parameters with idle power agree with trends shown in measured steady-state data in figures 13 and 15, e.g., the decrease (in absolute value) of C_{Z_α}, $C'_{m_{\delta e}}$, and C'_{m_q} and the increase of C'_{m_α}.

Lateral Characteristics

For the estimates of lateral parameters, 28 maneuvers initiated from steady-state level flights at different airspeeds were available. The measured data were obtained from two flights. The results from eight repeated measurements at the same airspeed are given in table XII. They include the ensemble mean values and standard errors of the EE and ML estimates, and the average standard errors of a single measurement. The mean values obtained from results of both methods are quite consistent; the only significant differences were found in two less important derivatives C_{Y_p} and $C_{l_{\delta r}}$.

The ensemble standard errors of the EE estimates are, for most parameters, smaller than those of the ML estimates. In both cases the standard errors estimated from the ensemble do not agree with the standard errors of a single measurement. The ratio of these two different estimates varies between 1 and 5 for the EE method, and between 2 and 18 for the ML estimates. High values and variability in these ratios could be caused by bias errors in the estimates resulting from various modeling errors and also from a small sample size.

As an example of the comparison between measured and computed data, the time histories of one of the eight runs analyzed are presented in figures 21 and 22. In figure 21, the computed responses are based on the EE estimates and in figure 22, on the ML estimates. These two figures indicate no significant differences for both sets of parameters, which is in agreement with results in table XII.

The residuals from figure 22 and their standard errors are given in figure 23. In all time histories of residuals, some deterministic components are visible, the most significant of which are in the yawing velocity residuals. This study did not determine which modeling errors could contribute to the deterministic components in residuals. Because of the small amplitude of residuals in the given case, and also in the remaining runs, the existing modeling errors did not significantly influence the accuracy of the estimates.

The estimated parameters from all 28 runs are plotted against C_L in figure 24 and figure 25. In figure 24, the ML estimates were fitted by linear or quadratic polynomials. In figure 25, the ML estimates are compared with

those obtained by the EE method. As with the results in table XII, the differences in both estimates are not, in general, significant; furthermore, the results from the two flights do not differ substantially.

The fitted curves in figure 24 can be used for the prediction of the lateral stability and control derivatives of the airplane. Table XIII shows the predicted values for $C_L = 0.62$ and the standard error boundaries on the prediction errors. These boundaries represent the maximum and minimum standard error of the fitted curve $\hat{\theta} = \hat{\theta}(C_L)$ within the given range of C_L. For comparison, the last column of table XIII presents the Cramér-Rao lower bound on the estimated standard error of a single measurement.

The estimates of the yawing-moment coefficient derivatives shown in figures 24 and 25 revealed increased scatter with the increasing value of C_L. For the investigation of this trend, the standard errors of all output variables were first plotted against C_L as shown in figure 26. However, these plots show only a moderate increase of this error for higher values of C_L. This increase indicates that the modeling errors do not change significantly for runs at higher angles of attack.

The next step involved the investigation of sensitivities and standard errors in the parameter estimates. These characteristics deteriorate with increasing values of C_L which might lead to the conclusion that the input form used was not suitable for excitation at higher angles of attack. All the input forms used resulted in strong correlations between some of the stability and control derivatives, mainly between $C_{l_p}, C_{l_{\delta e}}$ and $C_{n_p}, C_{n_{\delta a}}$. The results in figure 26 demonstrate the increase in standard errors caused by modeling errors when one compares the estimates based on the equations of motion, on kinematic equations only (compatibility check), and on the instrumentation system alone. The difference in the standard errors $s(r)$ in two flights was probably caused by more pronounced modeling errors in flight 21, where the input was similar to that in flight 26, but the rudder amplitude was higher.

Comparison of results from transient and steady-state measurements.- As with the longitudinal case, the results from the lateral transient flight data were compared with those obtained from steady nonsymmetric flights (steady straight sideslips). Unfortunately, the lateral steady-state data cannot provide estimates of aerodynamic derivatives directly without additional a priori information. For that reason, the measured relationships between the sideslip angle and the bank angle, the aileron deflection and the rudder deflection were compared with those predicted using the parameters estimated from transient data. If linearized lateral equations of motion are assumed, it can be shown that the aforementioned relationships are linear and that their slopes and intersects depend on certain combinations of derivatives. The analytical form of the relationships $\beta = \beta(\phi)$, $\beta = \beta(\delta_a)$ and $\beta = \beta(\delta_r)$ is presented in appendix B.

In figures 27 to 29, the measured lateral static aerodynamic characteristics for two values of C_L are presented. The estimates of those characteristics were computed from equations (B13) to (B15) using the ML estimates for the parameters. The agreement between measurements and computed lines is generally good. The only discrepancy is for the intersection of the line $\beta(\delta_r)$ at $C_L = 1.19$.

This intersection depends primarily on the parameter $C_{n,o}$. The estimates of this parameter were incorrect as to sign. One explanation could be the existence of modeling errors in the yawing-moment equation; however, the proof would require more detailed analysis.

The results in figures 27 to 29 verified to some extent the estimates of the derivative C_{Y_β}, and the combination of derivatives $C_{l_{\delta a}}/C_{l_\beta}$ and $C_{n_{\delta r}}/C_{n_\beta}$. For the verification of the control derivatives $C_{l_{\delta a}}$ and $C_{n_{\delta r}}$, the aileron and rudder effectiveness were measured in steady flights with $\beta \approx 0$ and with the additional rolling and yawing moments provided by the onboard rocket system. The resulting derivatives from these measurements are given in figure 30 and compared with the ML estimates taken from figure 24. The steady-state data resulted in slightly higher absolute values for both control derivatives than for the transient data. The differences are, however, not significant.

Effect of different input forms and power settings on estimated parameters.- All previous lateral data analyzed included only one type of input form for both the rudder and aileron deflection. To investigate for an effect of other input forms, five other types of input forms shown in figure 31 have been used. The input A1 is similar to the standard input, but the aileron doublet is shorter and has greater amplitude. The input A2 is composed of input A1 repeated three times. In the input B1 the rudder pulse is followed by the aileron doublet. As in the previous case the input B2 is composed of input B1 repeated three times. Finally, in the input C the aileron doublet precedes the rudder doublet.

Estimated parameters from several runs with the inputs described are presented in figure 32. They are compared with the ensemble mean values given in table XII which were estimated from runs where the standard inputs were used. In all cases the parameters are the ML estimates.

The results in figure 32 revealed a significant effect of input forms on virtually all estimated parameters. The changes in the estimates are, in general, greater in the derivatives of C_Y and C_l than those in derivatives of C_n if the ensemble mean value and its confidence interval are considered as a reference. In many cases it was not possible to determine which estimates are more accurate because the standard errors and the correlation coefficients were almost the same for significantly different values of the same parameter.

The variability in the lateral parameter estimates due to different input forms was found to be less pronounced in the study covered by reference 7. This could be explained by the dependence of the input form sensitivity on the characteristics of an airplane. The impossibility of selecting the best estimates of parameters from runs with different inputs demonstrates the existing problem of an optimal input form for parameter identification and the problem of accuracy assessment of the parameter estimates.

In figure 32, the effect of different power settings on the parameter estimates is also shown. The results from runs excited from steady-state climbs with full power agree with those from the measurements in horizontal flight. This agreement was expected because in both experiments the power setting dif-

fered only slightly. On the other hand, the results from runs with idle power show a decrease in the absolute value of static derivatives C_{Y_β} and C_{n_β}, and control derivatives $C_{Y_{\delta r}}$ and $C_{n_{\delta r}}$. These changes and their directions have been expected. They are caused by the slipstream effect on the sidewash angle and the dynamic pressure at the tail.

ASSESSMENT OF ESTIMATED PARAMETERS

A comparison of the results in table X shows the ML parameter estimates to be the best values for the longitudinal stability and control derivatives of the airplane under test within the range of C_L where these derivatives have constant values, e.g., $C_L < 0.9$. Power will not significantly change the value of these derivatives, with the exception of power settings close to zero-power conditions. For both methods, the standard error of all important derivatives is about 2 percent. This error can also be a measure of the overall accuracy because of the agreement between the results from steady-state and transient data, and between the EE and ML estimates as shown in figure 18 for the pulse input doublet and combination of both (input A). The values of derivatives for $C_L > 0.9$ can be obtained from figure 10. The accuracy of these derivatives will deteriorate with the increasing value of C_L because the estimates are influenced by the input form, power conditions, and the uncertainty in the aerodynamic model equations. The best values of the stability and control derivatives for the lateral motion are given by the fitted curves in figure 24. The bounds on their standard errors can be obtained from table XIII. The standard errors for the aerodynamic static derivatives are between 1 and 3 percent, for the damping derivatives between 2 and 10 percent, and for the primary control derivatives between 2 and 5 percent. For some less significant derivatives the standard error can be as high as 70 percent. There is a good agreement between some derivatives and their combinations obtained from steady-state and transient data.

The EE and ML estimates of all important derivates also agree provided that the data with the same input form were used in the analysis. On the other hand, the estimated derivatives depend strongly on the input form used which means that the input-form dependence degrades the accuracy of the estimates. The effect of power is insignificant with the exception of the idle power regimes.

CONCLUDING REMARKS

A complete set of stability and control parameters included in the aerodynamic model equations was estimated from maneuvering flight data for a low-wing, single-engine, general aviation airplane. Most of the estimated parameters obtained by using the equation error and maximum likelihood methods agreed within two-standard-deviation confidence intervals for the parameter. This agreement was made possible because sufficient accuracy of measured data was achieved from a thorough ground and flight calibration of the instrumentation system, a check of the system before and after each flight, and correction

of the measured data for bias errors determined from compatibility checks of measured response variables. The estimated static parameters also agreed with the results from steady flights. The comparison of parameters obtained from different methods and through repeated measurements resulted in the determination of the best values for the estimated parameter and in the specification of their accuracies.

Longitudinal Parameters

Both estimation methods provided identical values for most of the parameters. The significant difference was found in the derivative of the vertical-force coefficient with respect to the angle of attack. The maximum likelihood estimates agreed better with the computed parameters from steady-flight data than with those from the equation error method. The engine power did not change the values of parameters significantly, with the exception of power settings close to zero-power conditions. The standard error of all important parameters was about 2 percent. The accuracy of parameters deteriorated with the increasing value of the lift coefficient. The high angle of attack and rapid maneuvers created some uncertainties in aerodynamic model equations. The addition of nonlinear aerodynamic terms could improve the parameter estimates at high values of the lift coefficient.

Lateral Parameters

The results from eight repeated measurements under the same flight conditions showed that the mean values from both estimation methods agreed in general. The only significant differences were found in two less important derivatives. The ensemble standard errors of parameters obtained by the use of the equation error method were smaller than those of the maximum likelihood estimates. At the same time, the ensemble standard errors of the parameters from both methods were higher than the standard errors of a single measurement.

The comparison of parameters plotted against the lift coefficient indicated no significant differences between the results of the two methods. The standard errors of the main derivatives varied between 1 and 10 percent. For some less important derivatives, this error was as high as 70 percent. There was good agreement between combinations of the static stability and control parameters obtained from steady and transient data. The estimated parameters depended strongly on the input form used. The effect of power was not significant with the exception of the idle power regimes.

Langley Research Center
National Aeronautics and Space Administration
Hampton, VA 23665
January 26, 1979

APPENDIX A

AIRPLANE STATE AND OUTPUT EQUATIONS

The airplane equations of motion are referred to the body axes. They are based on the following assumptions:

(1) The airplane is a rigid body.

(2) The stabilator deflection excites only the longitudinal motion whereas the rudder and ailerons excite the lateral motion which is coupled with the longitudinal motion.

(3) There are no external disturbances to the airplane.

(4) The aerodynamic model equations include also the effect of propeller and have the form

$$C_X = C_{X,o} + C_{X_\alpha}$$

$$C_Y = C_{Y,o} + C_{Y_\beta}(\beta - \beta_o) + C_{Y_p}\frac{pb}{2V} + C_{Y_{\delta r}}(\delta_r - \delta_{r,o})$$

$$C_Z = C_{Z,o} + C_{Z_\alpha}(\alpha - \alpha_o) + C_{Z_q}\frac{q\bar{c}}{2V} + C_{Z_{\delta e}}(\delta_e - \delta_{e,o})$$

$$C_l = C_{l,o} + C_{l_\beta}(\beta - \beta_o) + C_{l_p}\frac{pb}{2V} + C_{l_r}\frac{rb}{2V} + C_{l_{\delta a}}(\delta_a - \delta_{a,o}) + C_{l_{\delta r}}(\delta_r - \delta_{r,o})$$

$$C_m = C_{m,o} + C_{m_\alpha}(\alpha - \alpha_o) + C_{m_{\dot{\alpha}}}\frac{\dot{\alpha}\bar{c}}{2V} + C_{m_q}\frac{q\bar{c}}{2V} + C_{m_{\delta e}}(\delta_e - \delta_{e,o})$$

$$C_n = C_{n,o} + C_{n_\beta}(\beta - \beta_o) + C_{n_p}\frac{pb}{2V} + C_{n_r}\frac{rb}{2V} + C_{n_{\delta a}}(\delta_a - \delta_{a,o}) + C_{n_{\delta r}}(\delta_r - \delta_{r,o})$$

where

$$C_X = C_T \cos \alpha_T + C_L \sin \alpha - C_D \cos \alpha$$

$$C_Z = -C_T \sin \alpha_T - C_L \cos \alpha - C_D \sin \alpha$$

and where the index o denotes the value of the coefficient, output, or input variable corresponding to the initial steady-state flight conditions.

These assumptions allow the longitudinal state equations to be expressed as

$$\dot{u} = -qw - g \sin \theta + \frac{\bar{q}S}{m}\left[C_{X,o} + C_{X_\alpha}(\alpha - \alpha_o)\right] \tag{A1}$$

$$\dot{w} = qu + g \cos \theta + \frac{\bar{q}S}{m}\left[C_{Z,o} + C_{Z_\alpha}(\alpha - \alpha_o) + C_{Z_q}\frac{q\bar{c}}{2V} + C_{Z_{\delta e}}(\delta_e - \delta_{e,o})\right] \tag{A2}$$

$$\dot{q} = \frac{\bar{q}S\bar{c}}{I_Y}\left[C'_{m,o} + C'_{m_\alpha}(\alpha - \alpha_o) + C'_{m_q}\frac{q\bar{c}}{2V} + C'_{m_{\delta e}}(\delta_e - \delta_{e,o})\right] \tag{A3}$$

$$\dot{\theta} = q \tag{A4}$$

and the output equations to be expressed as

$$\alpha_v = \tan^{-1}\left(\frac{w - qx_\alpha}{u}\right) \tag{A5}$$

$$a_X = \frac{1}{g}(\dot{u} + qw + g \sin \theta) \tag{A6}$$

$$a_Z = \frac{1}{g}(\dot{w} - qu - g \cos \theta) \tag{A7}$$

APPENDIX A

In the pitching-moment equation

$$C'_{m,o} = C_{m,o} + C_{m_{\dot{\alpha}}}\left(\frac{\rho S\bar{c}}{4m} C_{Z,o} + \frac{g\bar{c}}{2V^2}\cos\theta_o\right) \tag{A8}$$

$$C'_{m_\alpha} = C_{m_\alpha} + \frac{\rho S\bar{c}}{4m} C_{m_{\dot{\alpha}}} C_{Z_\alpha} \tag{A9}$$

$$C'_{m_q} = C_{m_q} + C_{m_{\dot{\alpha}}}\left(1 + \frac{\rho S\bar{c}}{4m} C_{Z_q}\right) \tag{A10}$$

$$C'_{m_{\delta e}} = C_{m_{\delta e}} + \frac{\rho S\bar{c}}{4m} C_{m_{\dot{\alpha}}} C_{Z_{\delta e}} \tag{A11}$$

True airspeed and angle of attack are computed from the equations

$$V = \sqrt{u^2 + w^2}$$

$$\alpha = \tan^{-1}\frac{w}{u}$$

For the equation error method the state equations were modified as

$$\frac{gm}{qS} a_X = C_{X,o} + C_{X_\alpha}(\alpha - \alpha_o) \tag{A12}$$

$$\frac{gm}{qS} a_Z = C_{Z,o} + C_{Z_\alpha}(\alpha - \alpha_o) + C_{Z_q}\frac{q\bar{c}}{2V} + C_{Z_{\delta e}}(\delta_e - \delta_{e,o}) \tag{A13}$$

$$\frac{I_Y}{qSc}\dot{q} = C'_{m,o} + C'_{m_\alpha}(\alpha - \alpha_o) + C'_{m_q}\frac{q\bar{c}}{2V} + C'_{m_{\delta e}}(\delta_e - \delta_{e,o}) \tag{A14}$$

APPENDIX A

The lateral equations can be expressed as

$$\dot{v} = -u_E r + w_E p + g \cos \theta_E \sin \phi + \frac{\bar{q}S}{m}\left[C_{Y,o} + C_{Y_\beta}(\beta - \beta_o) + C_{Y_p}\frac{pb}{2V} + C_{Y_{\delta r}}(\delta_r - \delta_{r,o})\right] \quad \text{(A15)}$$

$$\dot{p} = \frac{I_z}{I_x I_z - I_{xz}^2} F_1 + \frac{I_{xz}}{I_x I_z - I_{xz}^2} F_2 \quad \text{(A16)}$$

$$\dot{r} = \frac{I_x}{I_x I_z - I_{xz}^2} F_2 + \frac{I_{xz}}{I_x I_z - I_{xz}^2} F_1 \quad \text{(A17)}$$

$$\dot{\phi} = p + (q_E \sin \phi + r \cos \phi) \tan \theta_E \quad \text{(A18)}$$

where

$$F_1 = (I_Y - I_z)q_E r - I_{xz} q_E p + \bar{q}Sb\left[C_{l,o} + C_{l_\beta}(\beta - \beta_o) + C_{l_p}\frac{pb}{2V} + C_{l_r}\frac{rb}{2V} + C_{l_{\delta a}}(\delta_a - \delta_{a,o}) + C_{l_{\delta r}}(\delta_r - \delta_{r,o})\right] \quad \text{(A19)}$$

$$F2 = (I_x - I_Y)q_E p - I_{xz} q_E r + \bar{q}Sb\left[C_{n,o} + C_{n_\beta}(\beta - \beta_o) + C_{n_p}\frac{pb}{2V} + C_{n_r}\frac{rb}{2V} + C_{n_{\delta a}}(\delta_a - \delta_{a,o}) + C_{n_{\delta r}}(\delta_r - \delta_{r,o})\right] \quad \text{(A20)}$$

$$V = \sqrt{u_E^2 + v^2 + w_E^2}$$

$$\beta = \sin^{-1}\frac{v}{V}$$

APPENDIX A

$$u_E = V_E \cos \alpha_{v_E} \cos \beta_{v_E}$$

$$w_E = V_E \sin \alpha_{v_E} \cos \beta_{v_E} + q_E x_\alpha - p_E y_\alpha$$

the index E denotes the measured quantity.

The output equations related to the lateral motion have the form

$$\beta_v = \sin^{-1}\left(\frac{v + rx_\beta - pz_\beta}{V}\right) \tag{A21}$$

$$a_y = \frac{1}{g}(\dot{v} + u_E r - w_E p - g \cos \theta_E \sin \phi) \tag{A22}$$

For the equation error method, the lateral equations were modified as

$$\frac{gm}{\bar{q}S} a_Y = C_{Y,o} + C_{Y_\beta}(\beta - \beta_o) + C_{Y_p} \frac{pb}{2V} + C_{Y_{\delta_r}}(\delta_r - \delta_{r,o}) \tag{A23}$$

$$\frac{I_X}{\bar{q}Sb}\left[\dot{p} - \left(\frac{I_Y - I_Z}{I_X}\right)qr - \frac{I_{XZ}}{I_X}(pq + \dot{r})\right]$$

$$= C_{l,o} + C_{l_\beta}(\beta - \beta_o) + C_{l_p} \frac{pb}{2V} + C_{l_r} \frac{rb}{2V} + C_{l_{\delta_a}}(\delta_a - \delta_{a,o})$$

$$+ C_{l_{\delta_r}}(\delta_r - \delta_{r,o}) \tag{A24}$$

$$\frac{I_Z}{\bar{q}Sb}\left[\dot{r} - \left(\frac{I_X - I_Y}{I_Z}\right)pq - \frac{I_{XZ}}{I_Z} pq - \frac{I_{XZ}}{I_Z}(\dot{p} - qr)\right]$$

$$= C_{n,o} + C_{n_\beta}(\beta - \beta_o) + C_{n_p} \frac{pb}{2V} + C_{n_r} \frac{rb}{2V} + C_{n_{\delta_a}}(\delta_a - \delta_{a,o})$$

$$+ C_{n_{\delta_r}}(\delta_r - \delta_{r,o}) \tag{A25}$$

APPENDIX B

RELATIONSHIP BETWEEN AERODYNAMIC DERIVATIVES AND PARAMETERS ESTIMATED FROM STEADY-STATE DATA

From the measured steady-state data of the aircraft under test

$$C_L = C_L(\alpha, h, \delta_t, \text{power setting})$$

$$\delta_e = \delta_e(C_L, h, \delta_t, \text{power setting})$$

the following parameters for given power and trim tab setting can be determined:

Slope of the $C_L(\alpha)$ curve, $dC_L/d\alpha$

Slope of the $\delta_e(C_L)$ curve, $d\delta_e/dC_L$

$$V_T a_1 = \frac{\Delta h}{\Delta \delta_e} C_L \tag{B1}$$

and

$$H_n = \frac{\Delta h}{\Delta\left(\frac{d\delta_e}{dC_L}\right)} \frac{d\delta_e}{dC_L} \tag{B2}$$

where

$$V_T = \frac{1}{1 + F} \frac{S_t l}{S\bar{c}} \tag{B3}$$

$$F = \frac{\bar{c} h_{no}}{l_n} \tag{B4}$$

$$a_1 = \frac{\partial C_{L,t}}{\partial \alpha_t}$$

and where $\Delta\delta_e$ is an increment due to change of relative center-of-gravity position Δh for a given C_L.

Using these parameters allows the static stability and control derivatives to be obtained from the expressions

$$C_{m_{\delta e}} = \frac{-V_T a_1}{1 + \frac{\bar{c}}{l_t} H_n} \tag{B5}$$

$$C_{L_{\delta e}} = \frac{\bar{c}}{l_t} C_{m_{\delta e}} \tag{B6}$$

$$C_{L_\alpha} = \frac{dC_L/d\alpha}{1 + C_{L_{\delta e}} \frac{d\delta_e}{dC_L}} \tag{B7}$$

$$C_{m_\alpha} = -C_{L_\alpha} H_n \tag{B8}$$

The tail contribution to the damping derivatives can be approximated as

$$\left(C_{m_q}\right)_t = -2a_1 \frac{S_t}{S}\left(\frac{l_t}{\bar{c}}\right)^2 \approx -2V_T a_1 \frac{l_t}{\bar{c}} \tag{B9}$$

$$\left(C_{m_{\dot{\alpha}}}\right)_t \approx -2V_T a_1 \frac{l_t}{\bar{c}} \frac{\partial \varepsilon}{\partial \alpha} \tag{B10}$$

$$\left(C_{Z_q}\right)_t \approx -2V_T a_1 \tag{B11}$$

where the rate of downwash angle can be approximated as

$$\frac{\partial \varepsilon}{\partial \alpha} \approx \frac{2C_{L_\alpha}}{\pi A} \tag{B12}$$

For comparison of the estimated aerodyanmic derivatives from steady-state and transient flight data it was assumed that

$$C_{Z_\alpha} \approx -C_{L_\alpha}$$

$$C_{Z_{\delta e}} \approx -C_{L_{\delta e}}$$

$$C_{Z_q} \approx -\left(C_{L_q}\right)_t$$

The modified derivatives C'_{m_α} and C'_{m_q} were computed from equations (A9) and (A10). In the given case for $h\bar{c} = 0.206$ it was found that $C_{m_\alpha} = -1.015$, whereas $C'_{m_\alpha} = -0.80$. However, the difference between $C_{m_{\delta e}}$ and $C'_{m_{\delta e}}$ was negligible.

In steady-state nonsymmetric flights the following relationships can be measured:

$$\beta = \beta(\phi)$$

$$\beta = \beta(\delta_a)$$

$$\beta = \beta(\delta_r)$$

The analytical forms for these relationships are developed from equations (A15) to (A17) for $\dot{p} = \dot{r} = p = q = r = 0$ and $\beta_o = \delta_{a,o} = \delta_{r,o} = 0$ as

$$\beta \approx \frac{K_\phi}{C_{Y_\beta}}\left(C_{Y,o} - \frac{C_{Y_{\delta r}}}{C_{n_{\delta r}}}\frac{C_{n,o} - k_{\delta a}C_{l,o}}{1 - k_{\delta a}k_{\delta r}}\right) + \frac{K_\phi C_Z}{C_{Y_\beta}}\phi \tag{B13}$$

$$\beta = \frac{C_{l,o} - k_{\delta r}C_{n,o}}{C_{l_\beta}(1 - k_{\delta r}k_{nl\beta})} - \frac{C_{l_{\delta a}}}{C_{l_\beta}}\frac{1 - k_{\delta a}k_{\delta r}}{1 - k_{\delta r}k_{nl\beta}}\delta_a \tag{B14}$$

$$\beta = -\frac{C_{n,o} - k_{\delta a}C_{l,o}}{C_{n_\beta}(1 - k_{\delta a}k_{l n\beta})} - \frac{C_{n_{\delta r}}}{C_{n_\beta}}\frac{1 - k_{\delta a}k_{\delta r}}{1 - k_{\delta a}k_{l n\beta}}\delta_r \tag{B15}$$

In these equations,

$$C_Z = -\frac{2mg}{\rho S V^2} \cos\theta \cos\phi$$

$$K_\phi = \frac{1}{1 - \frac{C_{Y_{\delta r}}}{C_{n_{\delta r}}} \frac{C_{n_\beta}}{C_{Y_\beta}} \frac{1 - k_{\delta a} k_{l_{n\beta}}}{1 - k_{\delta a} k_{\delta r}}} \tag{B16}$$

$$k_{\delta a} = \frac{C_{n_{\delta a}}}{C_{l_{\delta a}}} \tag{B17}$$

$$k_{\delta r} = \frac{C_{l_{\delta r}}}{C_{n_{\delta r}}} \tag{B18}$$

$$k_{l_{n\beta}} = \frac{1}{k_{n_{l\beta}}} = \frac{C_{l_\beta}}{C_{n_\beta}} \tag{B19}$$

Equations (B13) to (B15) also define the relationship between the slope and intersect of the lateral steady-state characteristics and the lateral stability and control derivatives.

RFFERENCES

1. Gerlach, O. H.: Determination of Performance, Stability and Control Characteristics From Measurements in Non-Steady Manoeuvres. Stability and Control - Part 1, AGARD CP No. 17, Sept. 1966, pp. 499-523.

2. Howard, J.: The Determination of Lateral Stability and Control Derivatives From Flight Data. Can. Aeronaut. & Space J., vol. 13, no. 3, Mar. 1967, pp. 127-134.

3. Suit, William T.: Aerodynamic Parameters of the Navion Airplane Extracted From Flight Data. NASA TN D-6643, 1972.

4. Cannaday, Robert L.; and Suit, William T.: Effects of Control Inputs on the Estimation of Stability and Control Parameters of a Light Airplane. NASA TP-1043, 1977.

5. Denery, Dallas G.: Identification of System Parameters From Input-Output Data With Application to Air Vehicles. NASA TN D-6468, 1971.

6. Iliff, Kenneth W.; and Taylor, Lawrence W., Jr.: Determination of Stability Derivatives From Flight Data Using a Newton-Raphson Minimization Technique. NASA TN D-6579, 1972.

7. Klein, Vladislav; and Schiess, James R.: Compatibility Check of Measured Aircraft Responses Using Kinematic Equations and Extended Kalman Filter. NASA TN D-8514, 1977.

8. Grove, Randall D.; Bowles, Roland L.; and Mayhew, Stanley C.: A Procedure for Estimating Stability and Control Parameters From Flight Test Data by Using Maximum Likelihood Methods Employing a Real-Time Digital System. NASA TN D-6735, 1972.

9. Maine, Richard E.; and Iliff, Kenneth W.: A Fortran Program for Determining Aircraft Stability and Control Derivatives From Flight Data. NASA TN D-7831, 1975.

10. Klein, V.: On The Adequate Model for Aircraft Parameter Estimation. Rep. Aero No. 28, Cranfield Inst. Technol., Mar. 1975.

11. Klein, V.: Determination of Longitudinal Aerodynamic Derivatives From Steady-State Measurement of an Aircraft. AIAA Paper No. 77-1123, Aug. 1977.

TABLE I.- GEOMETRIC, MASS, AND INERTIA CHARACTERISTICS OF AIRPLANE

Wing:		
Area, m^2		13.56
Aspect ratio		7.35
Span, m		9.98
Mean aerodynamic chord, m		1.34
Ailerons:		
Area, m^2		0.94
Half-span, m		1.65
Vertical tail:		
Area, m^2		1.36
Rudder area, m^2		0.43
Horizontal tail (stabilator):		
Area, m^2		2.51
Aspect ratio		4.21
Span, m		3.25
Tail length (c.g. position at 0.206$\bar{c}$), m		4.21
Fuselage length, m		7.85
Mass:		
Aircraft mass at take-off, kg		974
Aircraft mass at landing (no fuel), kg		877
	No fuel	**Full fuel**
Inertia:		
I_X, kg-m^2	1568	1888
I_Y, kg-m^2	2125	2142
I_Z, kg-m^2	2326	3557
I_{XZ}, kg-m^2	140	142

TABLE II.- CHARACTERISTICS OF THE INSTRUMENTATION SYSTEM

Quantity measured	Transducer	Range (a)	Static sensitivity (b)	Resolution (c)	rms measurement error (c)	
					Unit (b)	Percent of full range
Longitudinal acceleration, g units	Servo accelerometer	-1 to 1	2.54	0.001	0.0046	0.23
Lateral acceleration, g units	Servo accelerometer	-1 to 1	2.48	.001	.0050	.25
Vertical acceleration, g units	Servo accelerometer	-3 to 6	.56	.001	.0050	.06
Rolling velocity, deg/sec	Rate gyro	-102 to 102	.025	.12	.20	.10
Pitching velocity, deg/sec	Rate gyro	-29 to 29	.088	.032	.19	.33
Yawing velocity, deg/sec	Rate gyro	-29 to 29	.084	.034	.080	.14
Roll angle, deg	Vertical gyro	-90 to 90	.028	.10	.077	.04
Pitch angle, deg	Vertical gyro	-87 to 87	.029	.098	.092	.05
Angle of sideslip, deg	Flow direction velocity sensor	-12 to 27	.127	.029	.027	.07
Angle of attack, deg	Flow direction velocity sensor	-29 to 32	.124	.018	.019	.03
Right aileron angle, deg	Control position transducer	-23 to 10	.147	.0020	.019	.06
Left aileron angle, deg	Control position transducer	-10 to 25	.142	.0020	.0061	.02
Stabilator angle, deg	Control position transducer	-16 to 3	.263	.010	.0037	.02
Rudder angle, deg	Control position transducer	-31 to 28	.084	.011	.0091	.02
Airspeed, m/sec	Pressure transducer	0 to 75	.067	.037	.89	1.2
Altitude, m	Altimeter	-150 to 2900	.0016	------	------	----
Air temperature, °C	Thermometer	-18 to 38	.089	------	------	----

[a]Working range of the channel.
[b]Obtained as volts per pertinent unit.
[c]Referred to a reading from the digitized tape.

TABLE III.- DYNAMIC CHARACTERISTICS OF INSTRUMENTATION SYSTEM

Quantity measured	Natural frequency, Hz	Damping ratio	Equivalent time constant, sec
Longitudinal acceleration, g units	402	1.58	0.0012
Lateral acceleration, g units	216	1.10	.0016
Vertical acceleration, g units	921	1.58	.0005
Rolling velocity, deg/sec Pitching velocity, deg/sec Yawing velocity, deg/sec	27	.64	.0075
Angle of sideslip, deg	(a)	(a)	
Angle of attack, deg	23	.085	.0012
Airspeed, m/sec	---	-----	

[a]At V = 50 m/sec.

TABLE IV.- FLIGHT CONDITIONS AND AVERAGE MASS AND INERTIA CHARACTERISTICS OF AIRPLANE IN TEST FLIGHTS

Flight	m, kg	h, percent $\frac{-}{c}$	I_X, kg-m^2	I_Y, kg-m^2	I_Z, kg-m^2	I_{XZ}, kg-m^2	ρ, kg/m^3	Experiment
8	911	16.7	1662	2135	3330	140	1.076	Longitudinal responses to short duration pulses; lateral responses; $V_i \sim 85$ knots
21	1033	20.6	2012	2206	3788	130	1.107	Lateral responses; 62 knots $< V_i <$ 100 knots
25	1050	20.6	----	2242	----	---	1.044	Longitudinal responses; 62 knots $< V_i <$ 100 knots
26	1050	20.6	2032	2242	3805	130	1.083	Lateral responses; $V_i \sim 85$ knots; different input forms and power settings
31A	1070	26.6	----	2354	----	---	1.066	Longitudinal responses; $V_i \sim 85$ knots; different power settings
31B	950	14.7	----	2127	----	---	.989	

TABLE V.- ESTIMATED INSTRUMENT BIAS ERRORS FROM STEADY-STATE AND TRANSIENT DATA FOR LONGITUDINAL MOTION

Parameter	Mean value from steady-state data	Estimate from transient data (a)	
		No fixed value	One fixed value
b_{a_X}, g units	0	0.000 (0.0030)	b_0
b_{a_Z}, g units	-.035	-.022 (.0067)	-.025 (0.0067)
b_q, deg/sec	.068	-.01 (.042)	-.01 (.042)
b_α, deg	-.14	-.28 (.078)	-.28 (.080)
b_β, deg	.81	.77 (.063)	.74 (.063)
λ_α	0	.01 (.0030)	.01 (.0030)

[a]Numbers in parentheses are Cramér-Rao lower bounds on standard errors.

[b]Fixed value.

TABLE VI.- ESTIMATED INSTRUMENT BIAS ERRORS FROM STEADY-STATE AND TRANSIENT DATA FOR LATERAL MOTION

Parameter	Mean value from steady-state data	Estimate from transient data (a)	
		No fixed value	One fixed value
b_{a_Y}, g units	0	-0.017 (0.0040)	[b]0
b_p, deg/sec	3.58	2.69 (.042)	2.69 (0.042)
b_r, deg/sec	.55	.24 (.037)	.26 (.036)
b_β, deg	0	.00 (.057)	-.02 (.057)
b_ϕ, deg	1.59	.88 (.080)	.09 (.080)
λ_β	0	.008 (.0021)	.003 (.0021)

[a]Numbers in parentheses are Cramér-Rao lower bounds on standard errors.

[b]Fixed value.

TABLE VII.- PARAMETERS AND THEIR STANDARD ERRORS ESTIMATED FROM FLIGHT DATA USING TWO ESTIMATION METHODS

[Flight 25, run 13B; C_L = 0.61]

Parameter	Equation error method		Maximum likelihood method	
	Estimate, $\hat{\Theta}$	Standard error, $s(\hat{\Theta})$	Estimate, $\hat{\Theta}$	Standard error, $s(\hat{\Theta})$ (a)
$C_{X,o}$	0.0400	0.0036	0.0461	0.00026
C_{X_α}	.46	.014	.50	.030
$C_{Z,o}$	-.604	.0010	-.611	.0016
C_{Z_α}	-4.82	.055	-5.67	.057
C_{Z_q}	-13	.27	-10.3	.92
$C_{Z_{\delta e}}$	-.7	.21	-.6	.16
$C'_{m,o}$	.0023	.00083	.0027	.00019
C'_{m_α}	-.71	.045	-.783	.0074
C'_{m_q}	-27	2.3	-26.6	.40
$C'_{m_{\delta e}}$	-3.3	.18	-3.21	.030

[a] Cramér-Rao lower bound.

TABLE VIII.- PARAMETERS ESTIMATED FROM TRANSIENT FLIGHT DATA USING TWO DIFFERENT AERODYNAMIC MODELS AND THE MAXIMUM LIKELIHOOD METHOD

[Flight 25, run 19B; $C_L = 1.26$]

Parameter	Linear aerodynamics			Nonlinear aerodynamics		
	Estimate, $\hat{\Theta}$	Sensitivity, $1/m_{jj}$, percent	Standard error, s_{jj}, percent	Estimate, $\hat{\Theta}$	Sensitivity, $1/m_{jj}$, percent	Standard error, s_{jj}, percent
$C_{X,o}$	0.252	0.17	0.31	0.251	0.11	0.25
C_{X_α}	1.15	1.0	1.5	1.17	1.1	1.5
$C_{Z,o}$	-1.214	.09	.25	-1.238	.04	.20
C_{Z_α}	-3.44	1.3	2.1	-3.22	.80	2.2
$C_{Z_{\alpha^2}}$	--------	----	----	11	2.0	9.6
C_{Z_q}	-33	3.1	6.8	-23	3.6	7.4
$C_{Z_{\delta e}}$	-2.67	3.9	8.7	-2.08	3.0	8.2
$C'_{m,o}$	-.0097	3.1	6.6	-.0033	3.5	17
C'_{m_α}	-1.301	.65	1.0	-1.473	.21	1.1
$C'_{m_{\alpha^2}}$	--------	----	----	-4.8	.66	5.4
C'_{m_q}	-18.6	.97	2.4	-15.6	.40	2.5
$C'_{m_{q\alpha}}$	--------	----	----	52	2.6	14
$C'_{m_{\delta e}}$	-3.44	.56	1.4	-3.12	.18	.97
s(V), m/sec	.19	----	----	.17	----	-----
s(α), deg	.33	----	----	.24	----	-----
s(q), deg/sec	.77	----	----	.61	----	-----
s(θ), deg	.43	----	----	.12	----	-----
$s(a_X)$, g units	.0049	----	----	.0057	----	-----
$s(a_Z)$, g units	.087	----	----	.029	----	-----

TABLE IX.- HIGH CORRELATION COEFFICIENTS FOR ESTIMATED PARAMETERS USING TWO DIFFERENT AERODYNAMIC MODELS AND THE MAXIMUM LIKELIHOOD METHOD

[Flight 25, run 19B; $C_L = 1.26$]

Parameter	Correlation coefficient	
	Linear aerodynamics	Nonlinear aerodynamics
$C_{Z,o}, C_{m,o}$	0.82	0.66
$C_{Z_q}, C_{Z_{\delta e}}$	.71	.65
$C'_{m_q}, C'_{m_{\delta e}}$	.83	.80
$C_{Z_\alpha}, C_{Z_{\alpha 2}}$	----	.64
$C'_{m_\alpha}, C'_{m_{\alpha 2}}$	----	.83
$C'_{m_q}, C'_{m_{q\alpha}}$	----	.65

TABLE X.- LONGITUDINAL PARAMETERS ESTIMATED FROM STEADY-STATE AND TRANSIENT FLIGHT DATA

Derivative	Steady-state data	Transient data (a)	
		EE method	ML method
[b] C_{Z_α}	[b]-5.10	[b]-4.68 (0.04)	[b]-5.3 (0.1)
C_{Z_q}	[c]-18	-16 (1)	[b]-19 (3)
$C_{Z_{\delta e}}$	-1.04	-1.02 (.06)	-1.2 (.2)
[d] C'_{m_α}	[d]-.80	[d]-.68 (.03)	[d]-.80 (.02)
[d] C'_{m_q}	[c]-30.6	[d]-27.3 (.2)	[d]-24.2 (.4)
$C'_{m_{\delta e}}$	-3.26	-3.32 (.04)	-3.32 (.05)

[a]Numbers in parentheses are standard errors of ensemble mean.
[b]For $C_L \leq 1.0$.
[c]Tail contribution only.
[d]For $C_L \leq 0.7$.

TABLE XI.- PARAMETERS ESTIMATED FROM TRANSIENT FLIGHT DATA WITH TWO DIFFERENT INPUTS BY MAXIMUM LIKELIHOOD METHOD

Parameter	Flight 25, run 13B			Flight 8, run 14		
	Estimate, $\hat{\Theta}$	Sensitivity, $1/m_{jj}$, percent	Standard error, s_{jj}, percent	Estimate, $\hat{\Theta}$	Sensitivity, $1/m_{jj}$, percent	Standard error, s_{jj}, percent
$C_{Z,o}$	-0.611	0.04	0.27	-0.548	0.27	0.38
C_{Z_α}	-5.67	.57	1.0	-5.23	.82	1.4
C_{Z_q}	-10	6.6	22	.76	88	161
$C_{Z_{\delta e}}$	-.64	9.1	25	-1.12	3.3	6.8
$C'_{m,o}$	.00027	.95	7.1	.00093	32	44
C'_{m_α}	[a]-.783	.49	.95	[a]-.946	1.1	1.4
C'_{m_q}	-26.6	.34	1.5	-22.13	.93	2.5
$C'_{m_{\delta e}}$	-3.21	.24	.96	-3.11	.55	1.4
s(α), deg	.24	----	-----	.15	-----	------
s(q), deg/sec	.28	----	-----	2.3	-----	------
$s(a_Z)$, g units	.010	----	-----	.018	-----	------

[a]Estimates for $h\bar{c} = 0.206$.

TABLE XII.- PARAMETERS AND THEIR STANDARD ERRORS ESTIMATED FROM REPEATED MEASUREMENTS USING TWO ESTIMATION METHODS

Parameter	Equation error method			Maximum likelihood method		
		Standard errors			Standard errors	
	Mean value $\bar{\Theta}$ (a)	$s(\hat{\Theta})$ (b)	$s(\hat{\Theta})$ (c)	Mean value $\bar{\Theta}$ (a)	$s(\hat{\Theta})$ (b)	$s(\hat{\Theta})$, lower bound (c)
C_{Y_β}	-0.647	0.012	0.0061	-0.649	0.0097	0.0064
C_{Y_p}	-.04	.093	.016	-.09	.12	.016
$C_{Y_{\delta r}}$	.097	.011	.0065	.094	.014	.0068
C_{l_β}	-.0810	.0025	.0025	-.0816	.0042	.00079
C_{l_p}	-.532	.018	.018	-.559	.053	.0055
C_{l_r}	.16	.040	.016	.13	.027	.0053
$C_{l_{\delta a}}$	-.227	.010	.0065	-.241	.022	.0018
$C_{l_{\delta r}}$	.015	.0051	.0036	.007	.0068	.0012
C_{n_β}	.0745	.0043	.00090	.0772	.0055	.00031
C_{n_p}	-.042	.029	.0064	-.024	.031	.0028
C_{n_r}	-.130	.017	.0059	-.145	.030	.0022
$C_{n_{\delta a}}$	.019	.0087	.0022	.024	.0096	.0010
$C_{n_{\delta r}}$	-.072	.0031	.0013	-.074	.0073	.00060

[a]Ensemble mean value.
[b]Ensemble standard error.
[c]Average standard error of estimates.

TABLE XIII.- PREDICTED VALUES OF PARAMETERS AND VARIOUS STANDARD ERROR ESTIMATES

Parameter	Estimate, $\hat{\theta}_p$, for $C_L = 0.62$	Standard error boundaries		Standard error, $s(\hat{\theta})$ (a)
		$s(\hat{\theta}_p)$ min.	$s(\hat{\theta}_p)$ max.	
C_{Y_β}	-0.662	0.0059	0.010	0.0064
C_{Y_p}	-.09	.025	.044	.016
$C_{Y_{\delta r}}$	.094	.0058	.012	.0068
C_{l_β}	-.079	.0016	.0032	.00079
C_{l_p}	-.55	.010	.021	.0055
C_{l_r}	.13	.010	.020	.0053
$C_{l_{\delta a}}$	-.238	.0040	.0080	.0018
$C_{l_{\delta r}}$	.007	.0025	.0049	.0012
C_{n_β}	.077	.0015	.0023	.00031
C_{n_p}	-.020	.0068	.012	.0028
C_{n_r}	-.139	.0077	.013	.0022
$C_{n_{\delta a}}$	.027	.0028	.0055	.0010
$C_{n_{\delta r}}$	-.072	.0020	.0034	.00060

[a]Average value for single measurement, lower bound.

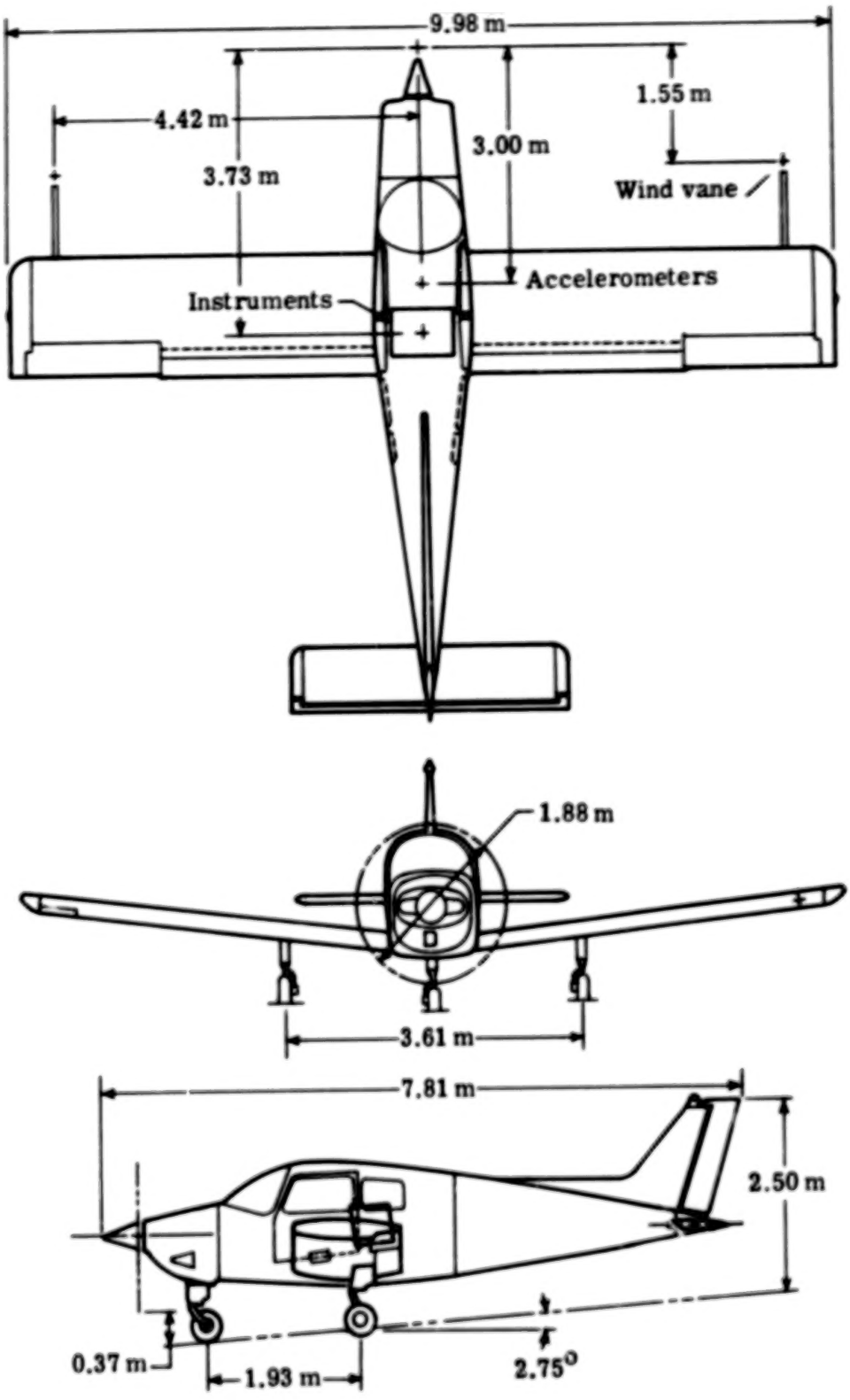

Figure 1.- Three-view drawing of test airplane.

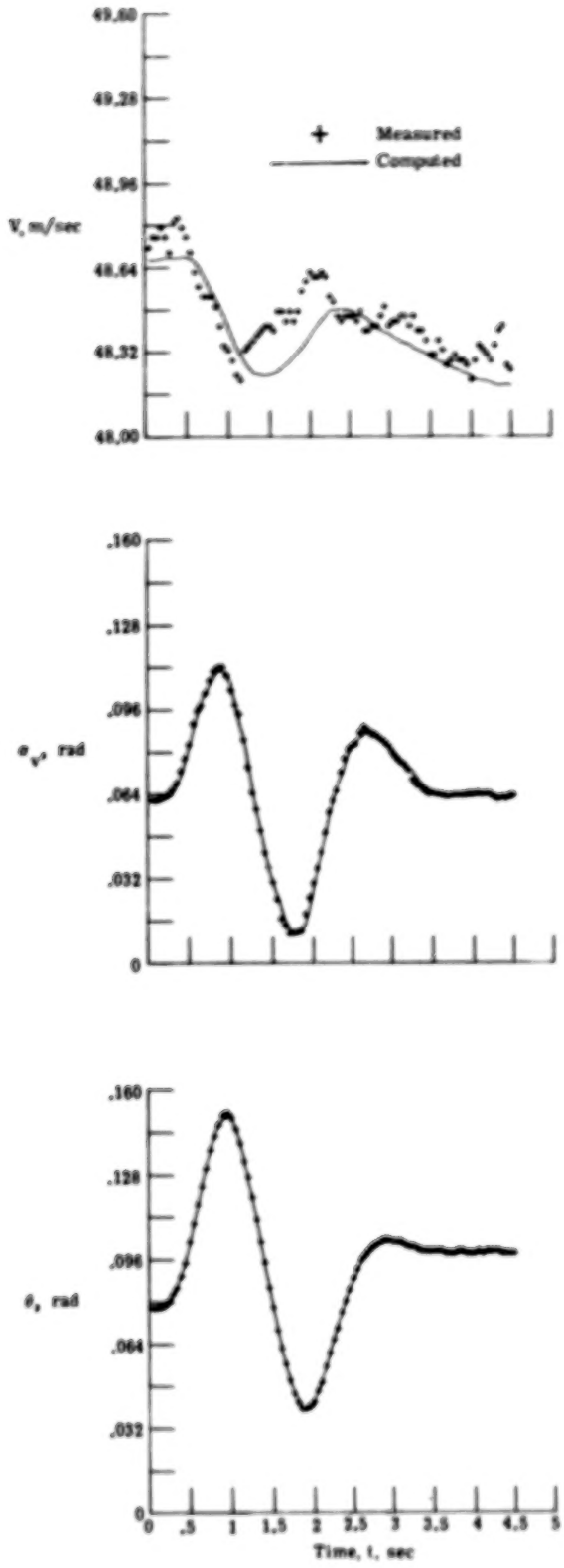

Figure 2.- Time histories of measured and predicted output variables. Longitudinal motion; flight 25, run 13B.

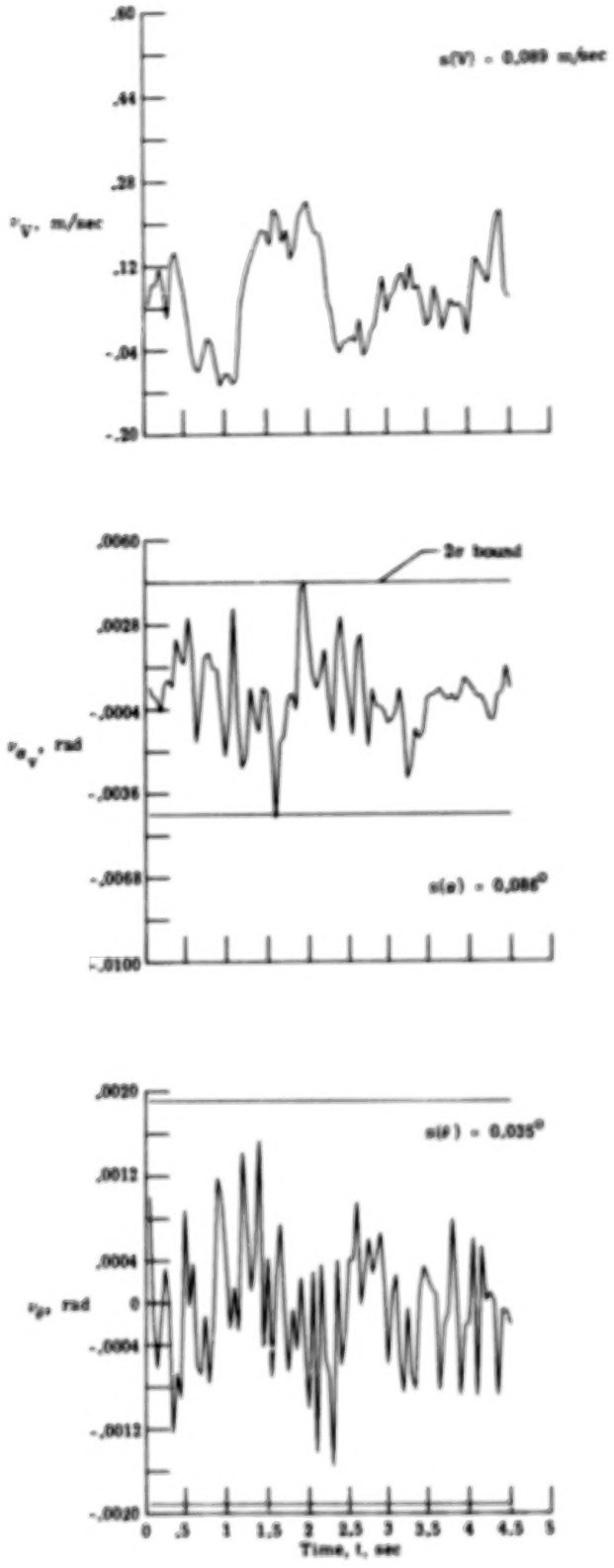

Figure 3.- Time histories and standard errors of residuals. Longitudinal motion; flight 25, run 13B.

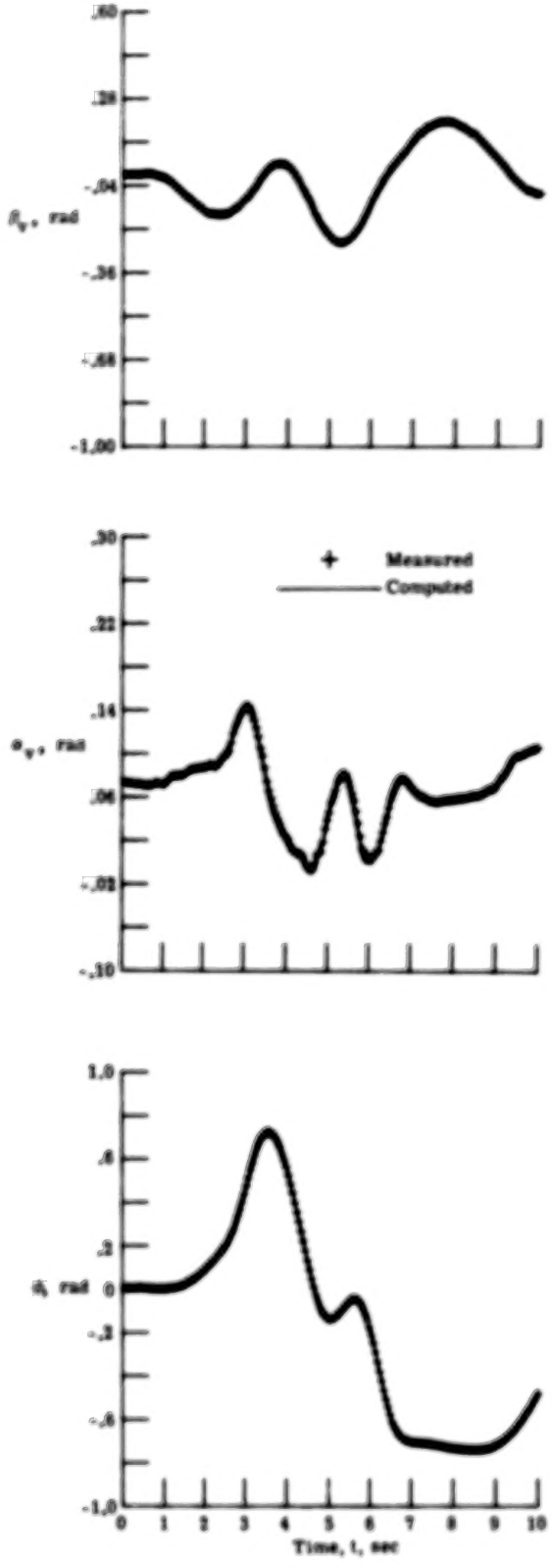

Figure 4.- Time histories of measured and predicted output variables. Lateral motion; flight 21, run 26.

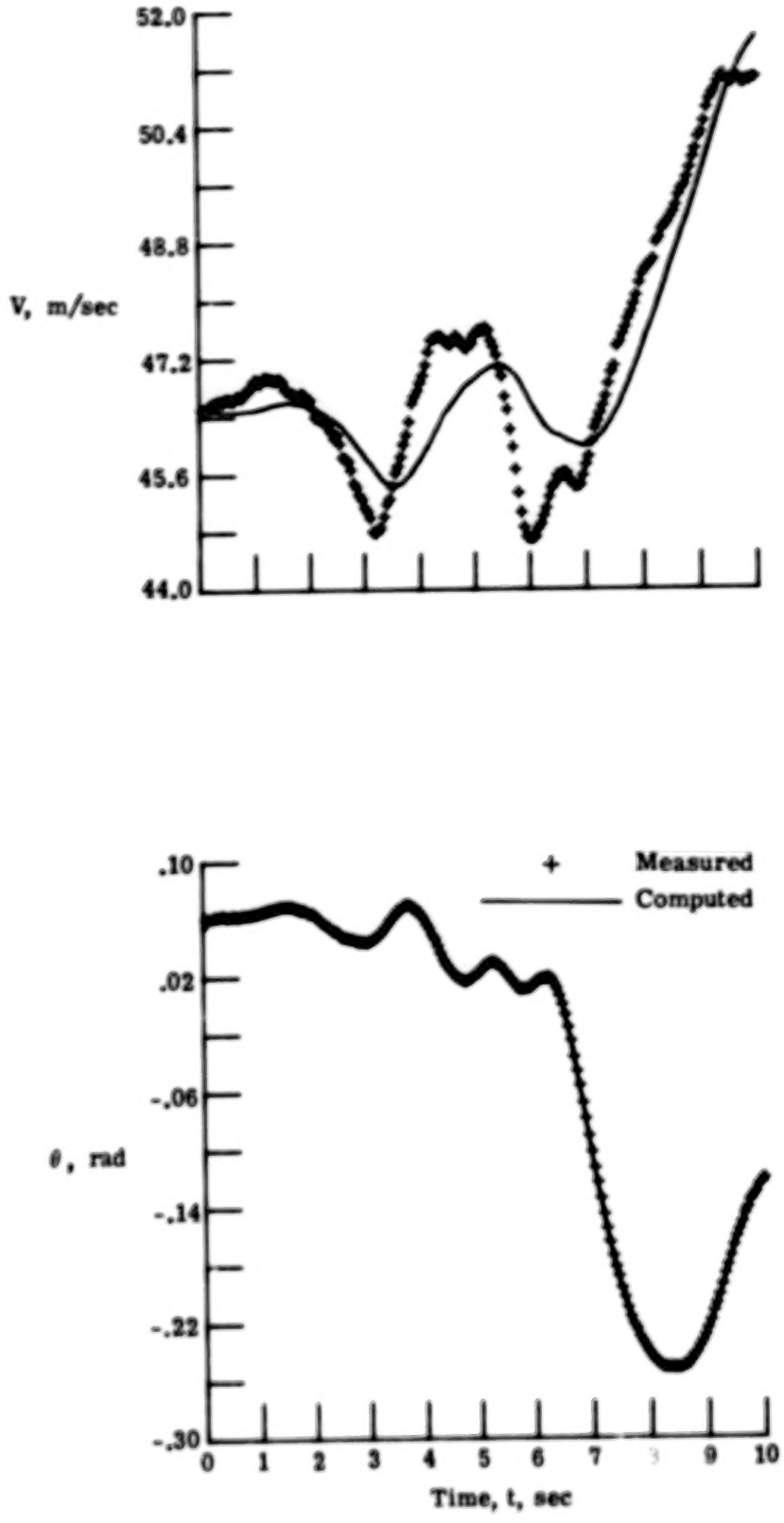

Figure 4.- Concluded.

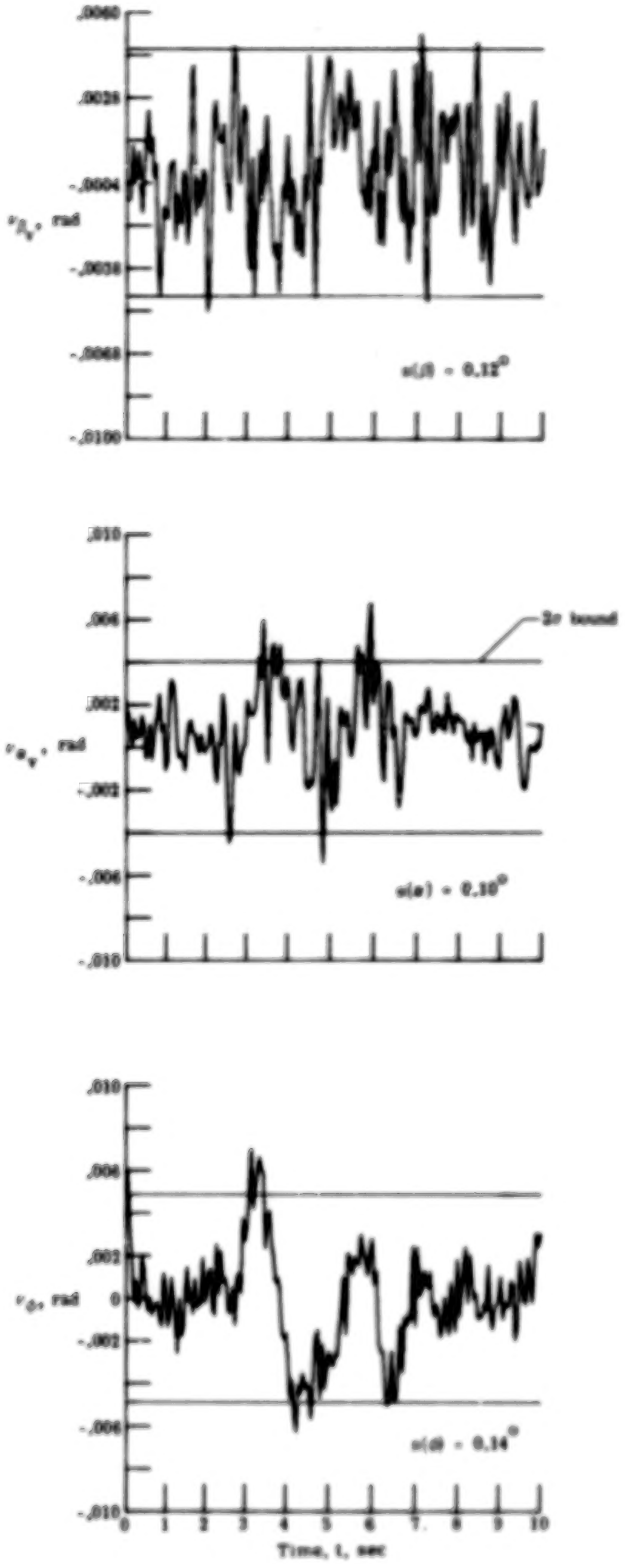

Figure 5.- Time histories and standard errors of residuals. Lateral motion; flight 21, run 26.

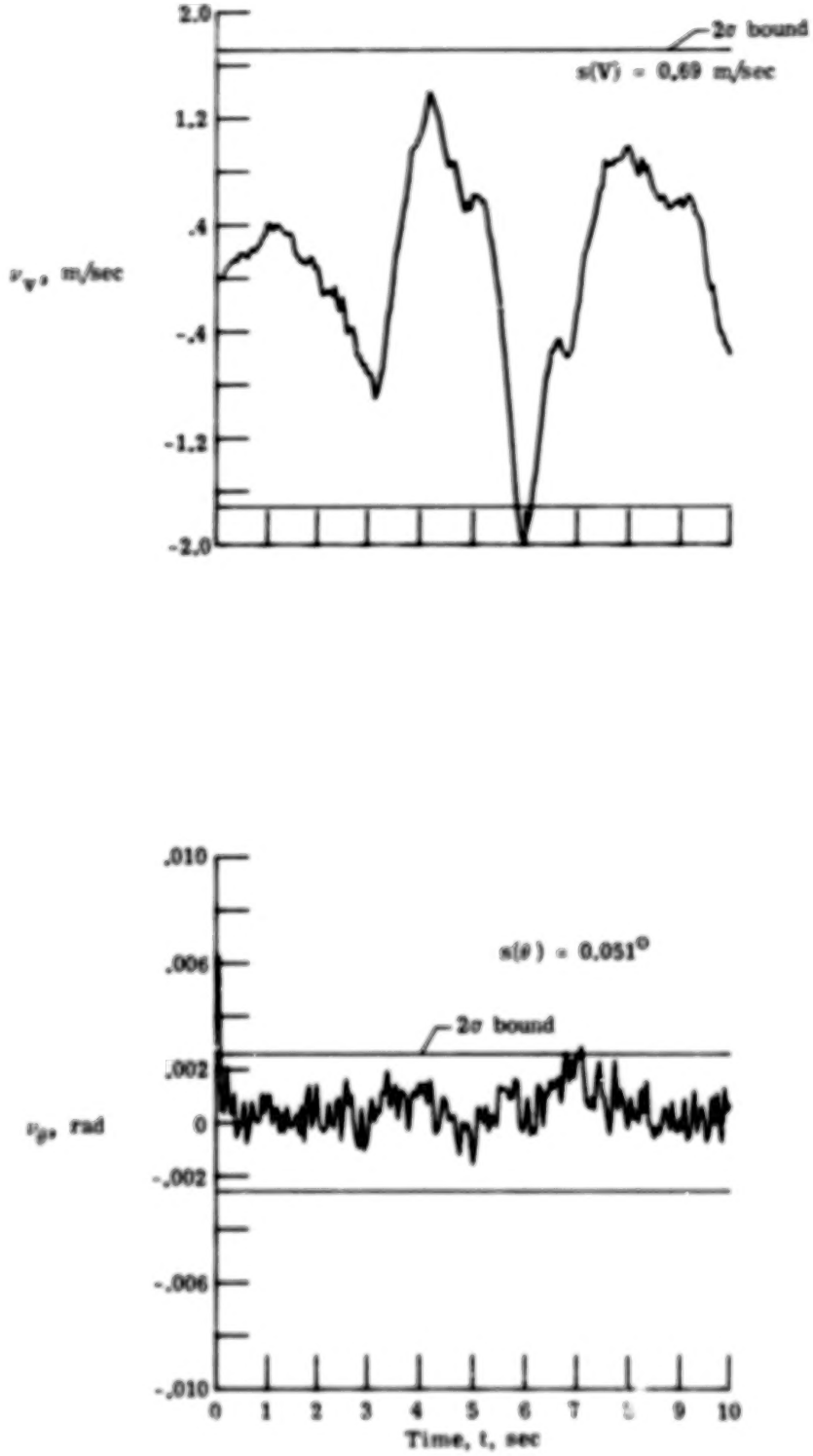

Figure 5.- Concluded.

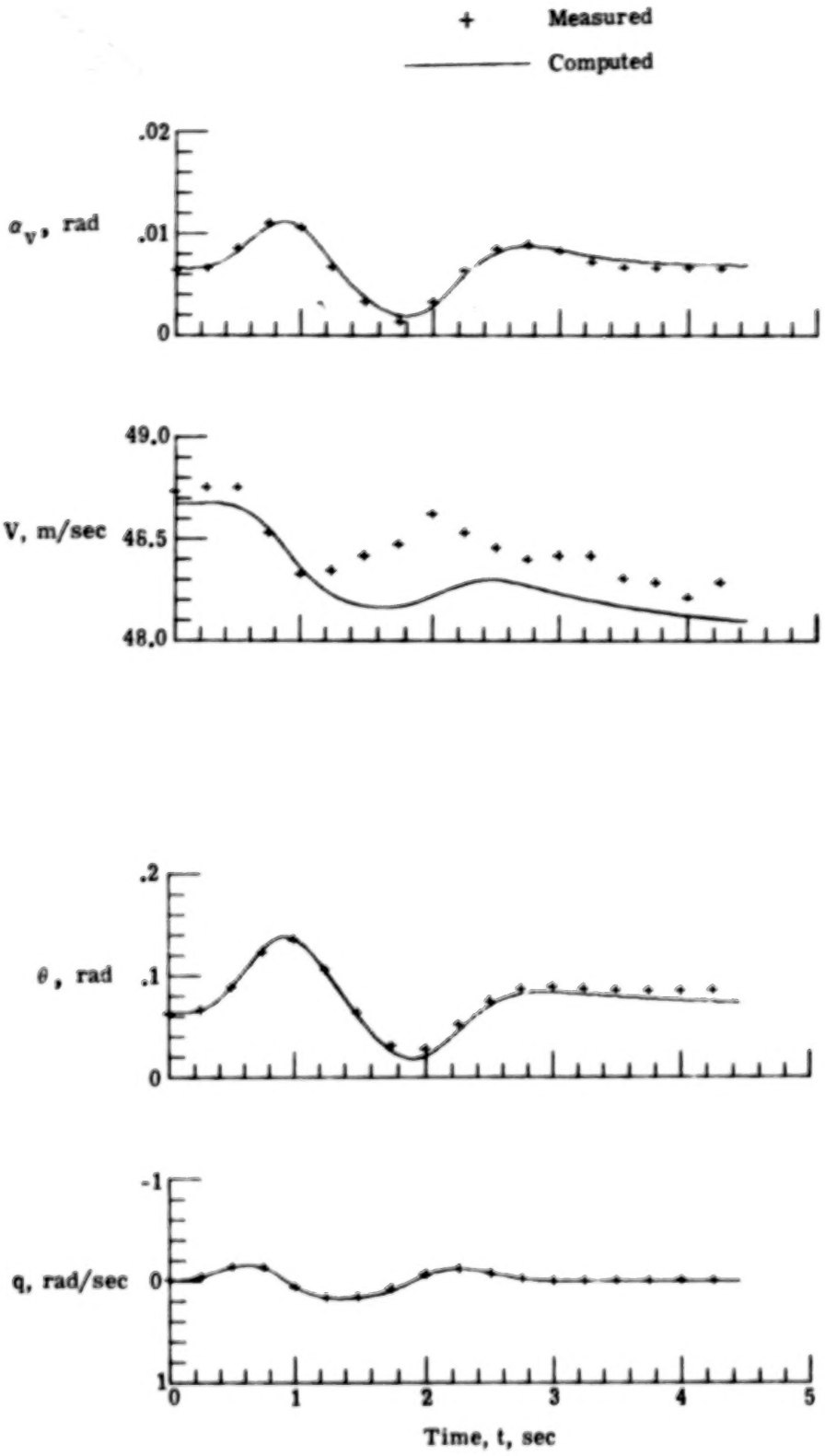

Figure 6.- Measured longitudinal flight data time histories and those computed by using parameters obtained by equation error method. Flight 25, run 13B.

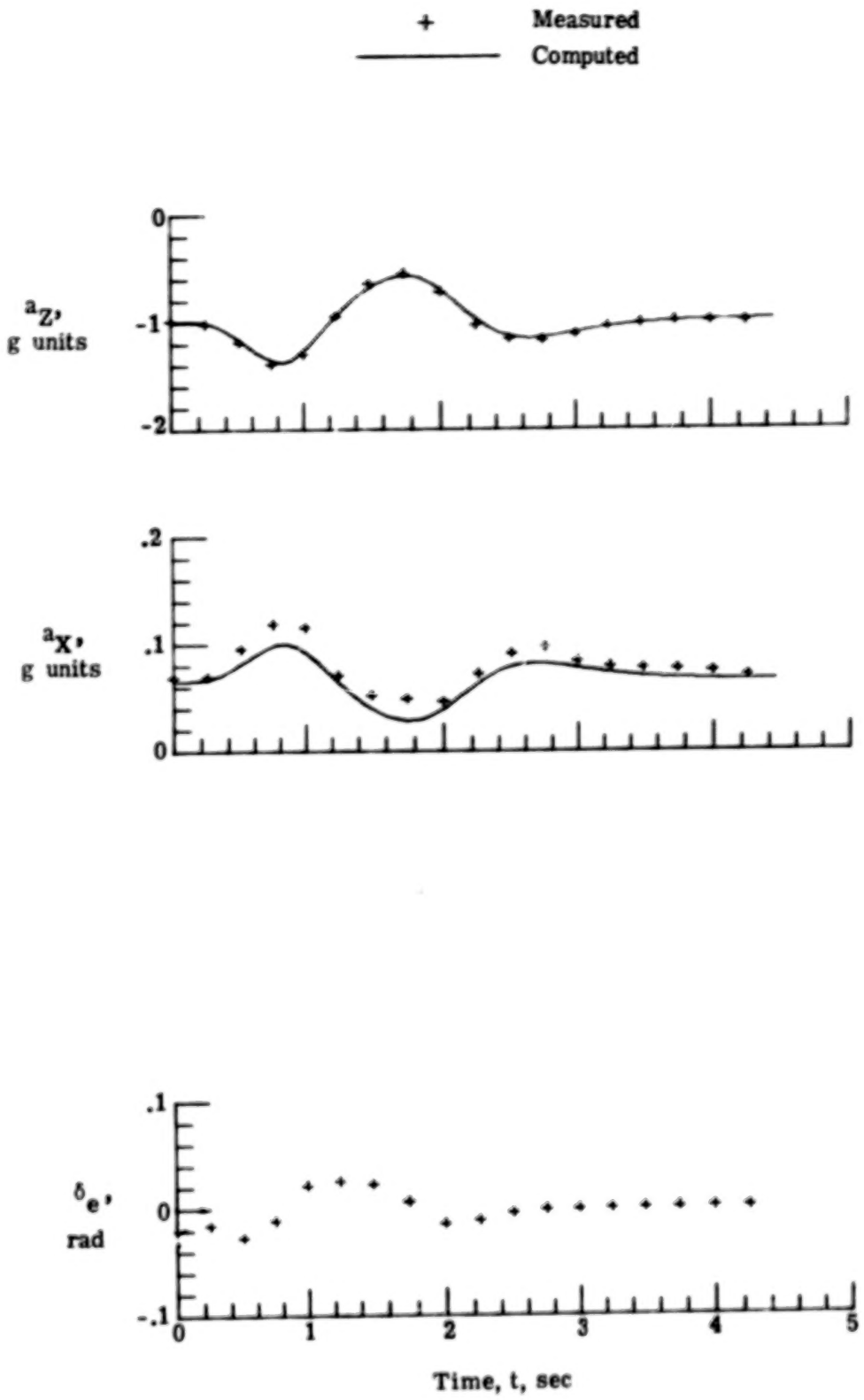

Figure 6.- Concluded.

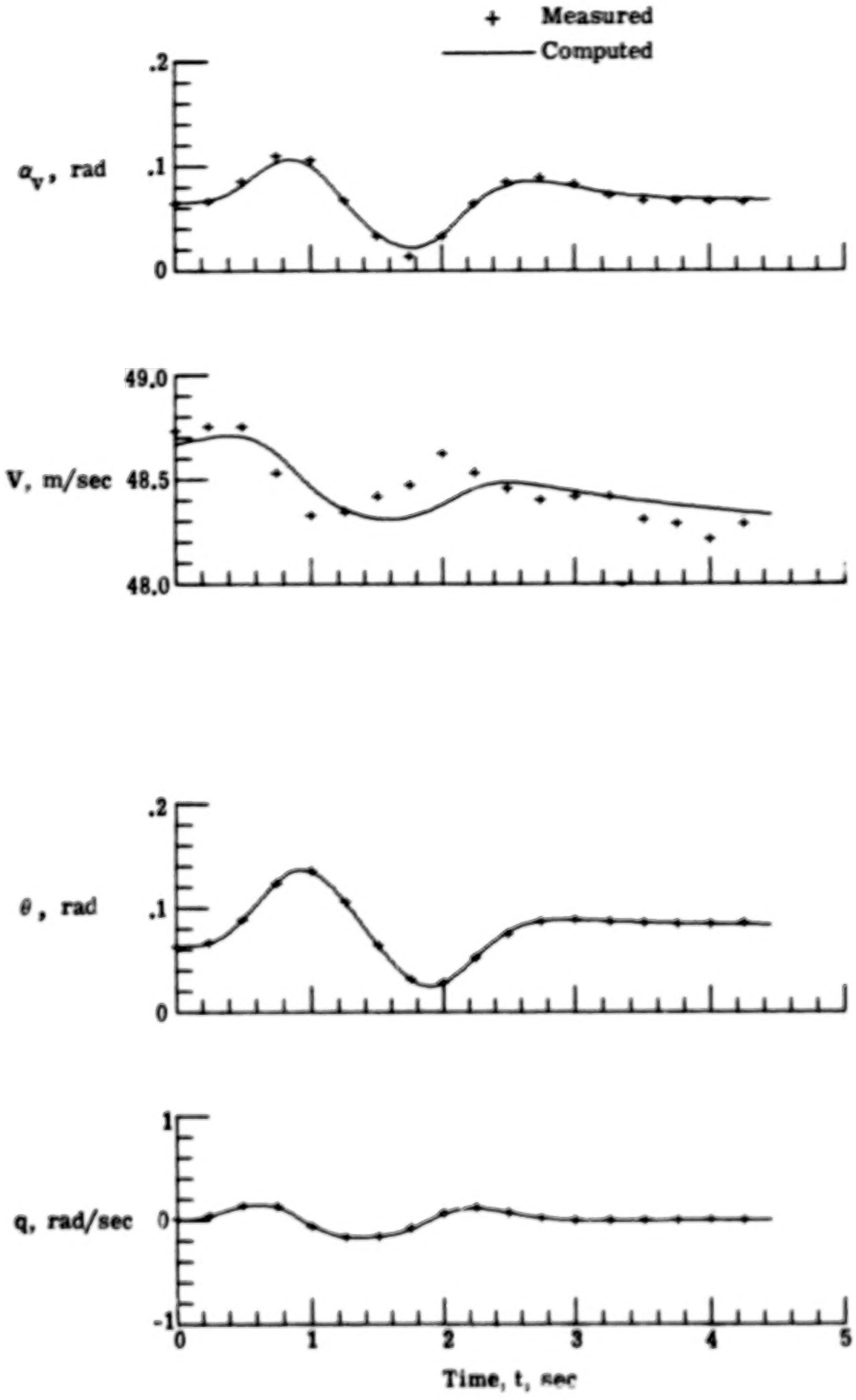

Figure 7.- Measured longitudinal flight data time histories and those computed by using parameters obtained by maximum likelihood method. Flight 25, run 13B.

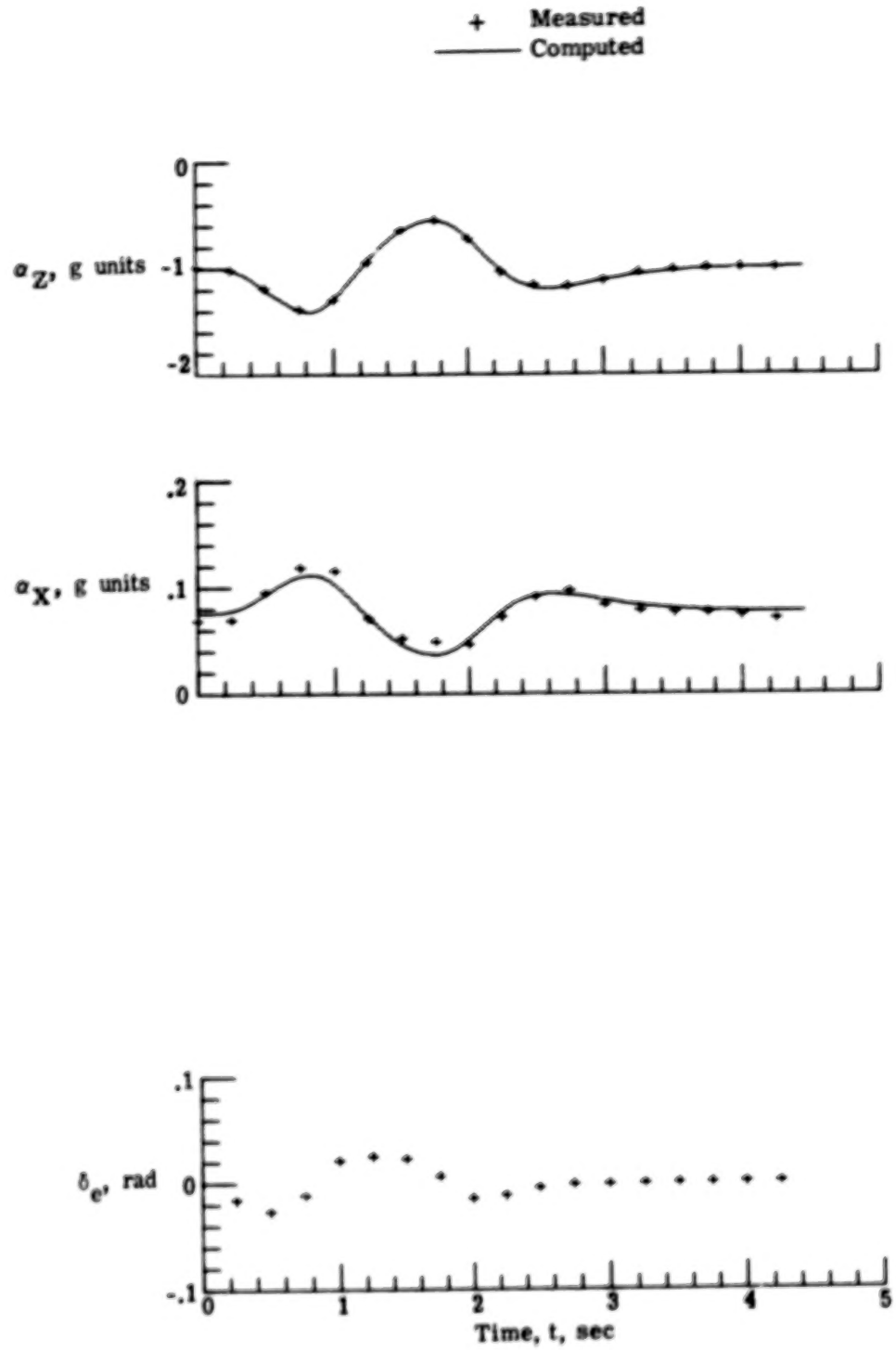

Figure 7.- Concluded.

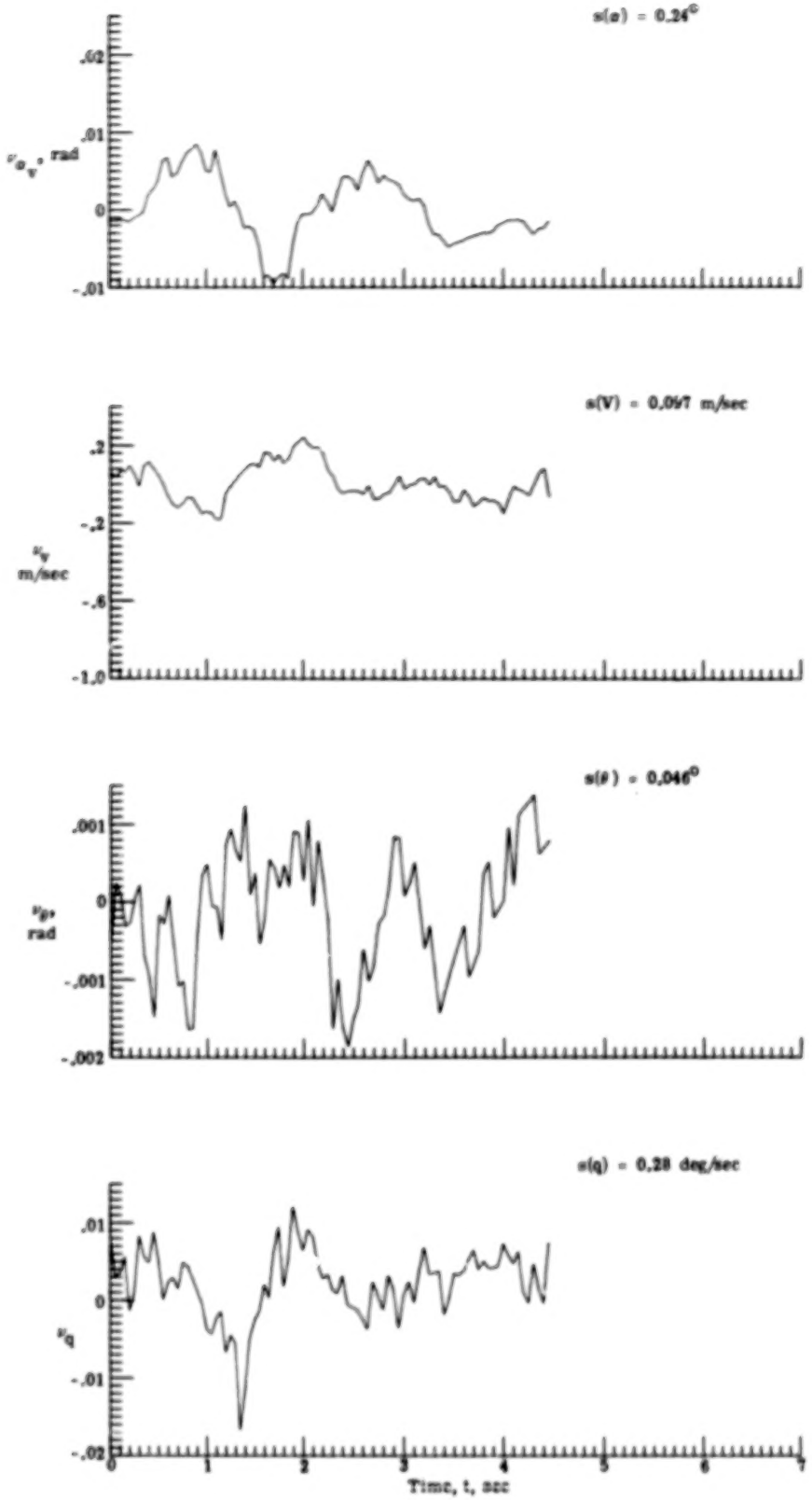

Figure 8.- Time histories and standard errors of residuals. Maximum likelihood method; flight 25, run 13B.

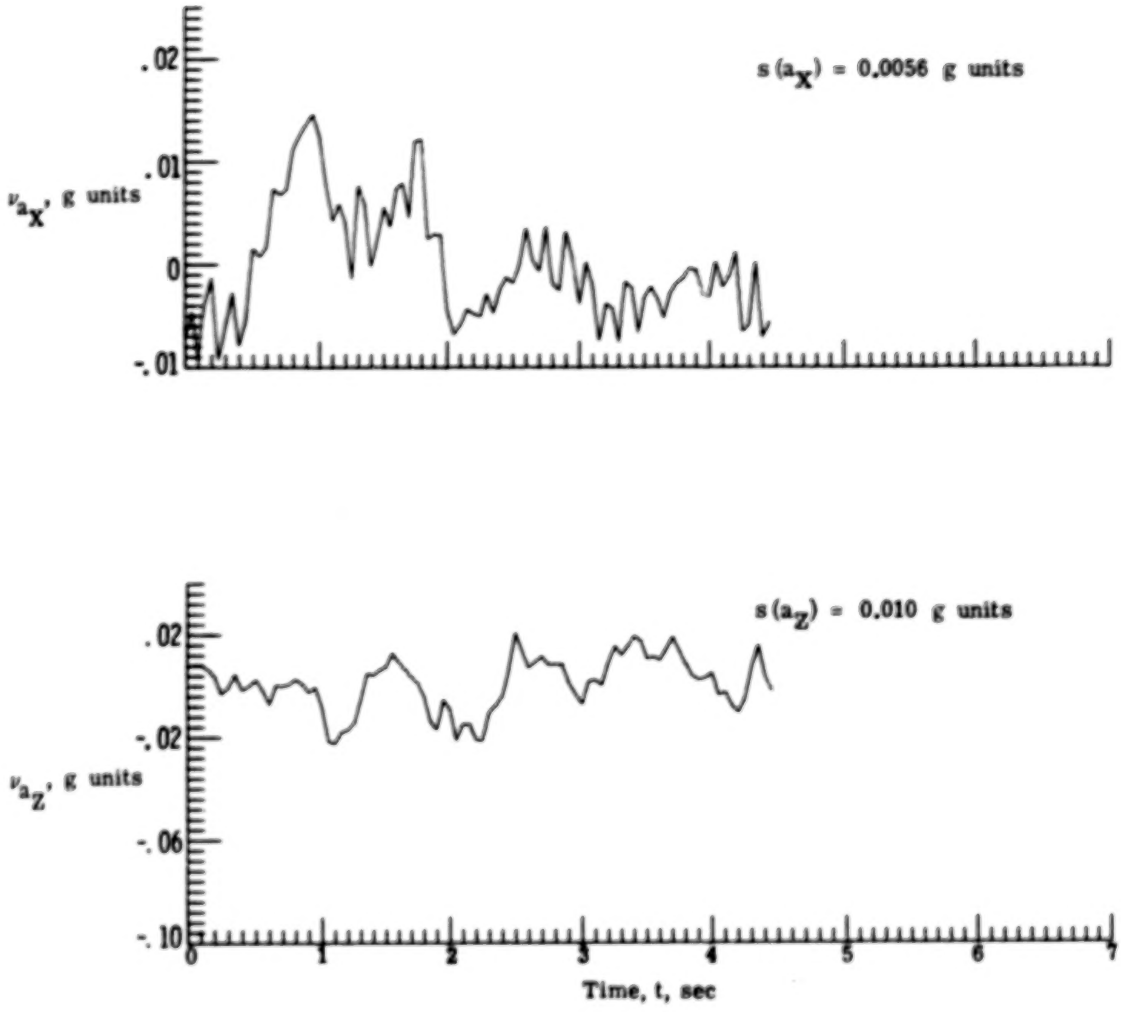

Figure 8.- Concluded.

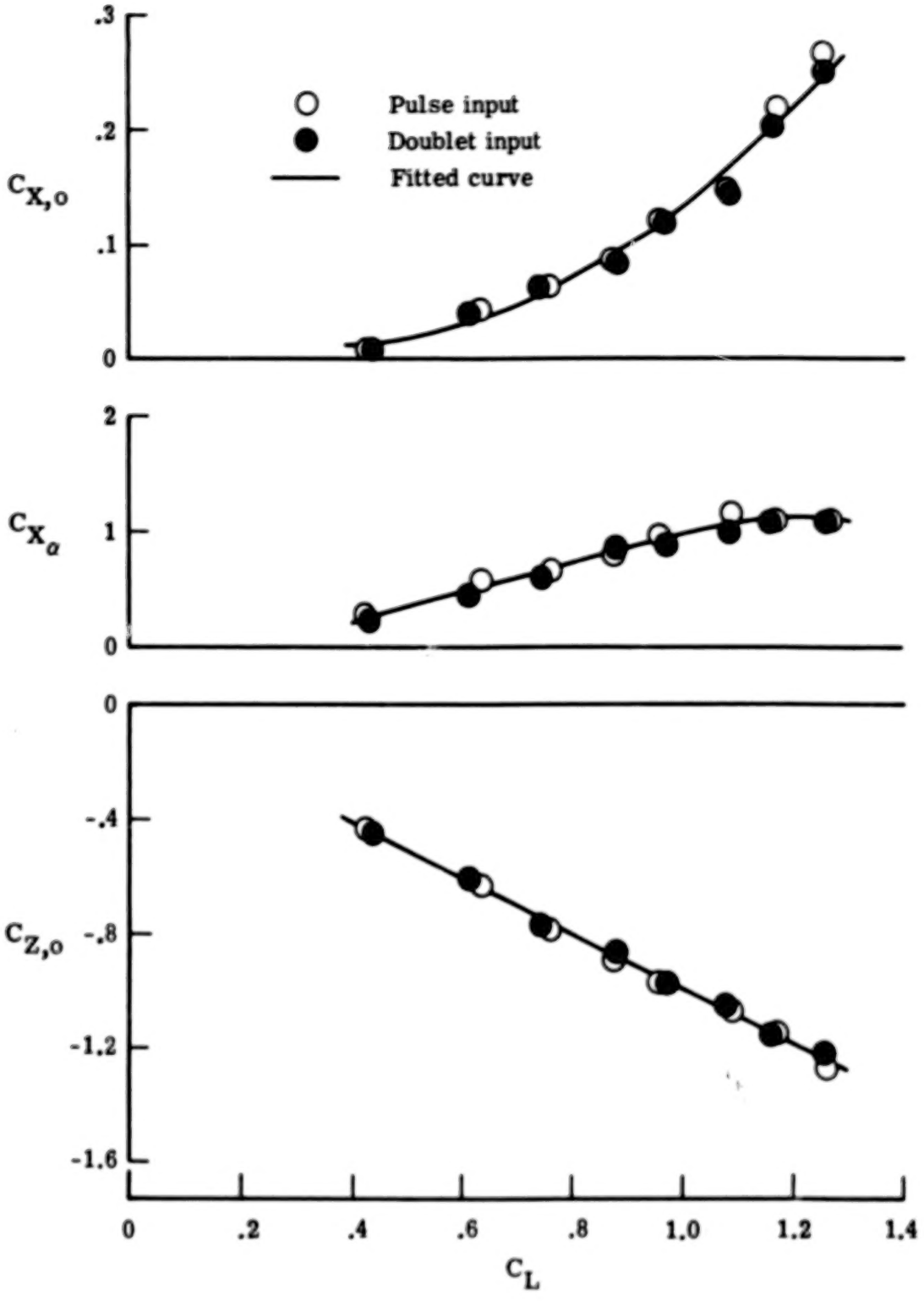

Figure 9.- Estimated longitudinal parameters from flight data. Equation error method.

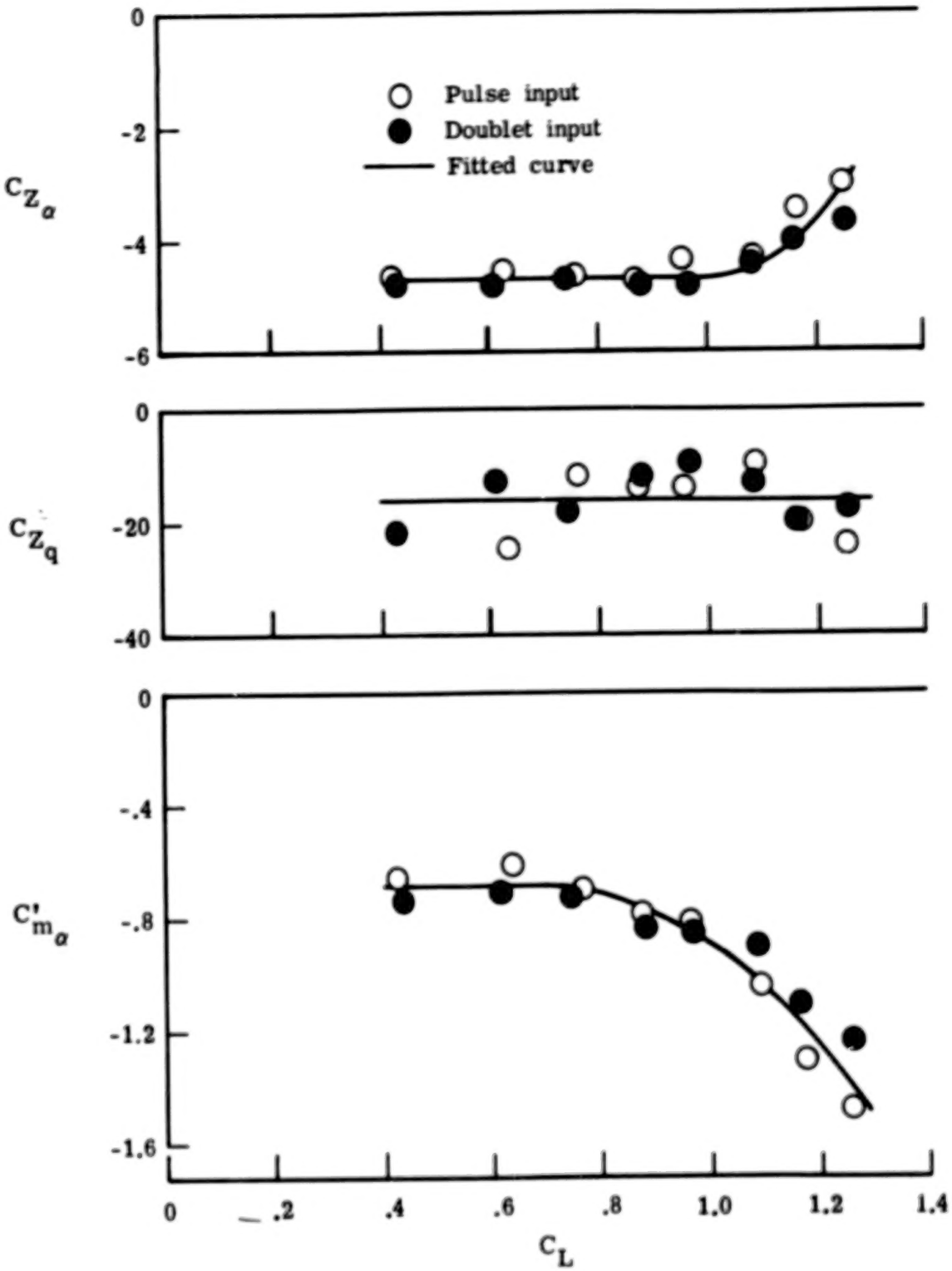

Figure 9.- Continued.

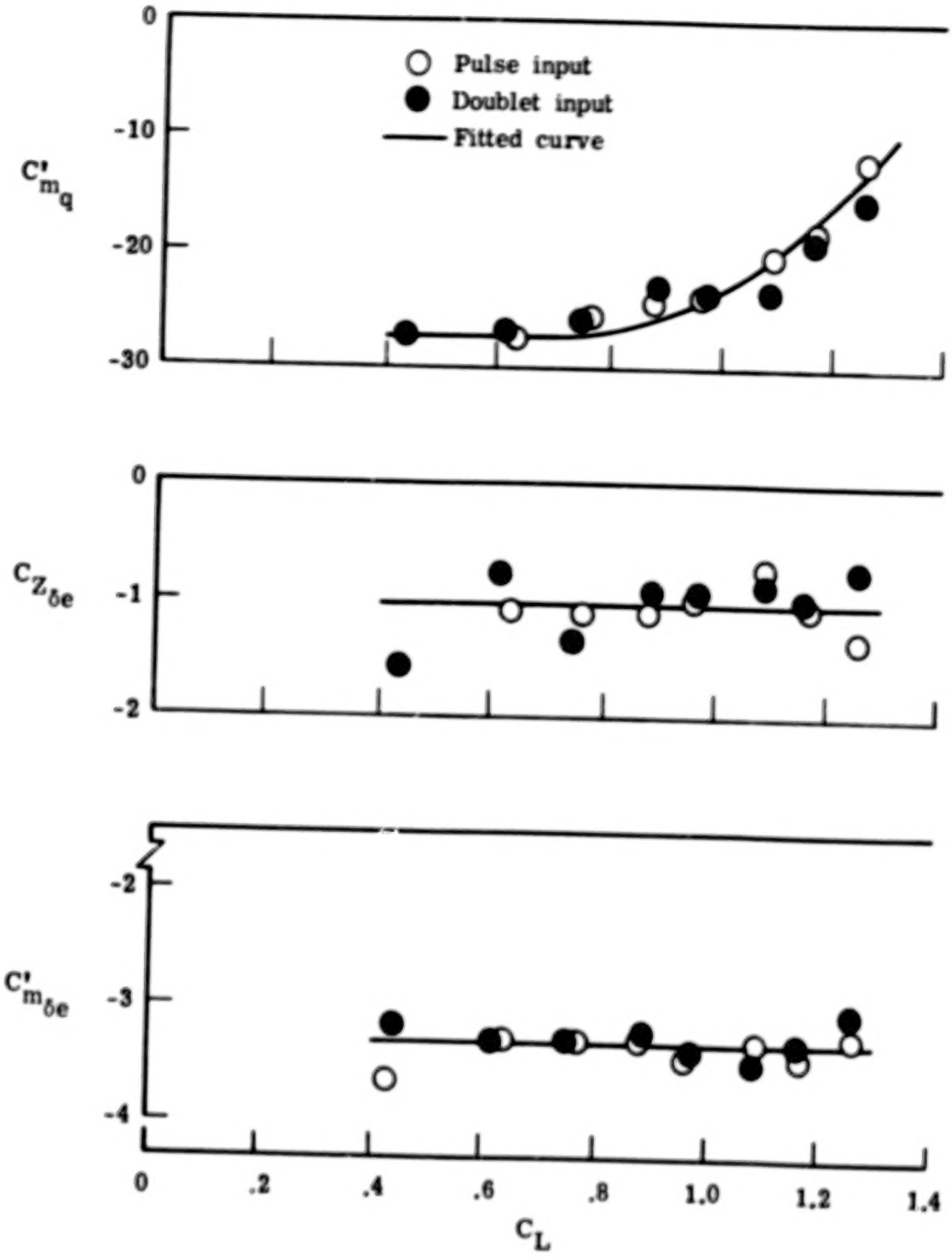

Figure 9.- Concluded.

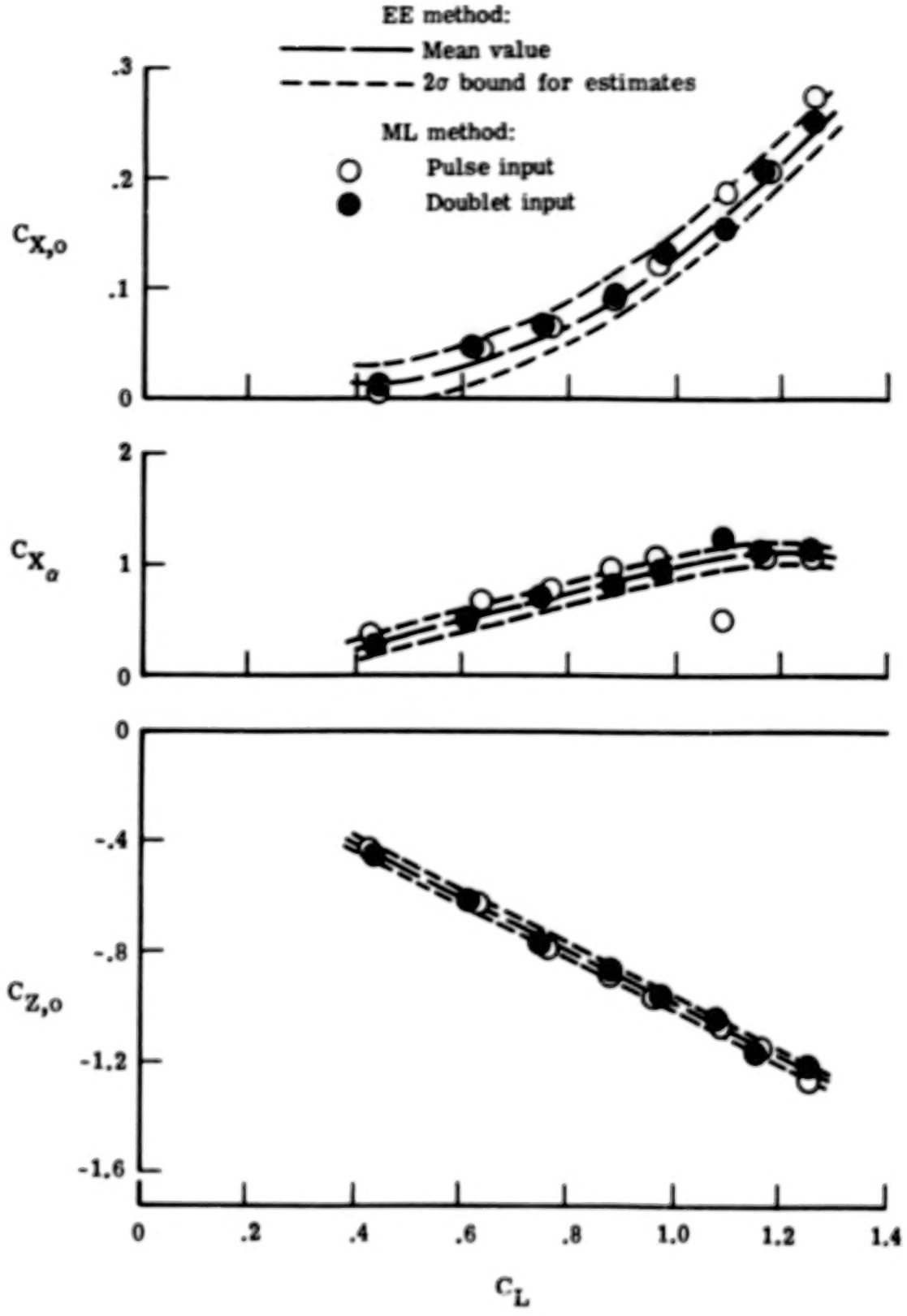

Figure 10.- Comparison of longitudinal parameters estimated from flight data using equation error and maximum likelihood methods.

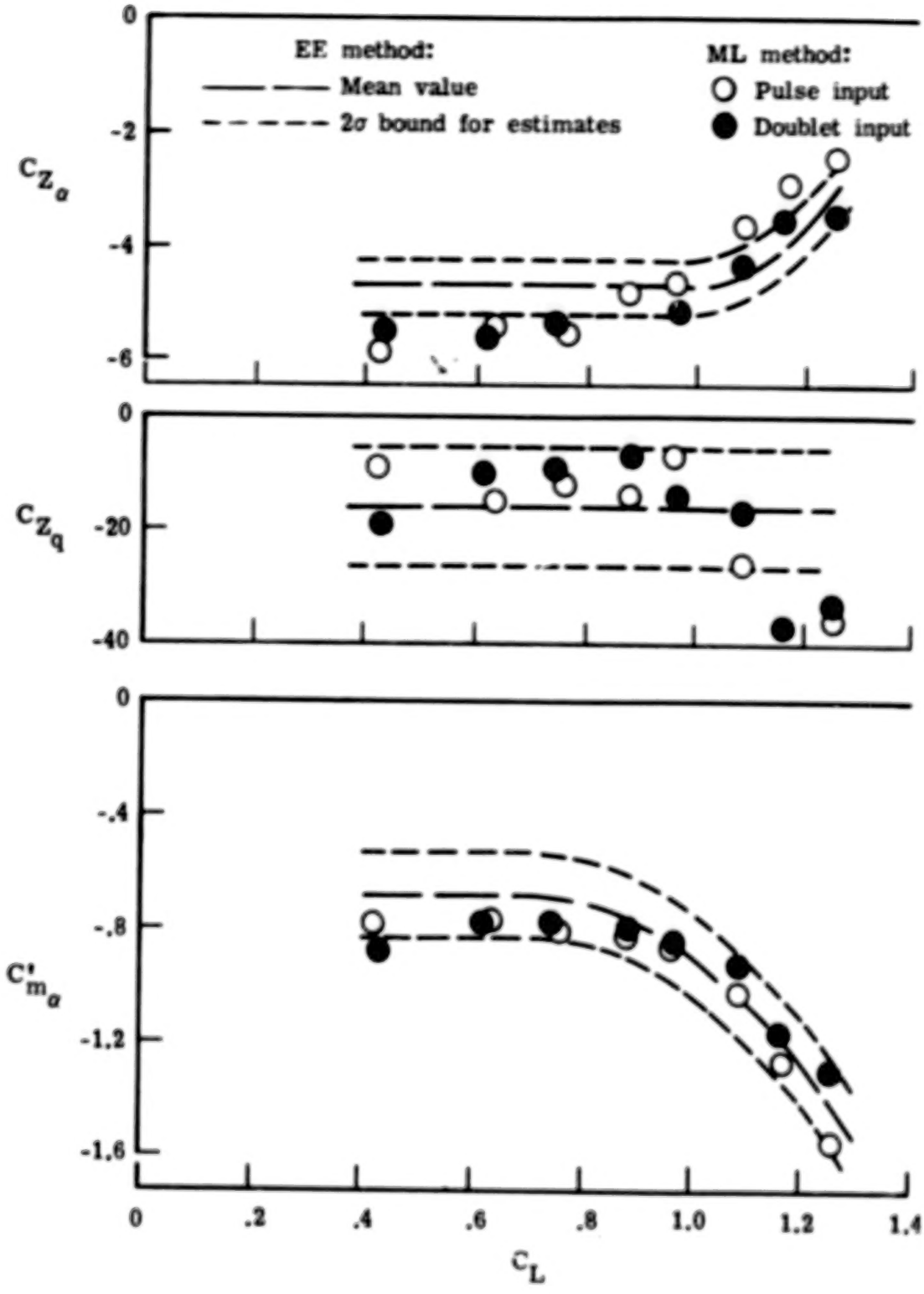

Figure 10.- Continued.

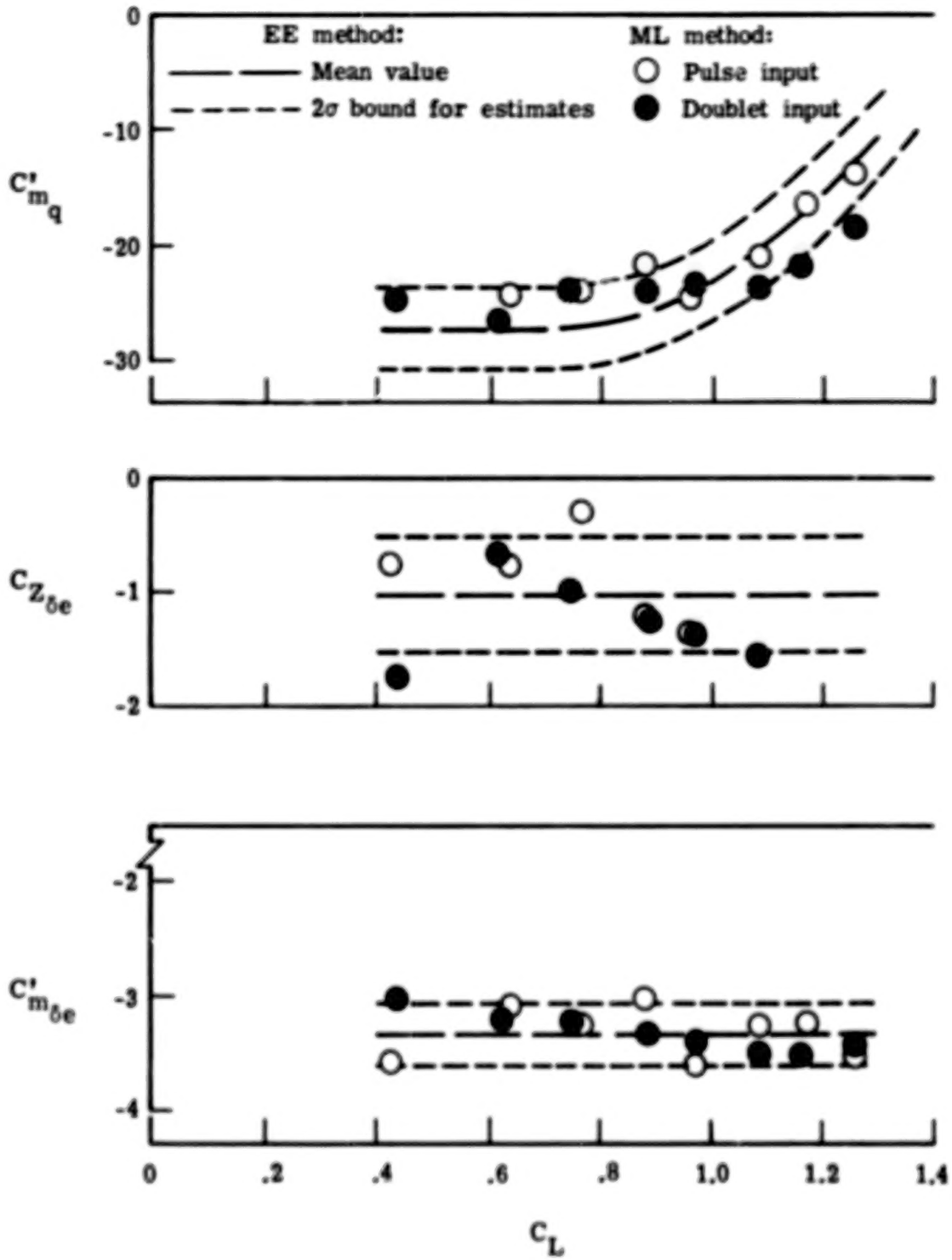

Figure 10.- Concluded.

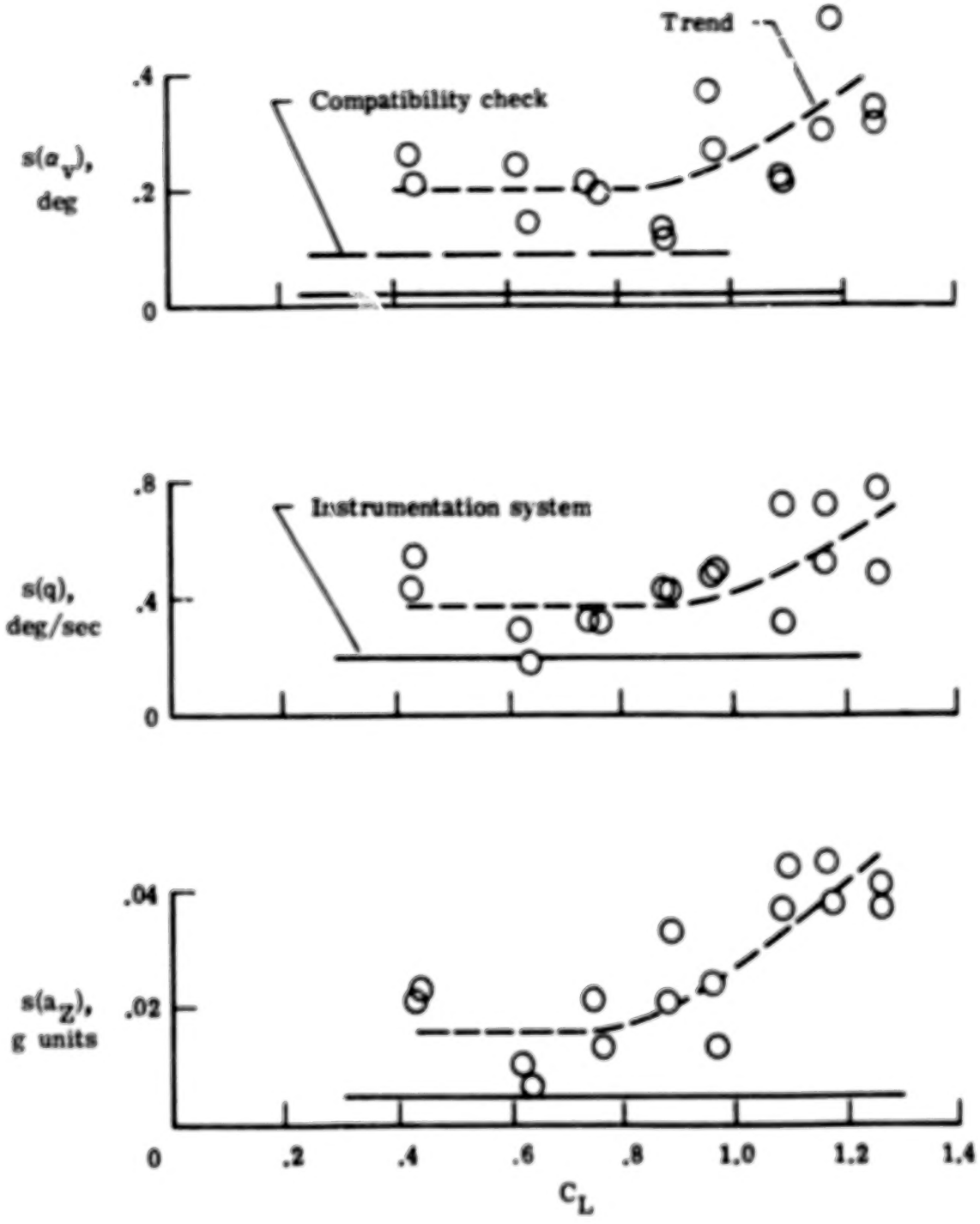

Figure 11.- Estimated standard errors of measurement noise. Longitudinal flight data.

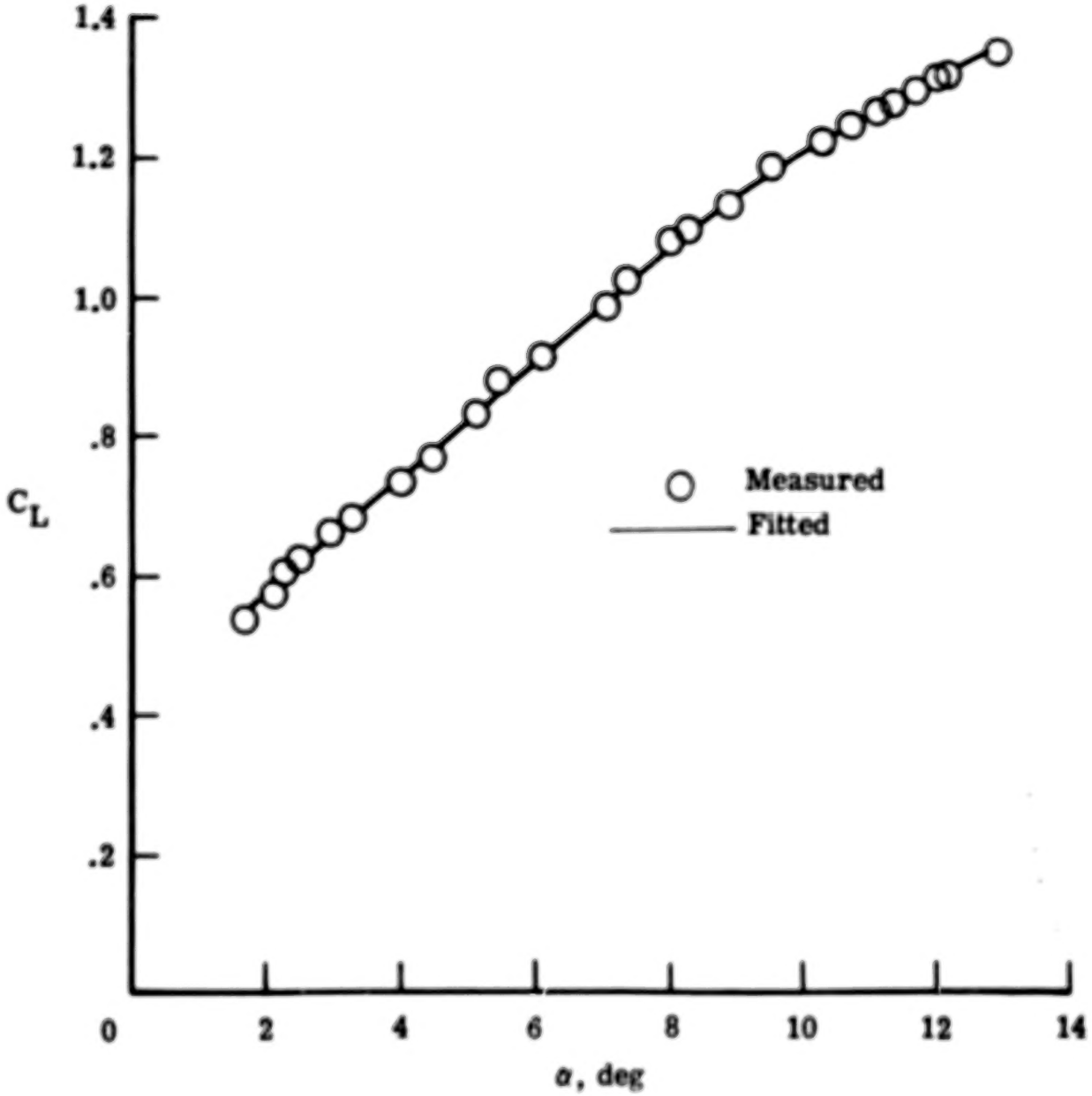

Figure 12.- Measured and fitted lift coefficient plotted against angle of attack. Acceleration-deceleration levels.

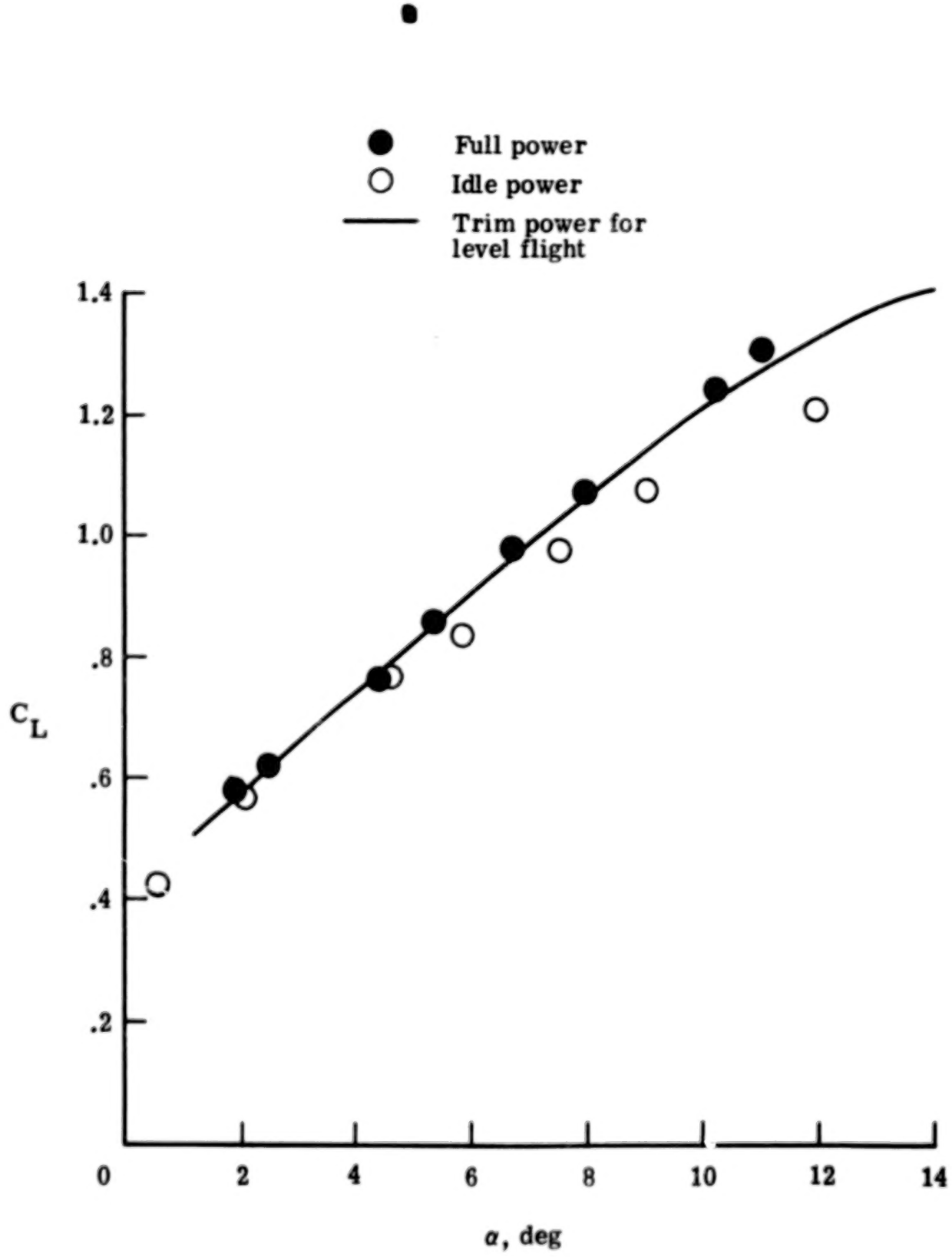

Figure 13.- Effect of power setting on relationships of measured lift coefficient angle of attack.

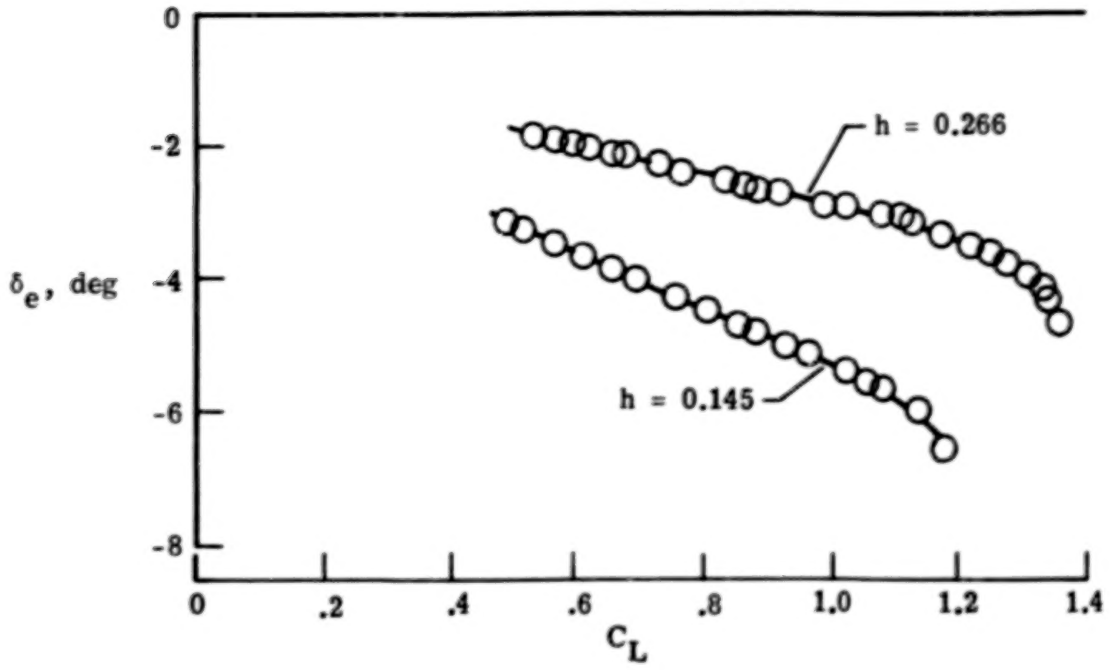

Figure 14.- Measured and fitted elevator deflection plotted against lift coefficient. Acceleration-decleration levels.

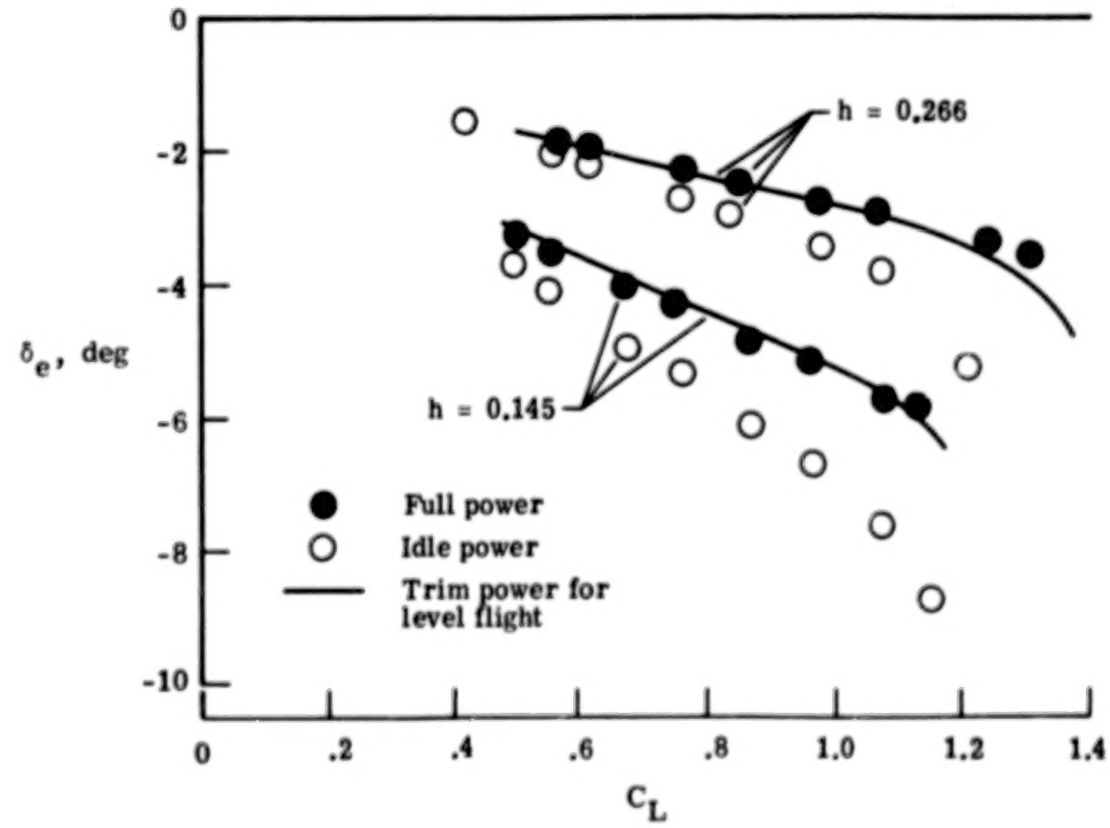

Figure 15.- Effect of power setting on relationship of measured elevator deflection to lift coefficient.

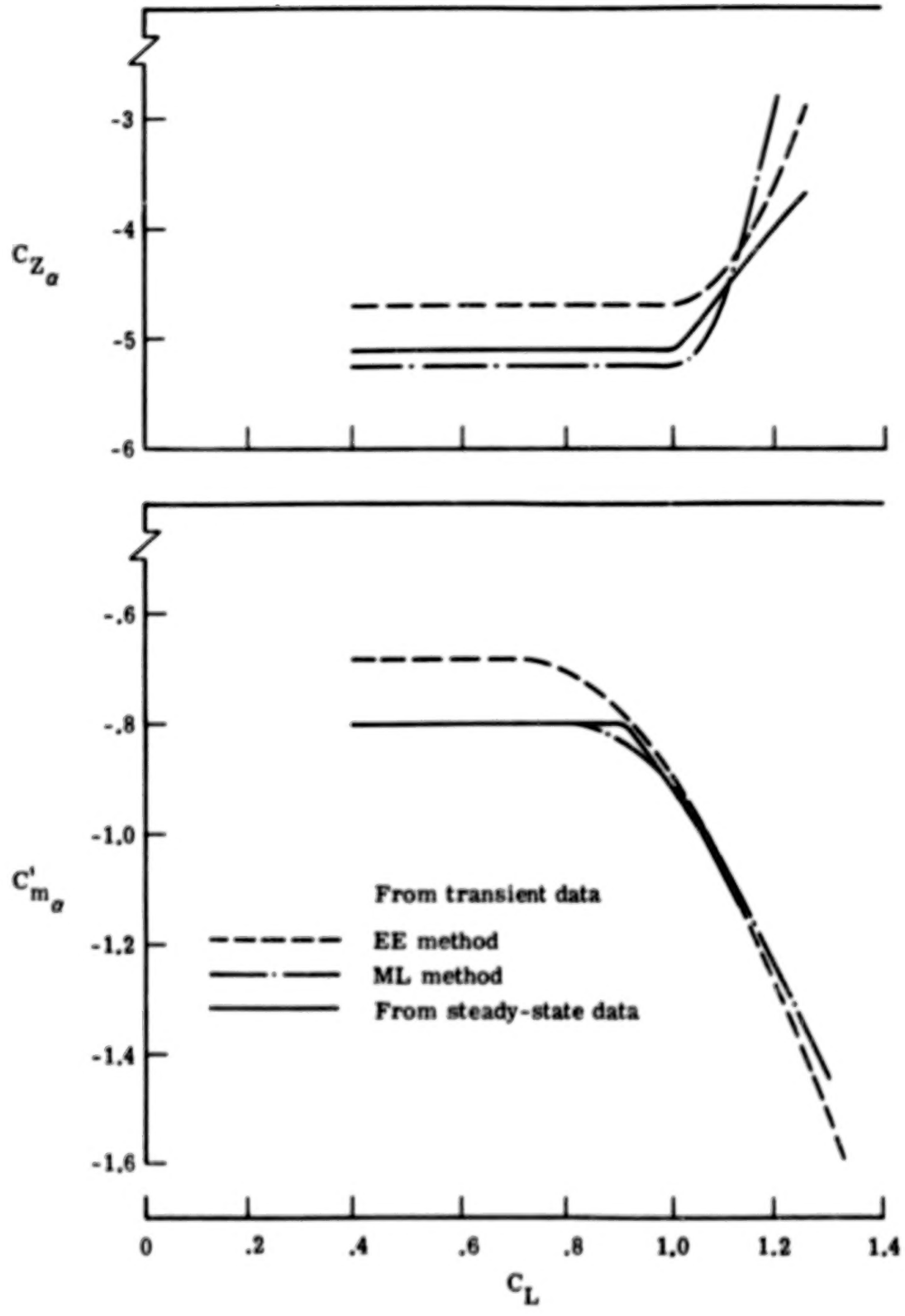

Figure 16.- Comparison of two parameters estimated from steady-state and transient flight data.

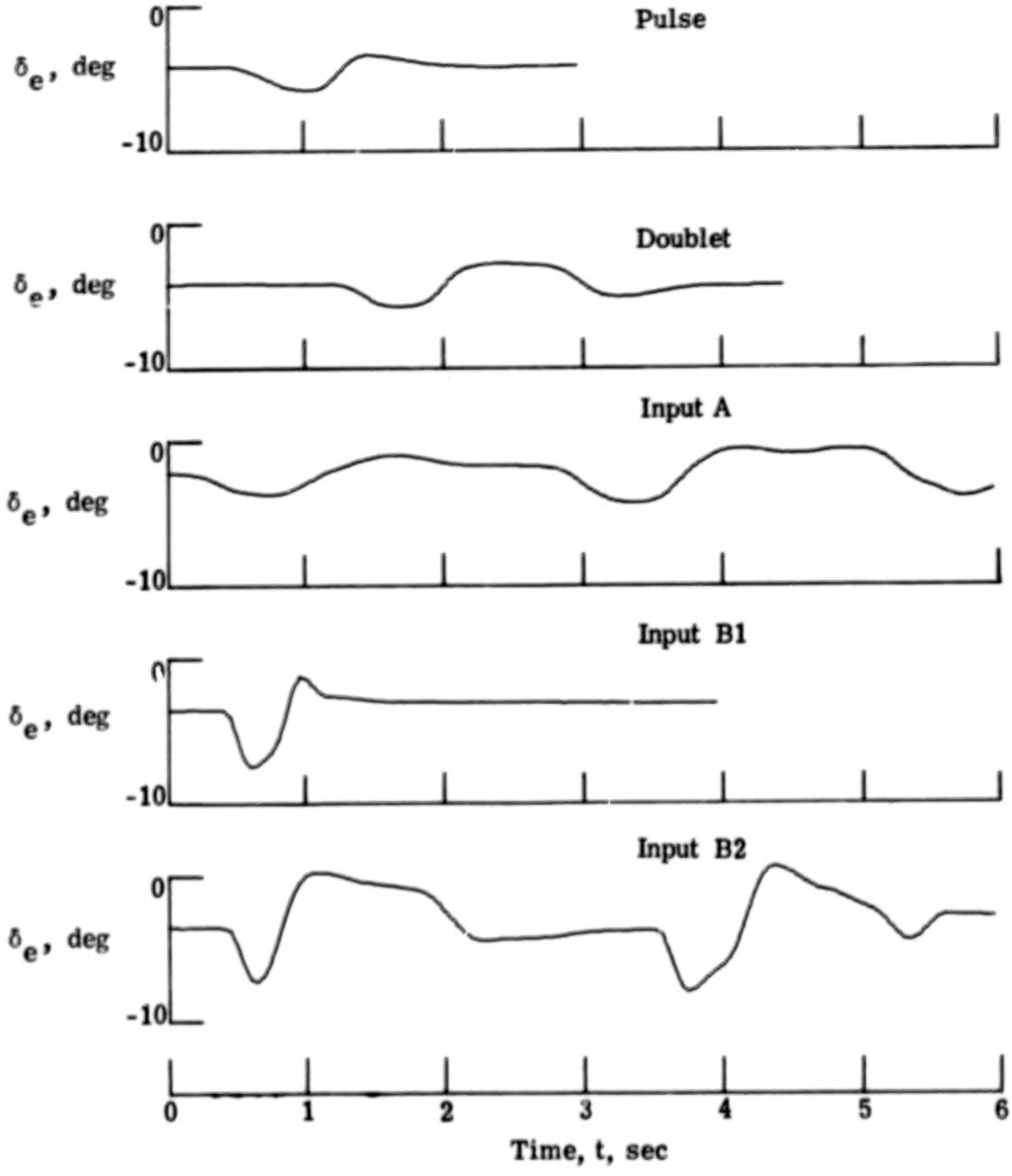

Figure 17.- Different forms of elevator deflection used in test.

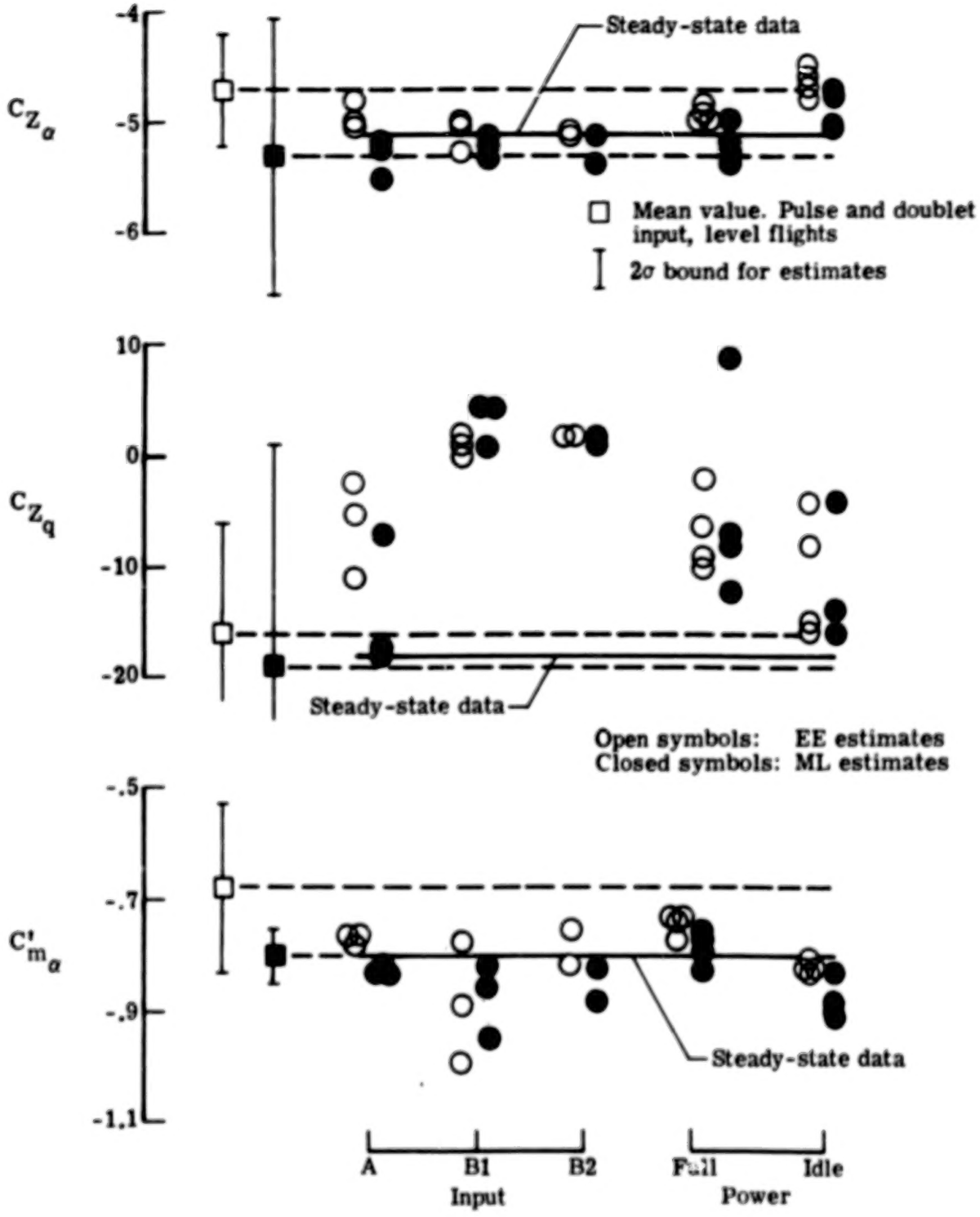

Figure 18.- Effect of different input forms and power settings on estimated longitudinal parameters.

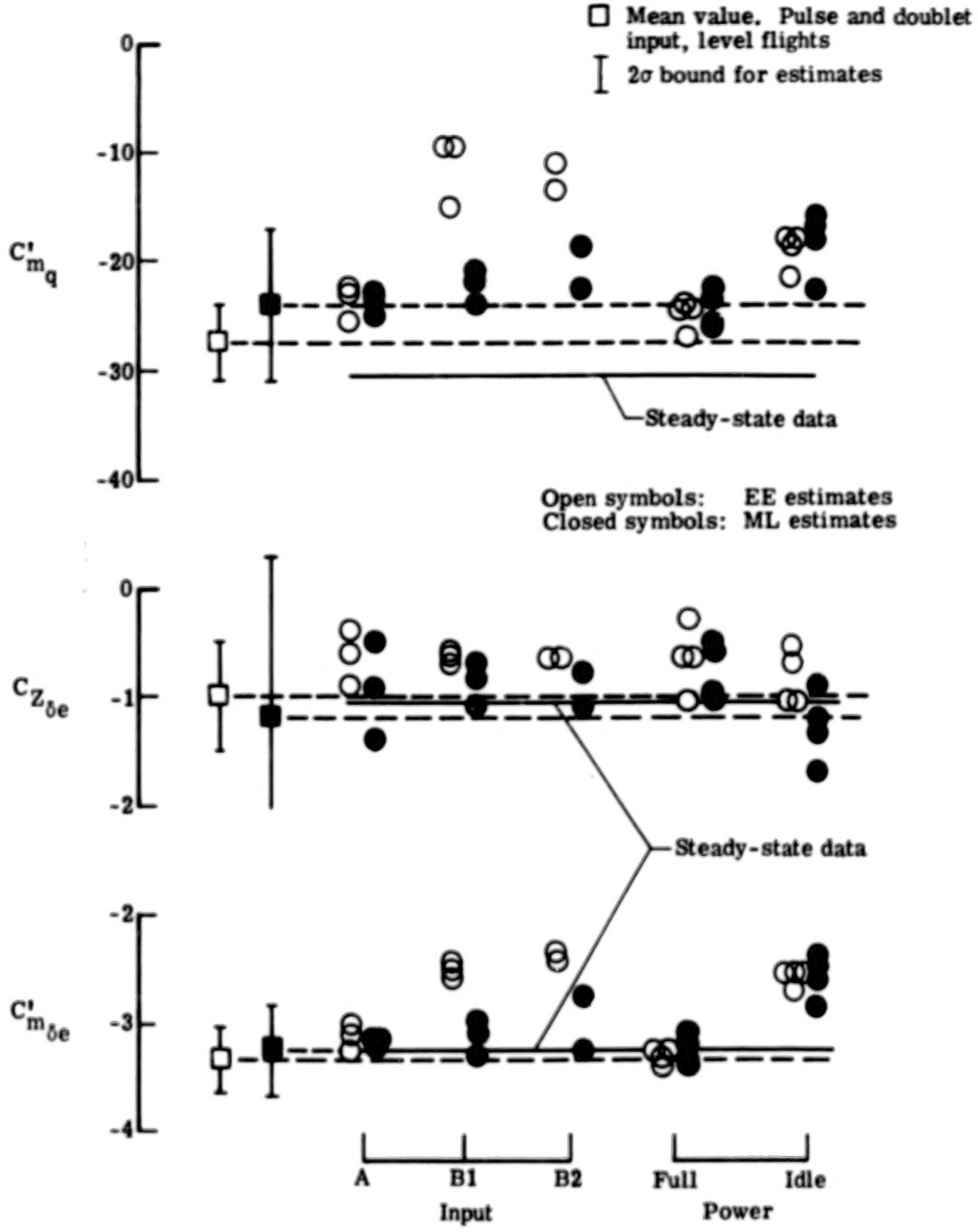

Figure 18.- Concluded.

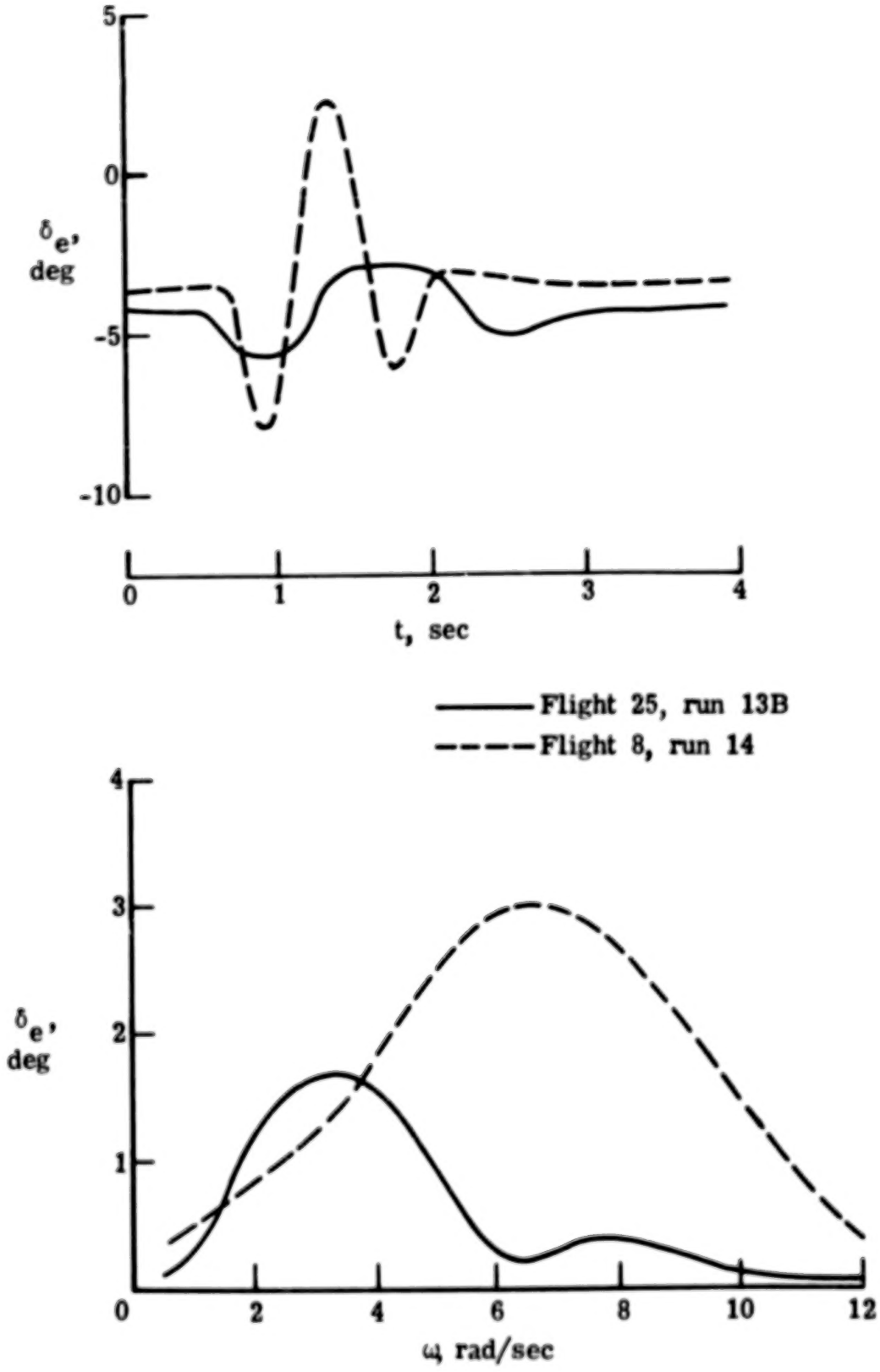

Figure 19.- Two input forms and their harmonic contents.

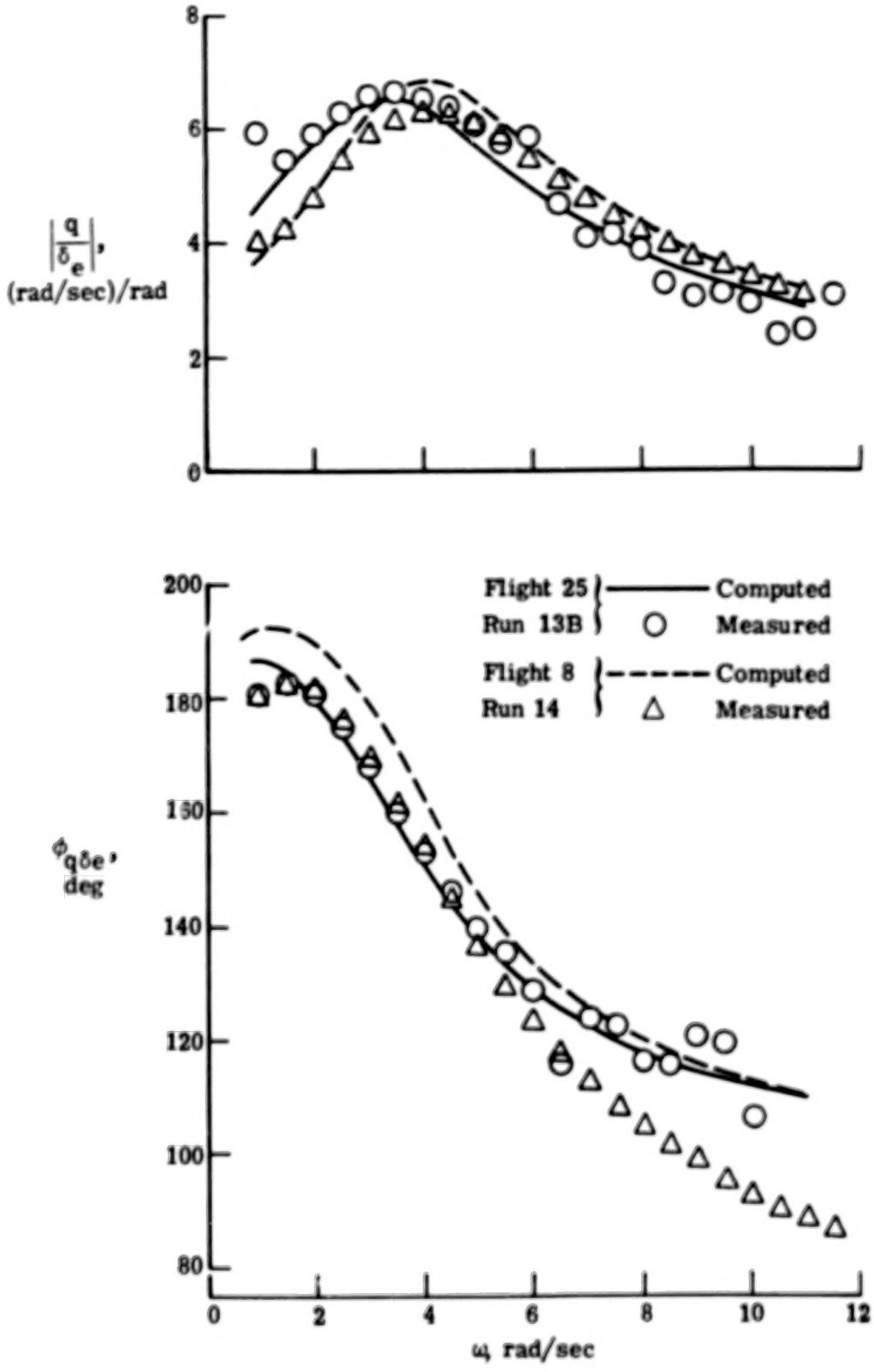

Figure 20.- Comparison of measured frequency response curves for two different inputs with those computed by using parameters obtained by maximum likelihood method in time domain.

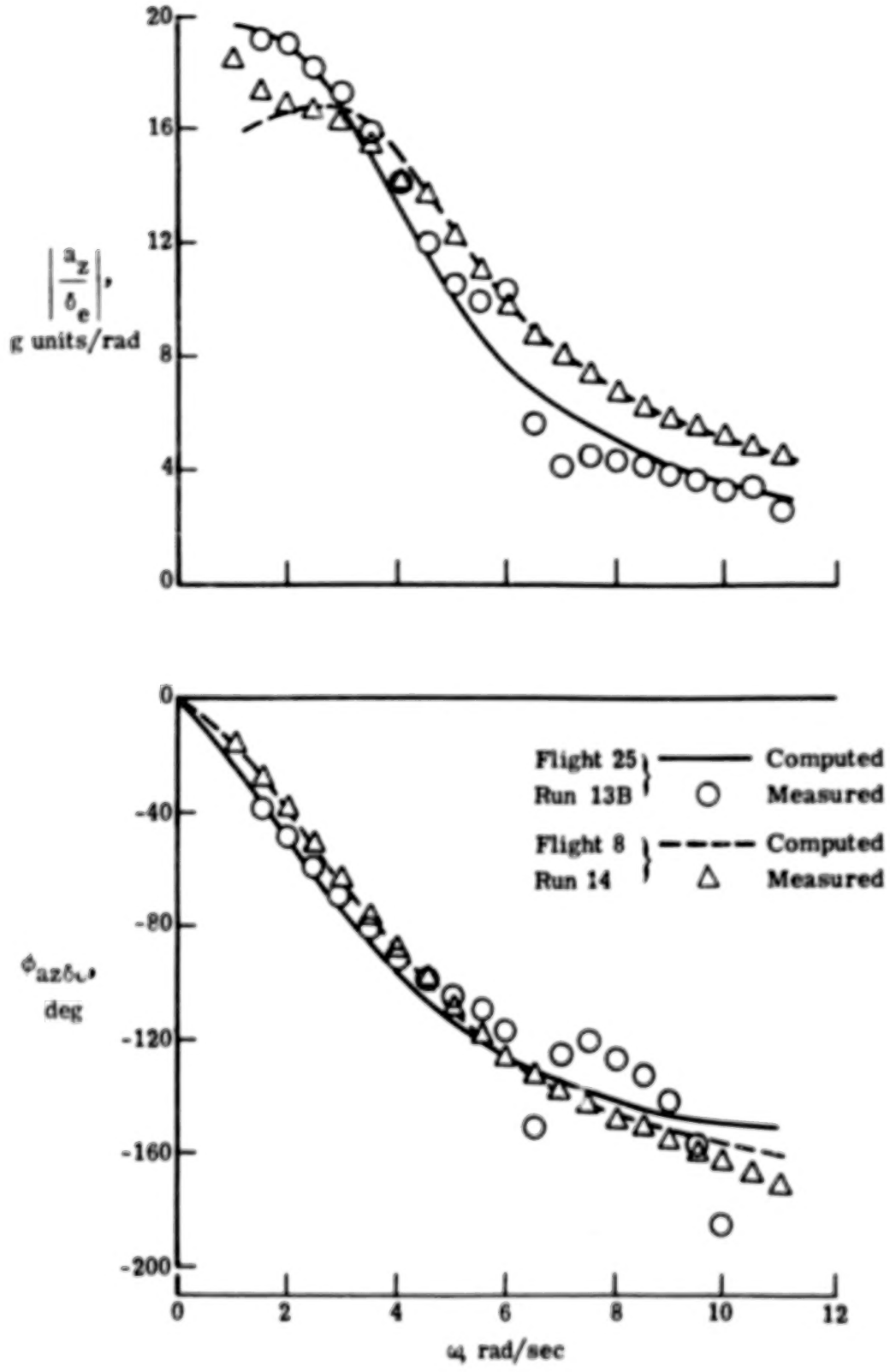

Figure 20.- Concluded.

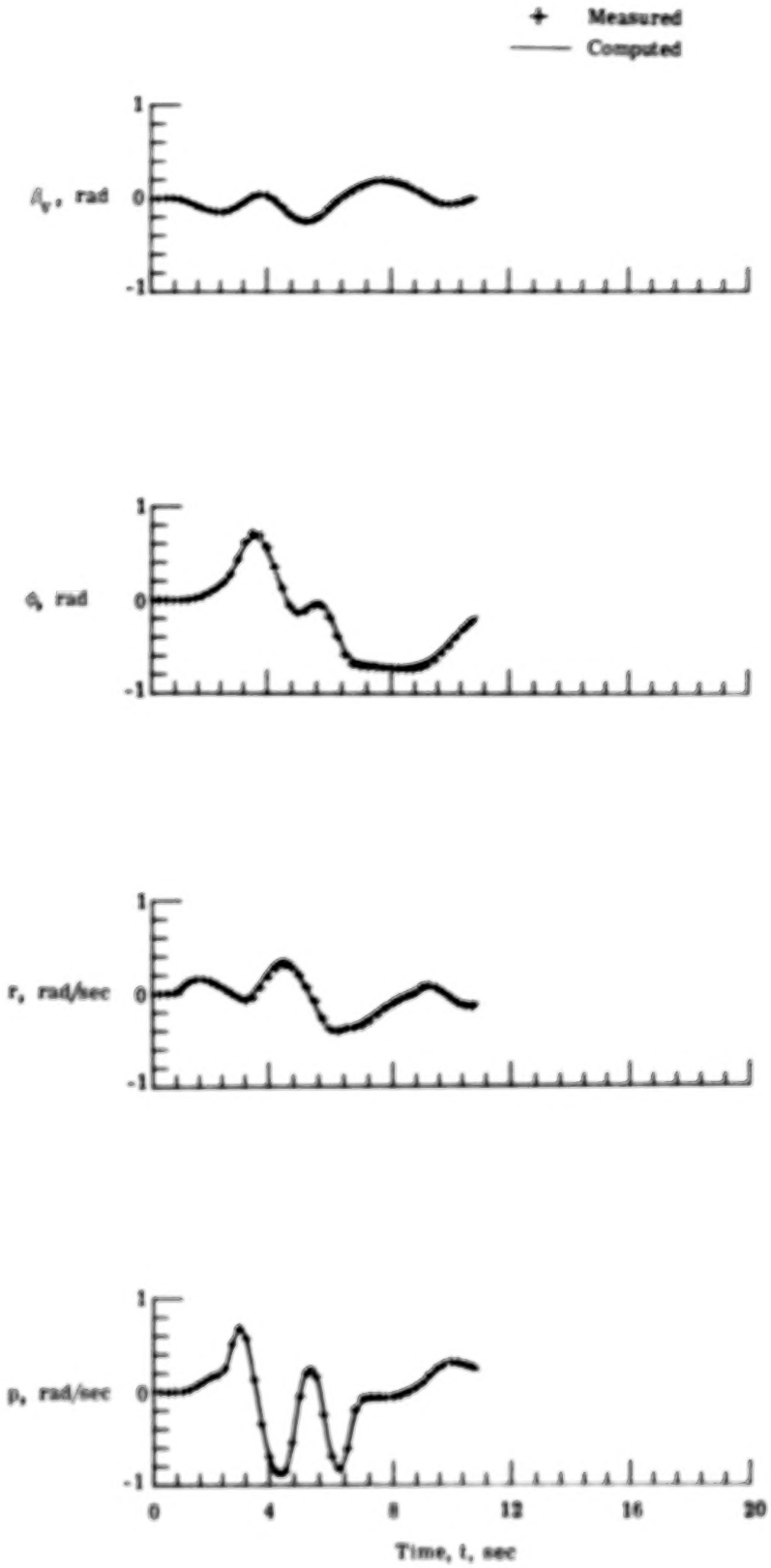

Figure 21.- Measured lateral flight data time histories and those computed by using parameters obtained by equation error method. Flight 21, run 26.

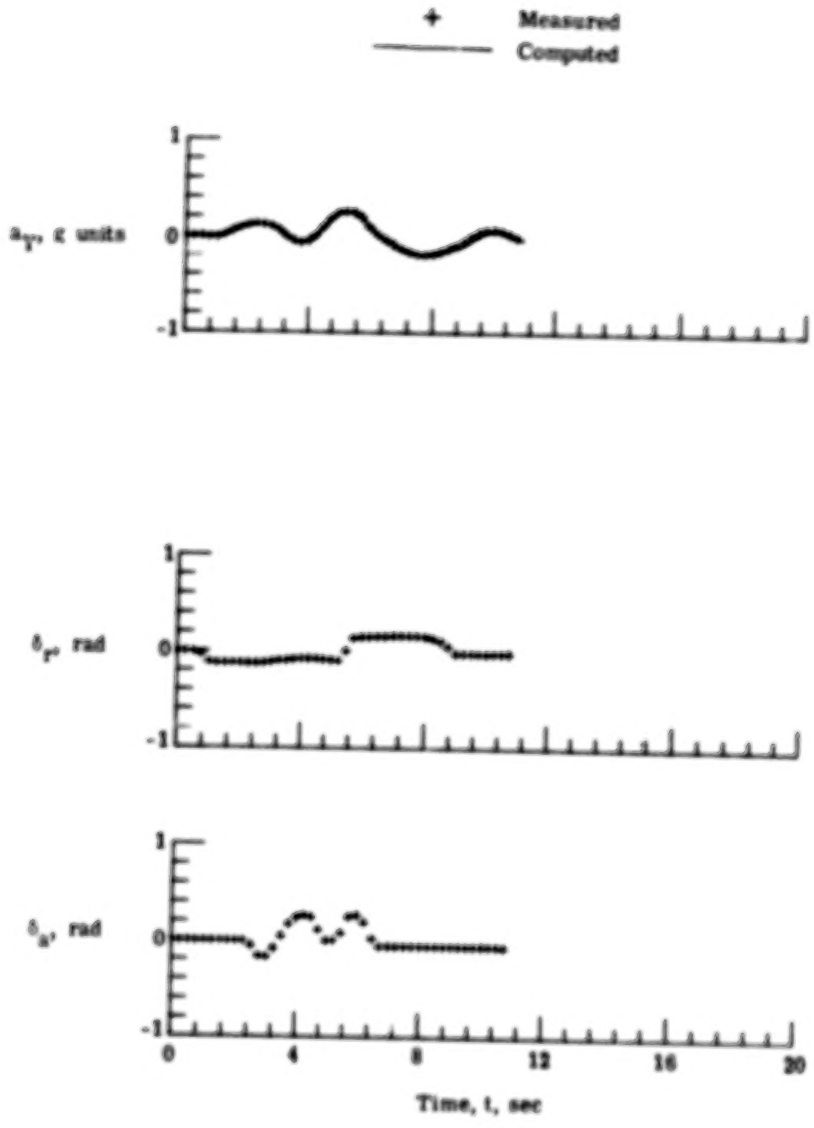

Figure 21.- Concluded.

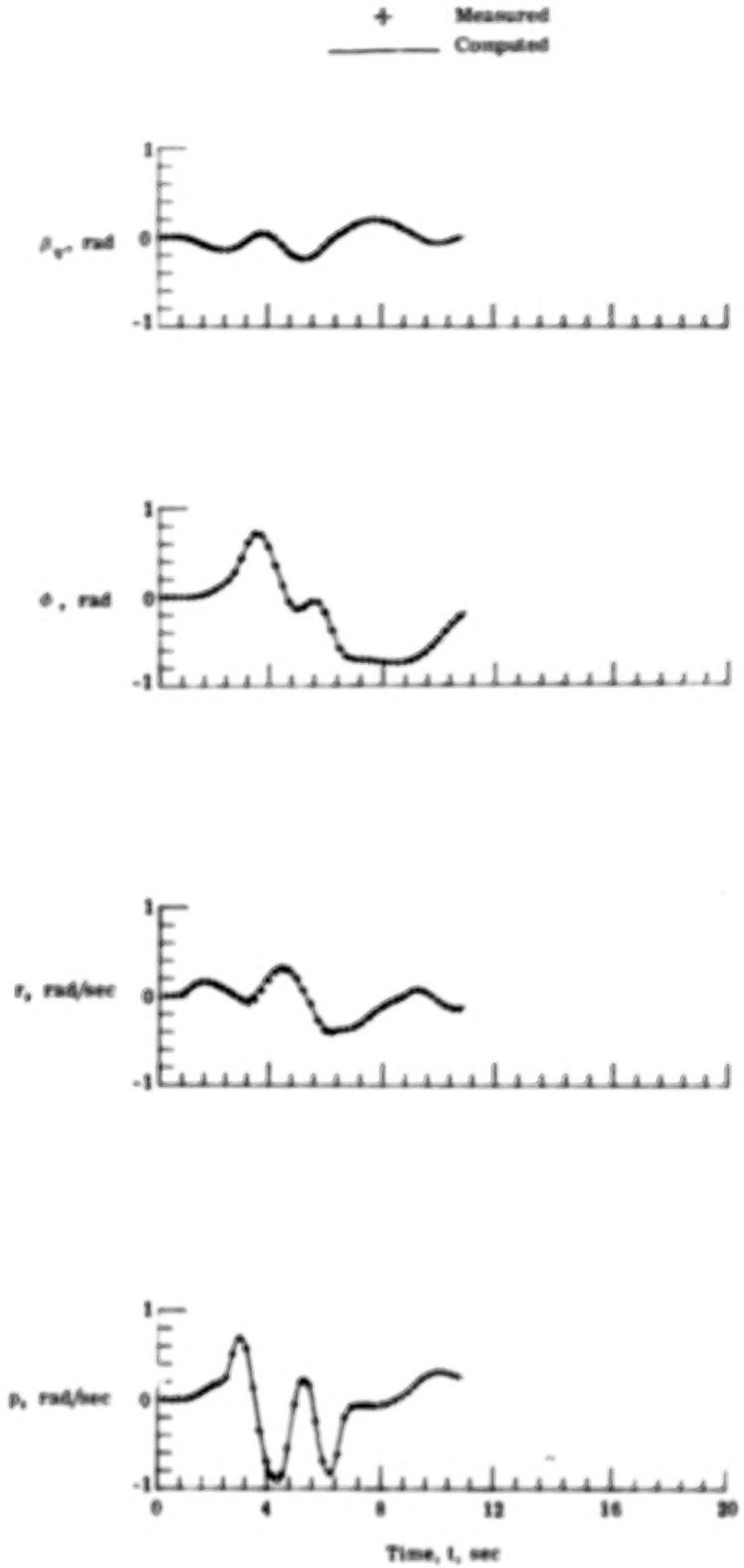

Figure 22.- Measured lateral flight data time histories and those computed by using parameters obtained by maximum likelihood method. Flight 21, run 26.

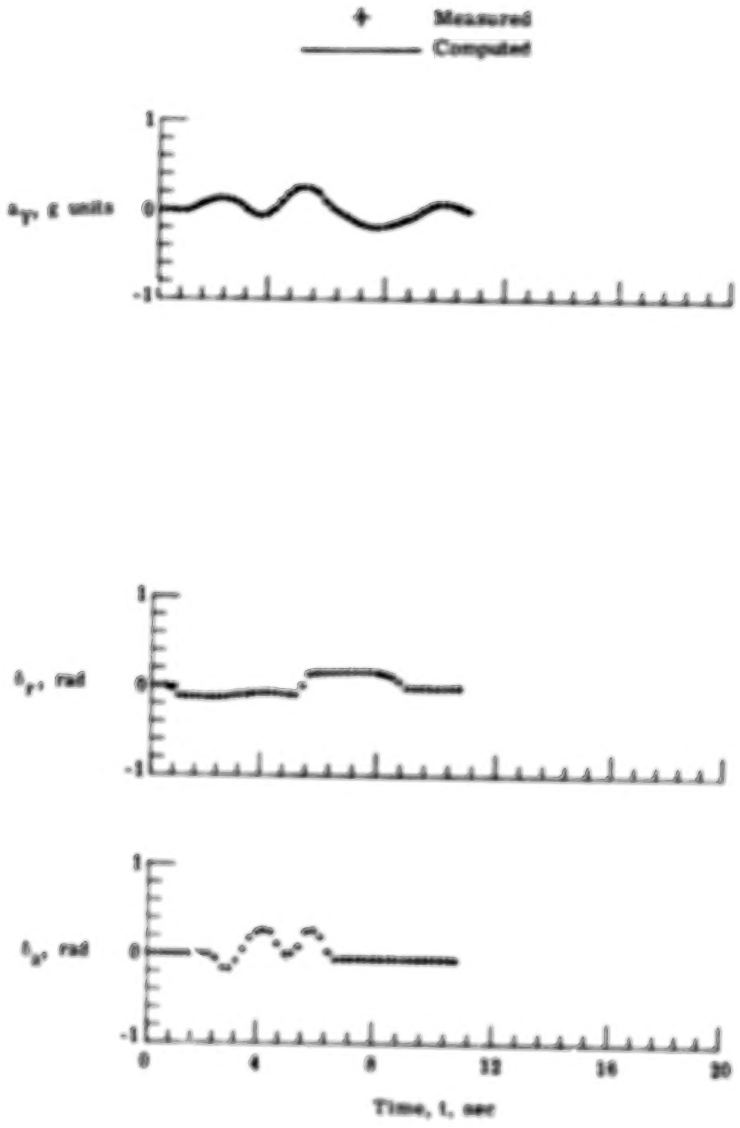

Figure 22.- Concluded.

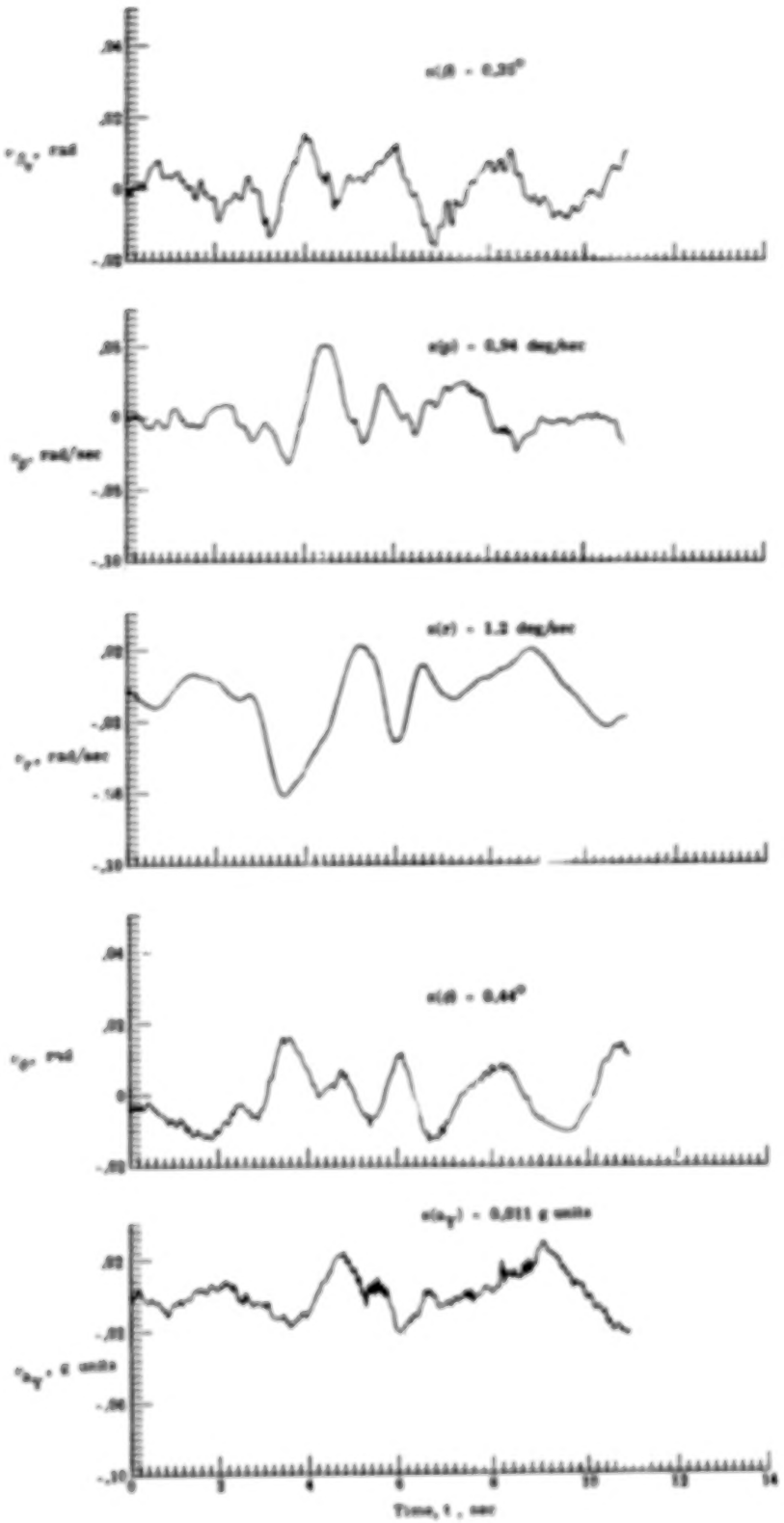

Figure 23.- Time histories and standard errors of residuals. Maximum likelihood method; flight 21, run 26.

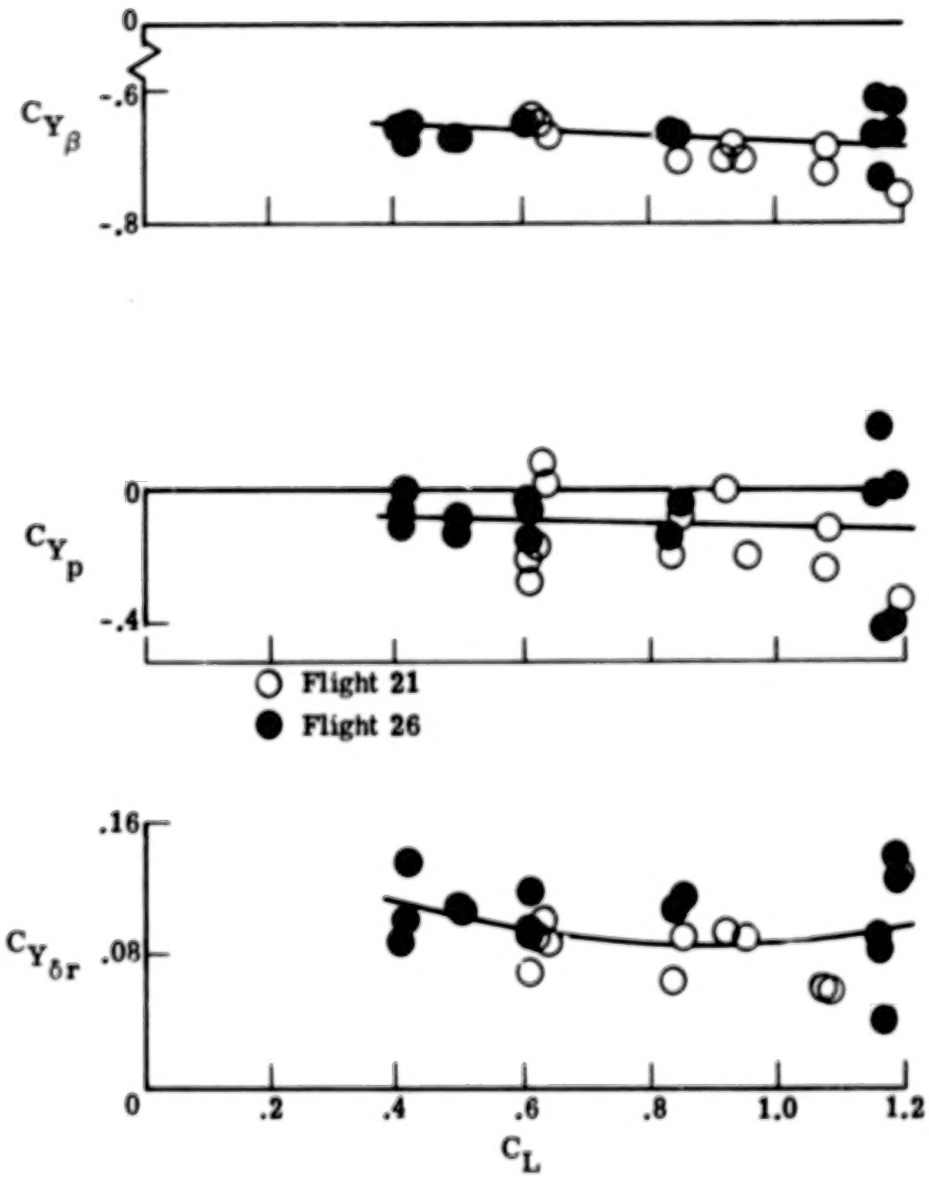

Figure 24.- Estimated lateral parameters from flight data. Maximum likelihood method.

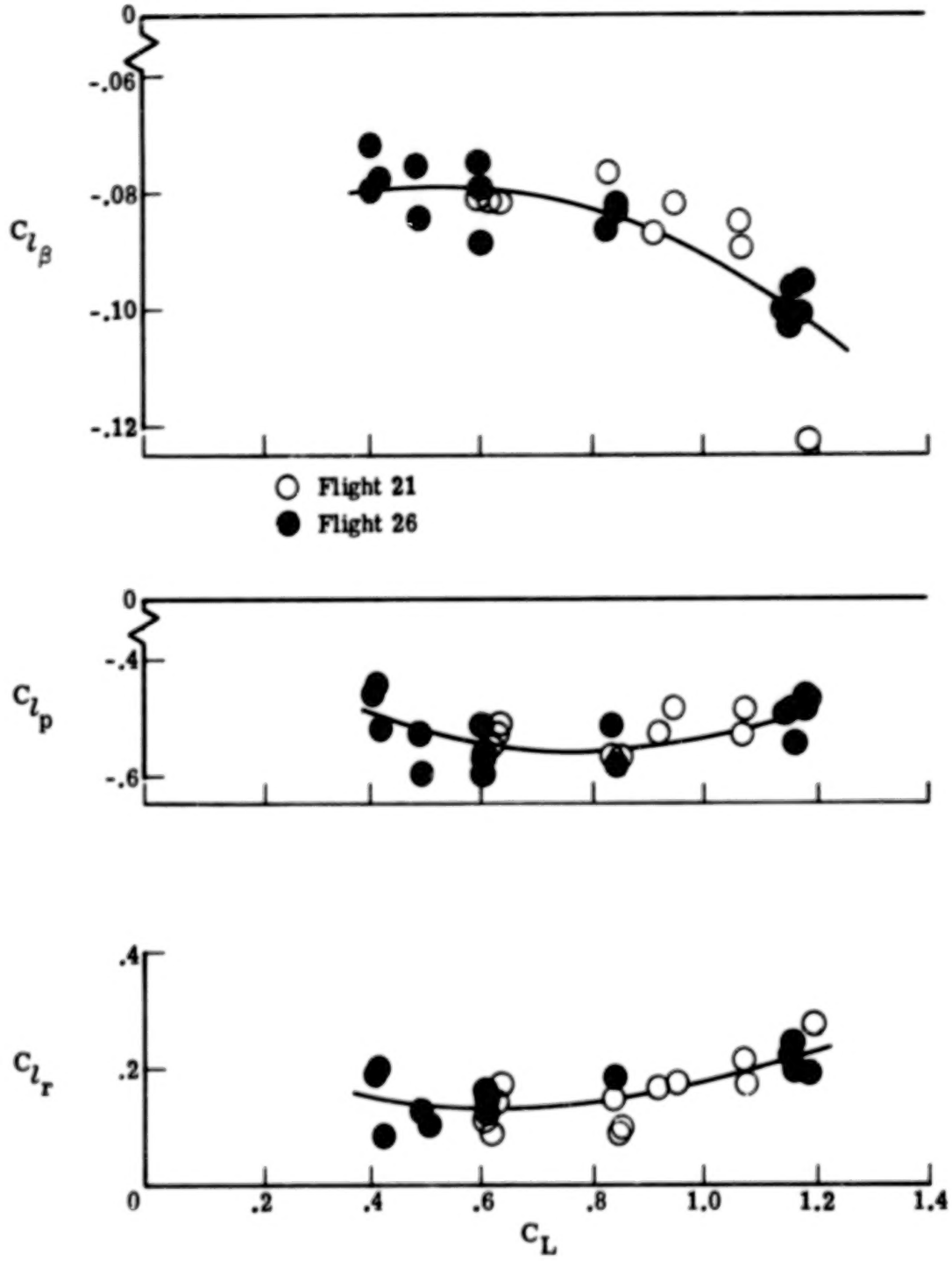

Figure 24.- Continued.

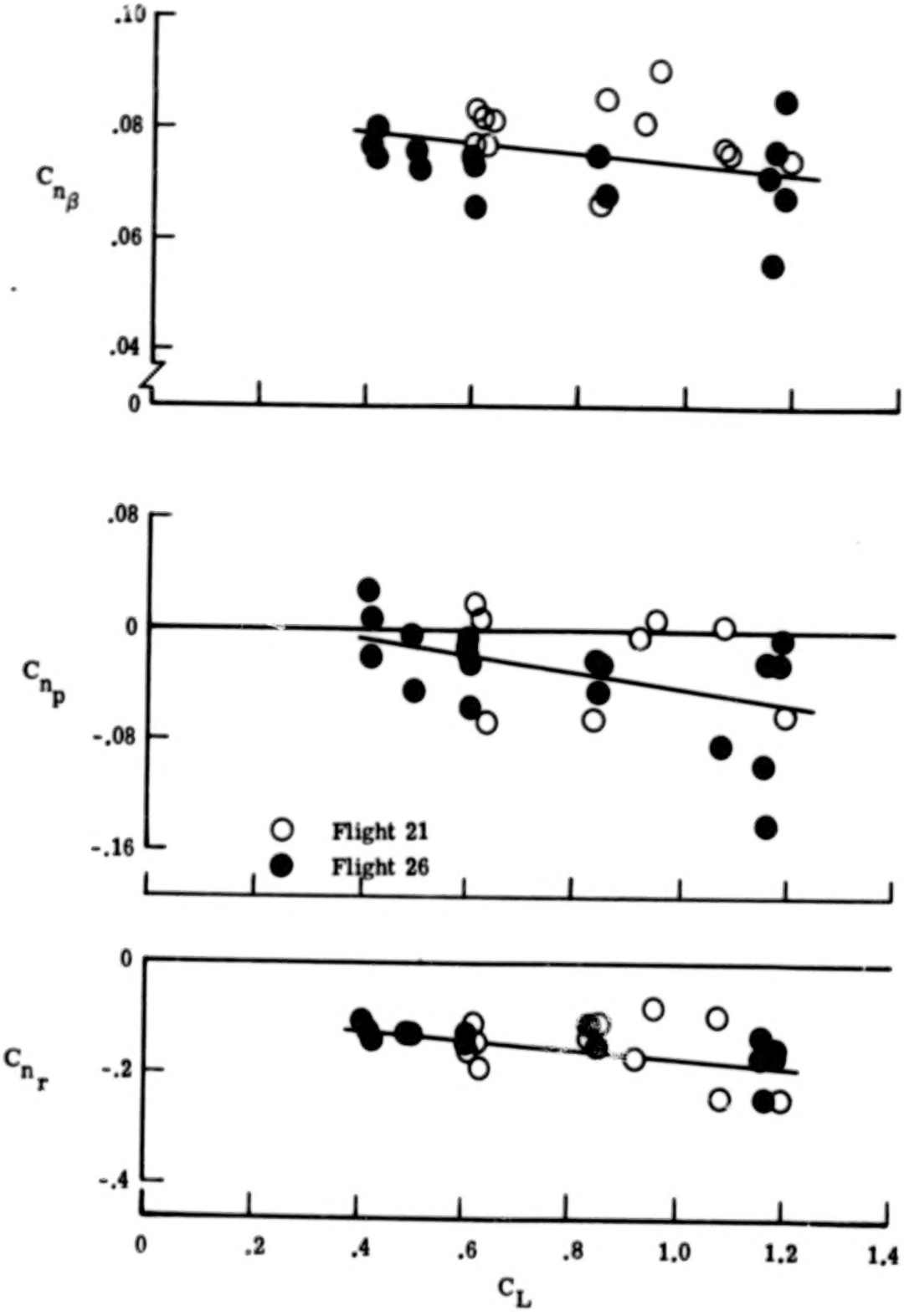

Figure 24.- Continued.

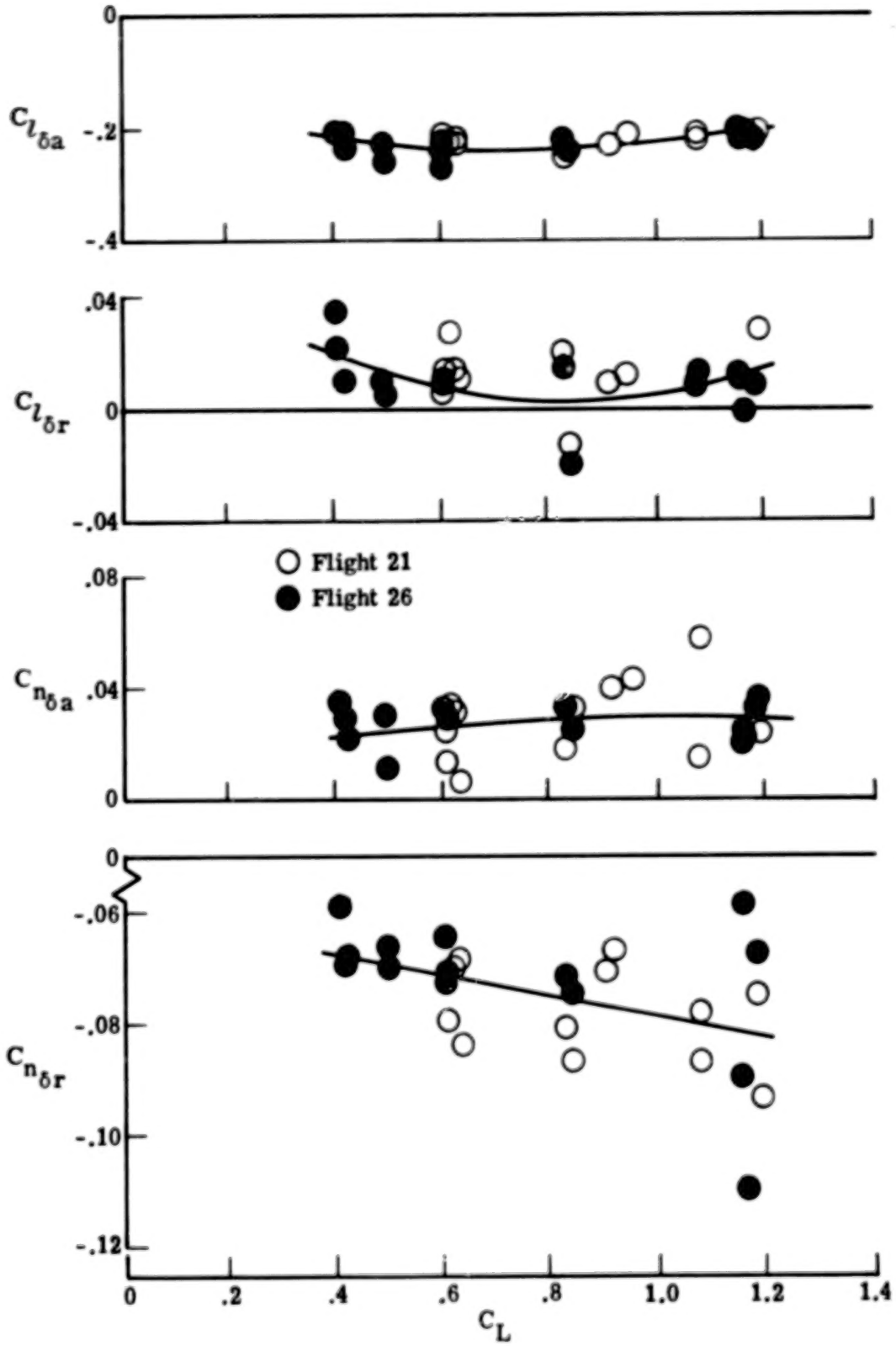

Figure 24.- Continued.

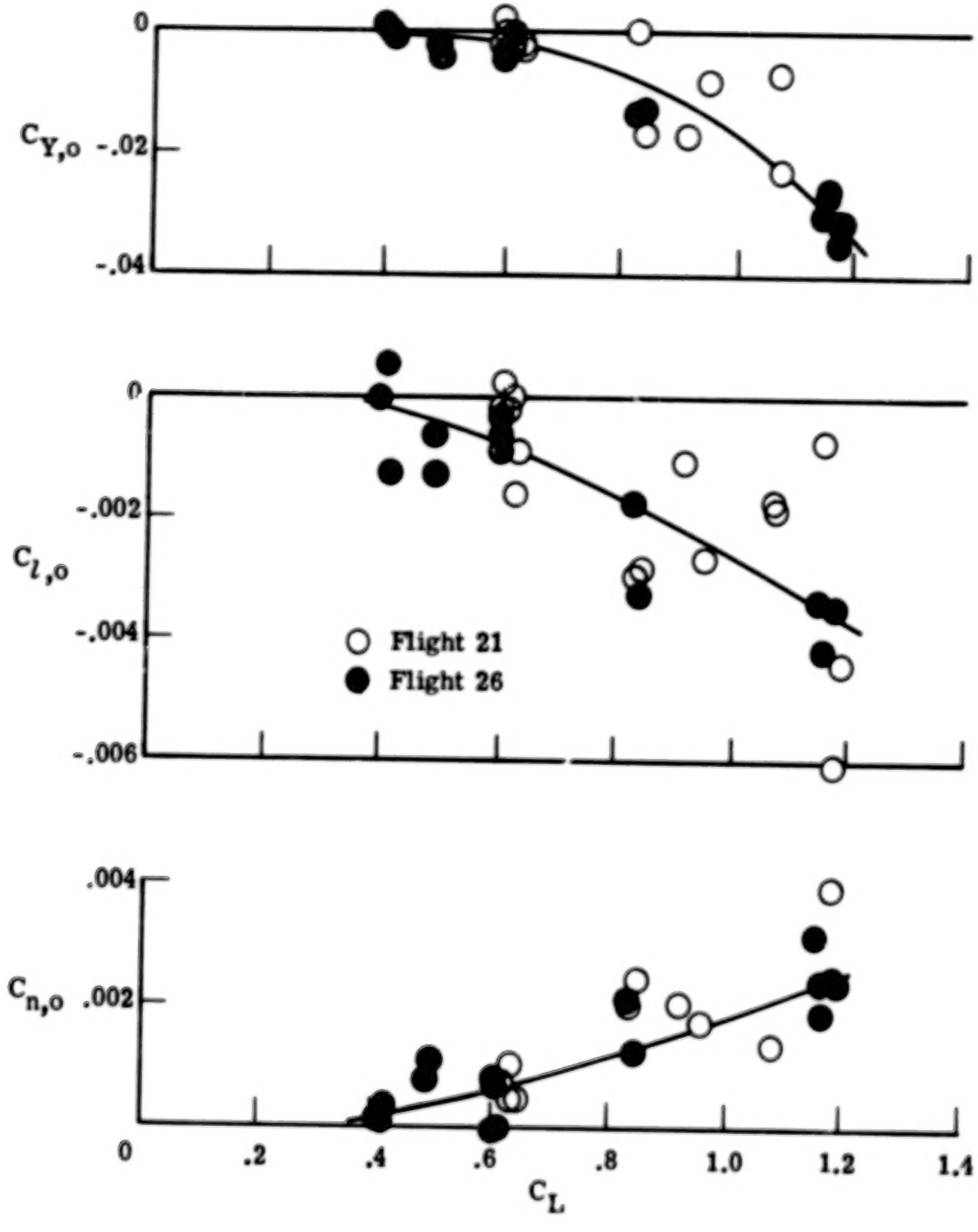

Figure 24.- Concluded.

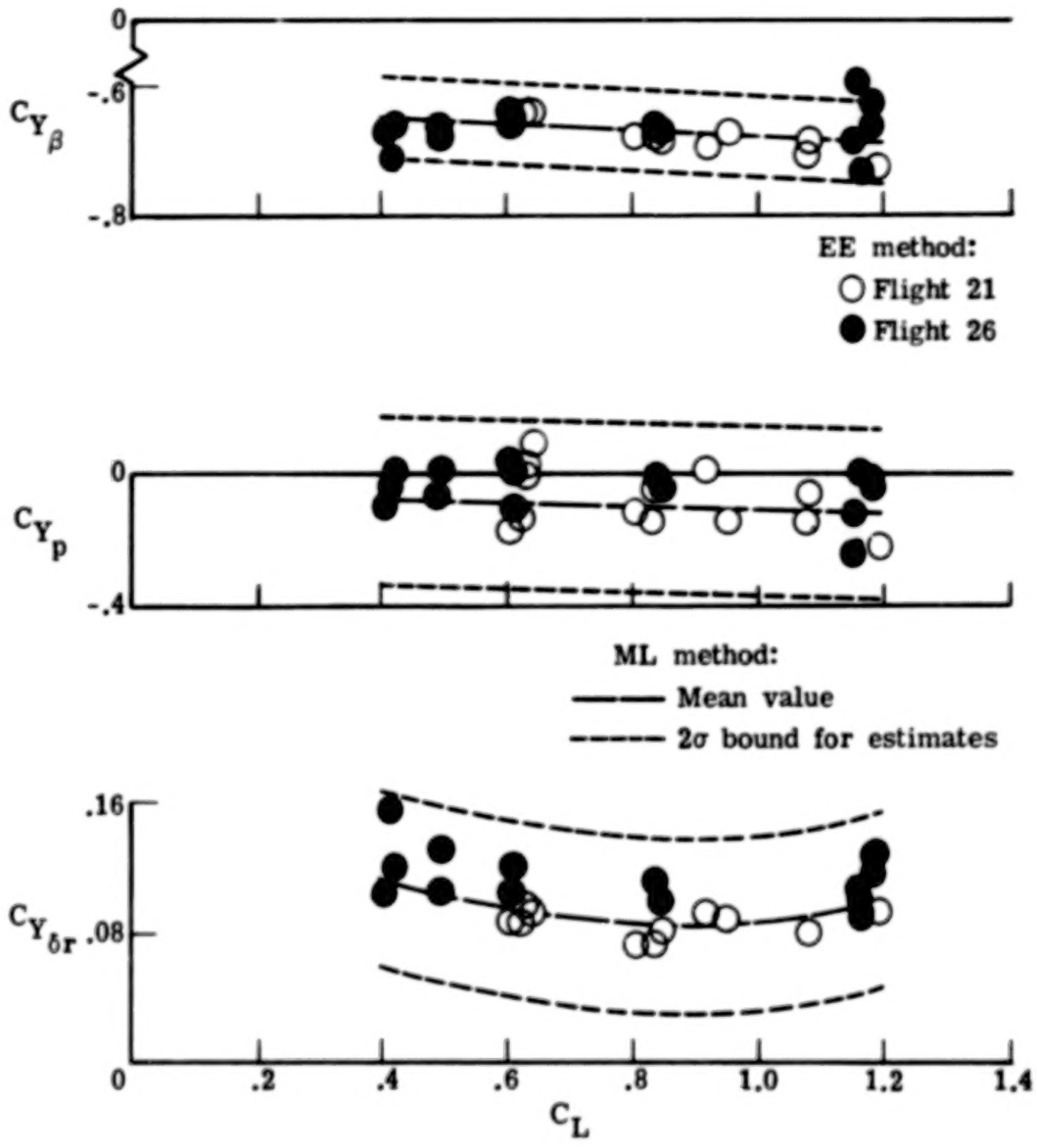

Figure 25.- Comparison of lateral parameter estimates obtained from flight data using equation error and maximum likelihood methods.

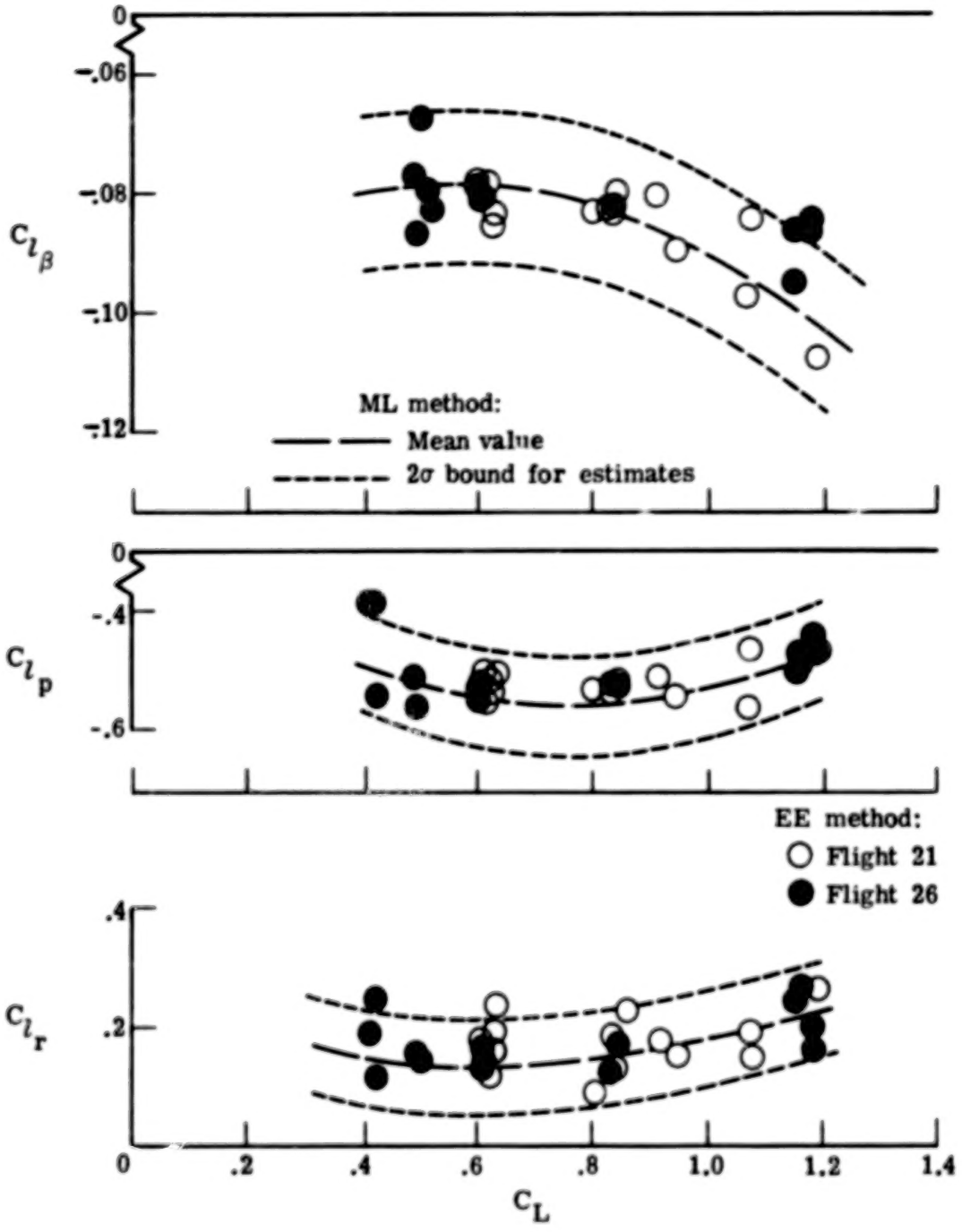

Figure 25.- Continued.

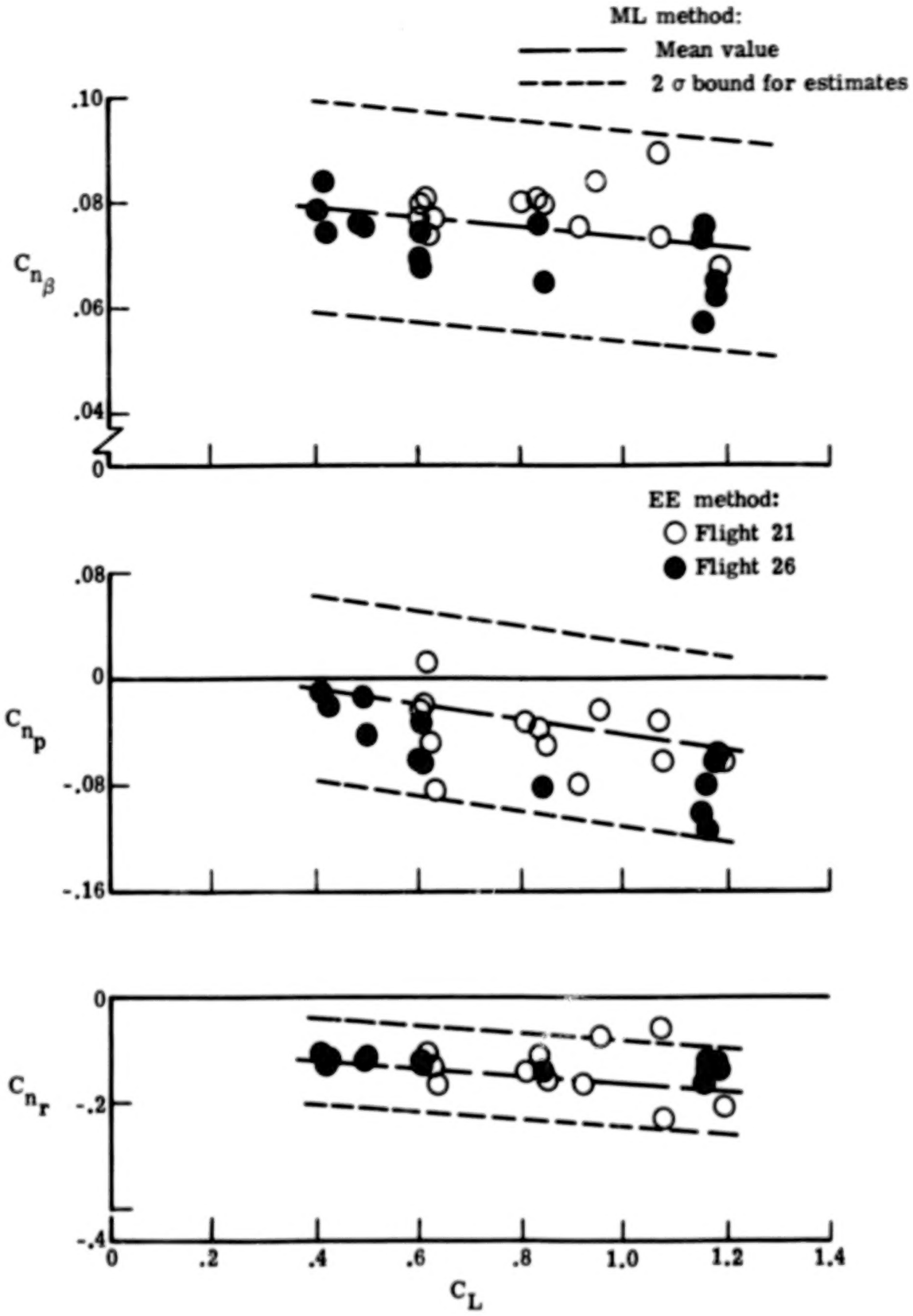

Figure 25.- Continued.

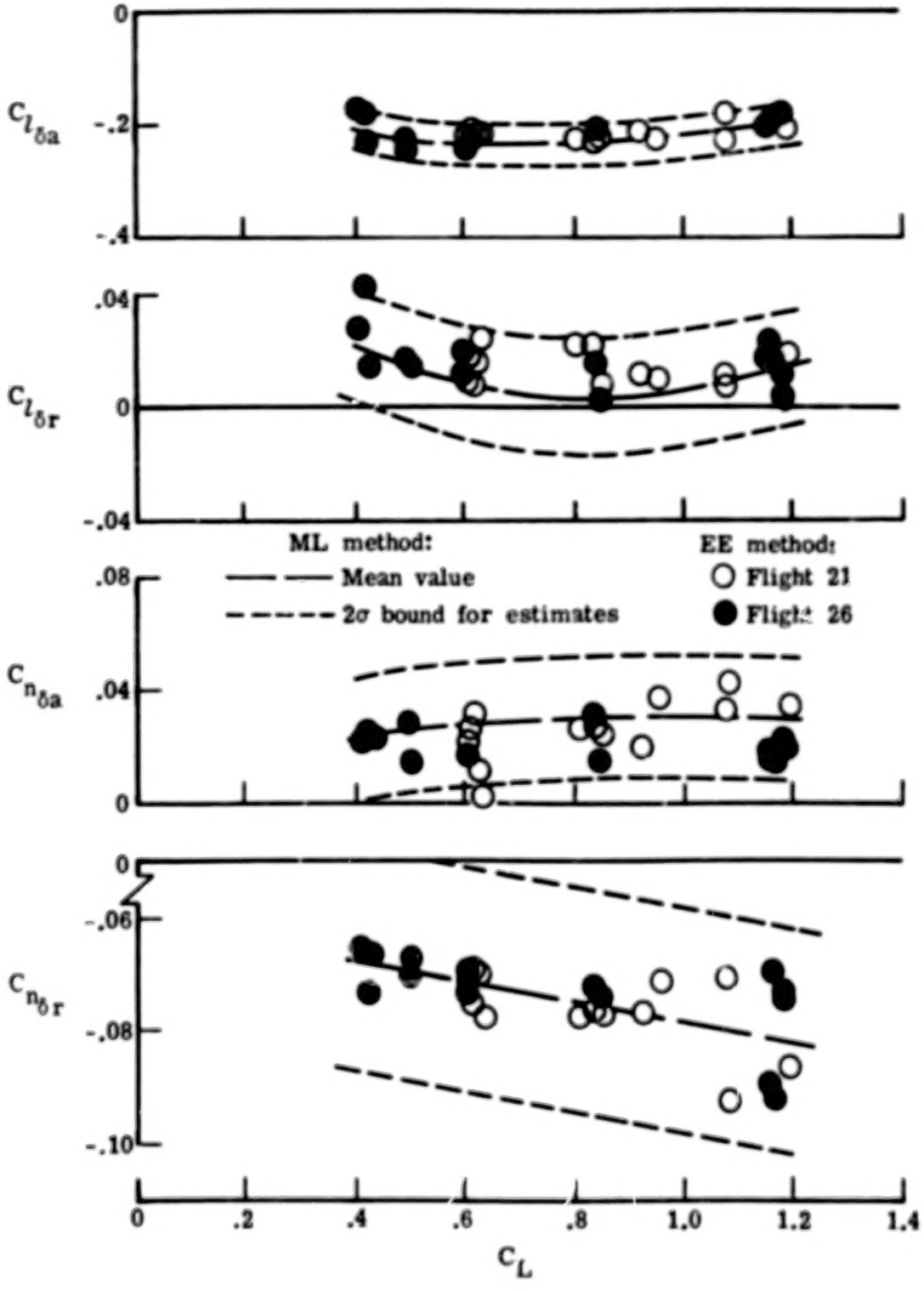

Figure 25.- Concluded.

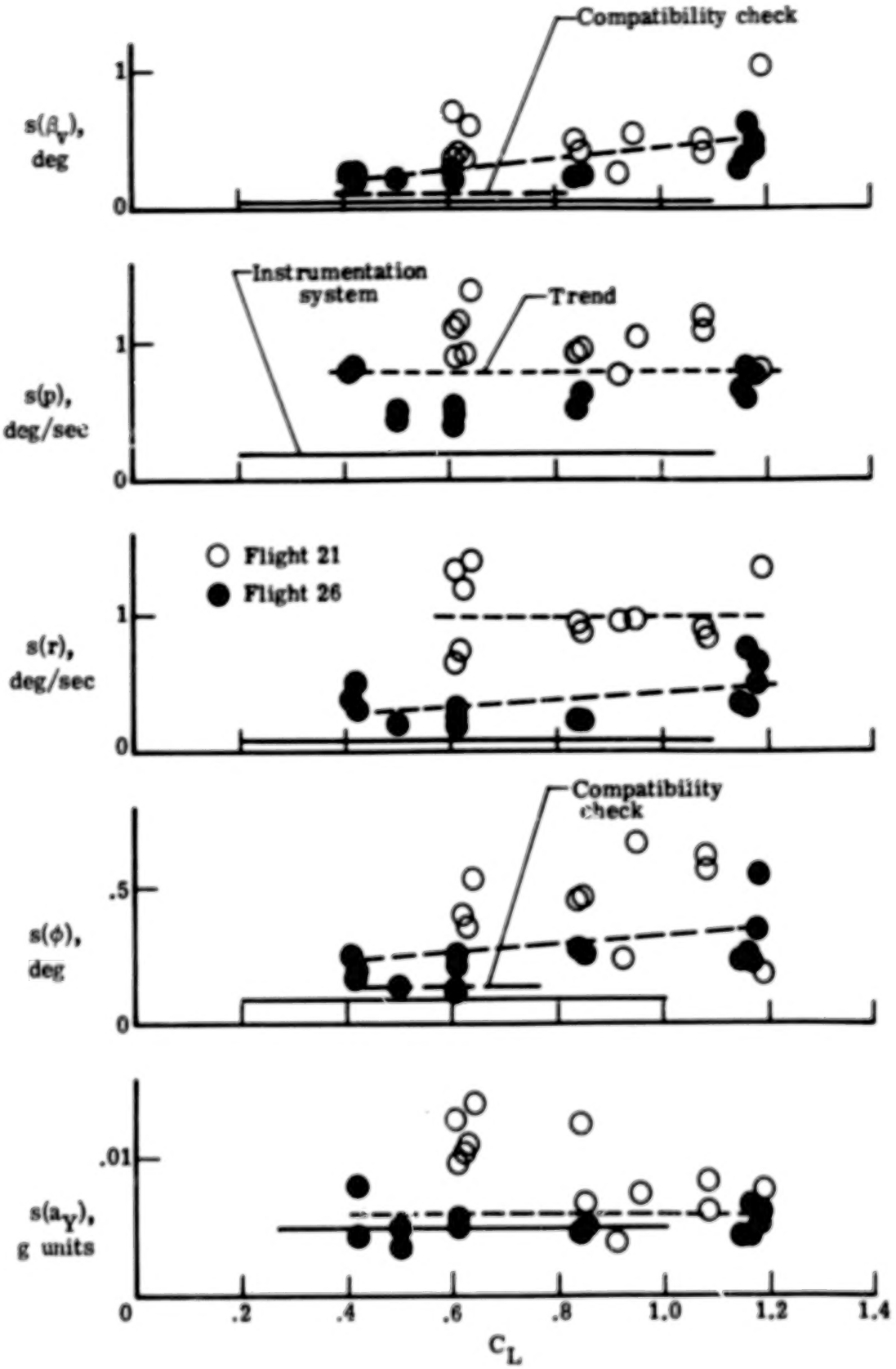

Figure 26.- Estimated standard errors of measurement noise. Lateral flight data.

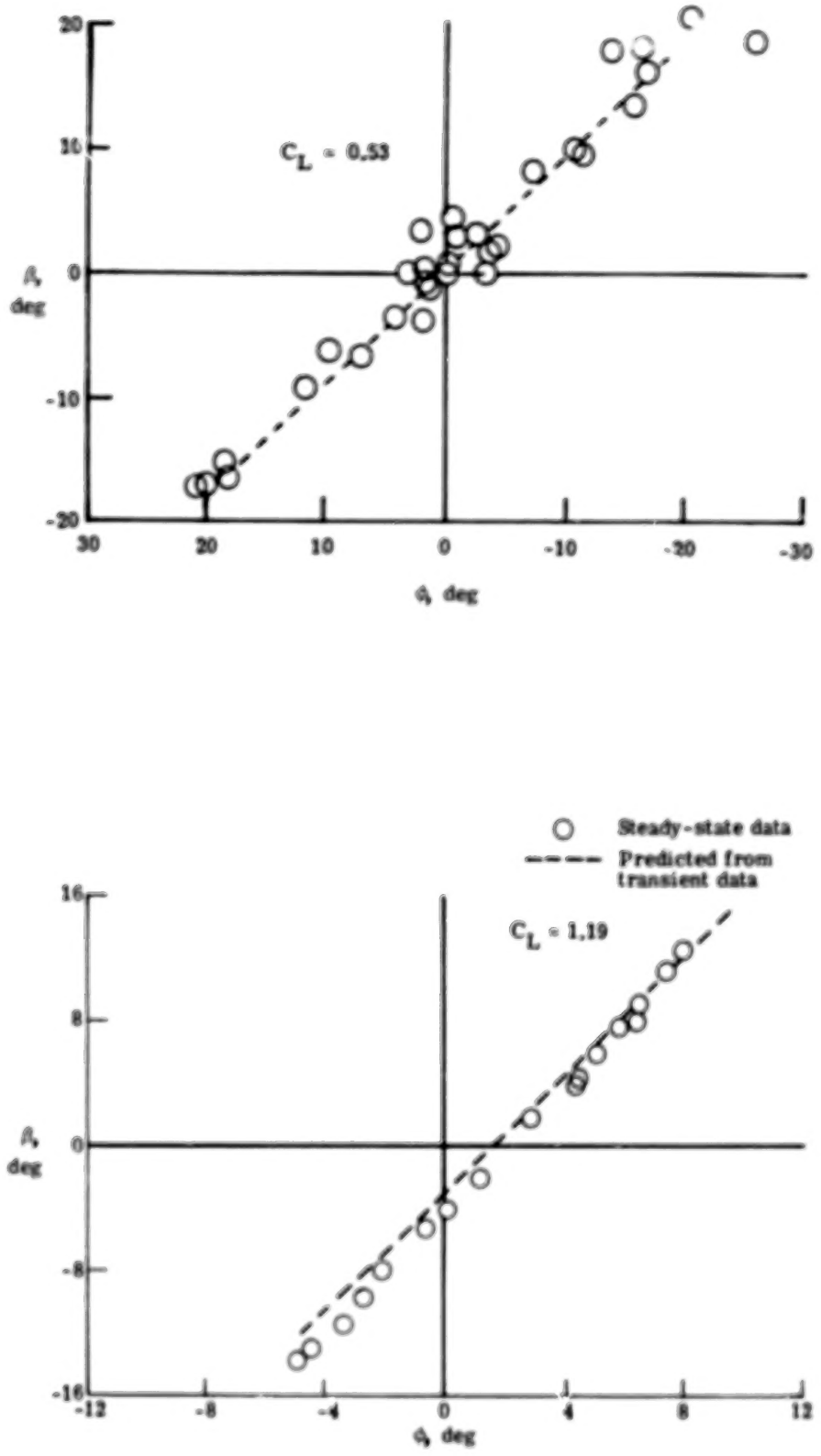

Figure 27.- Measured and predicted sideslip angles plotted against bank angle in nonsymmetric steady-state flights.

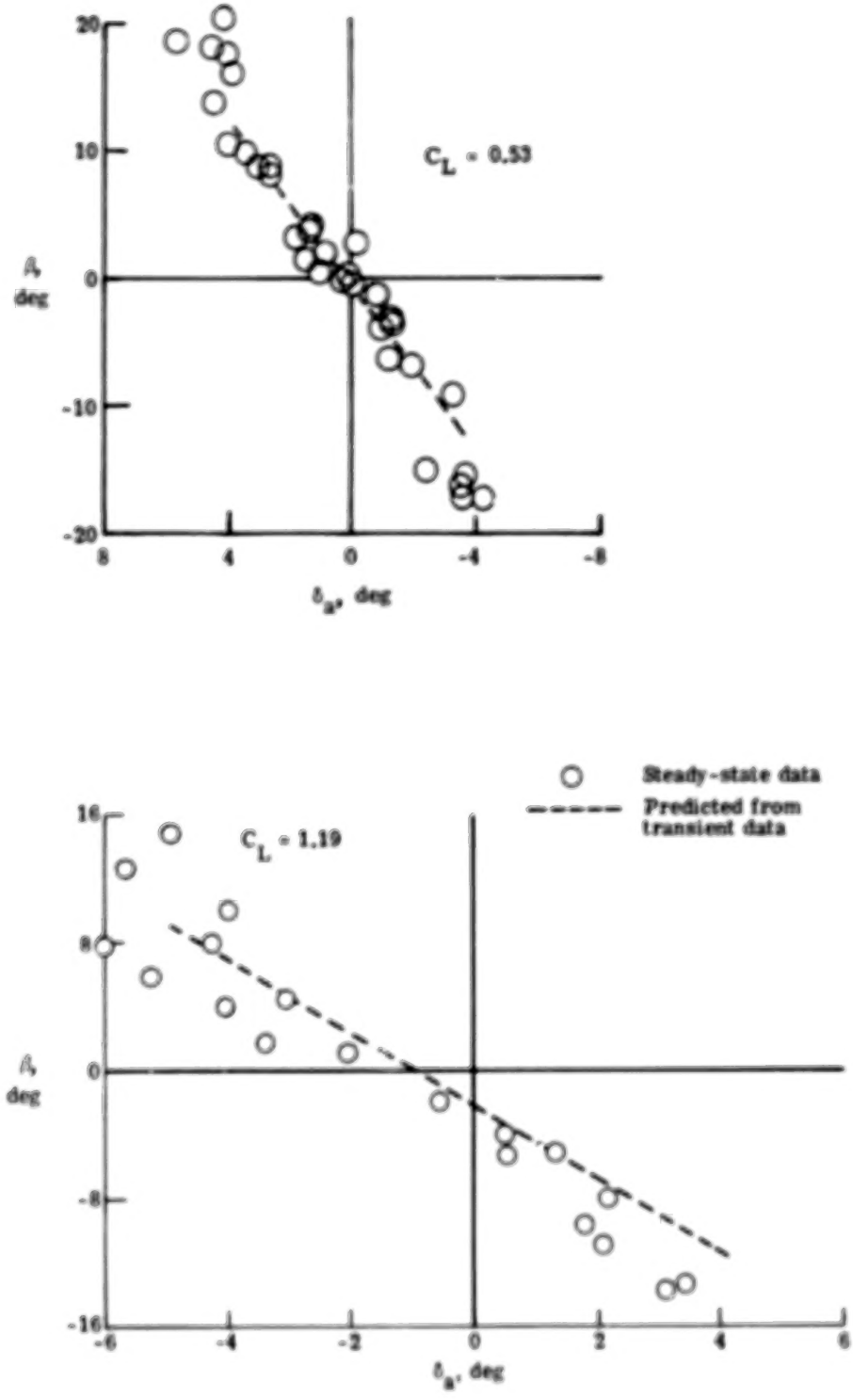

Figure 28.- Measured and predicted sideslip angle plotted against aileron deflection in nonsymmetric steady-state flights.

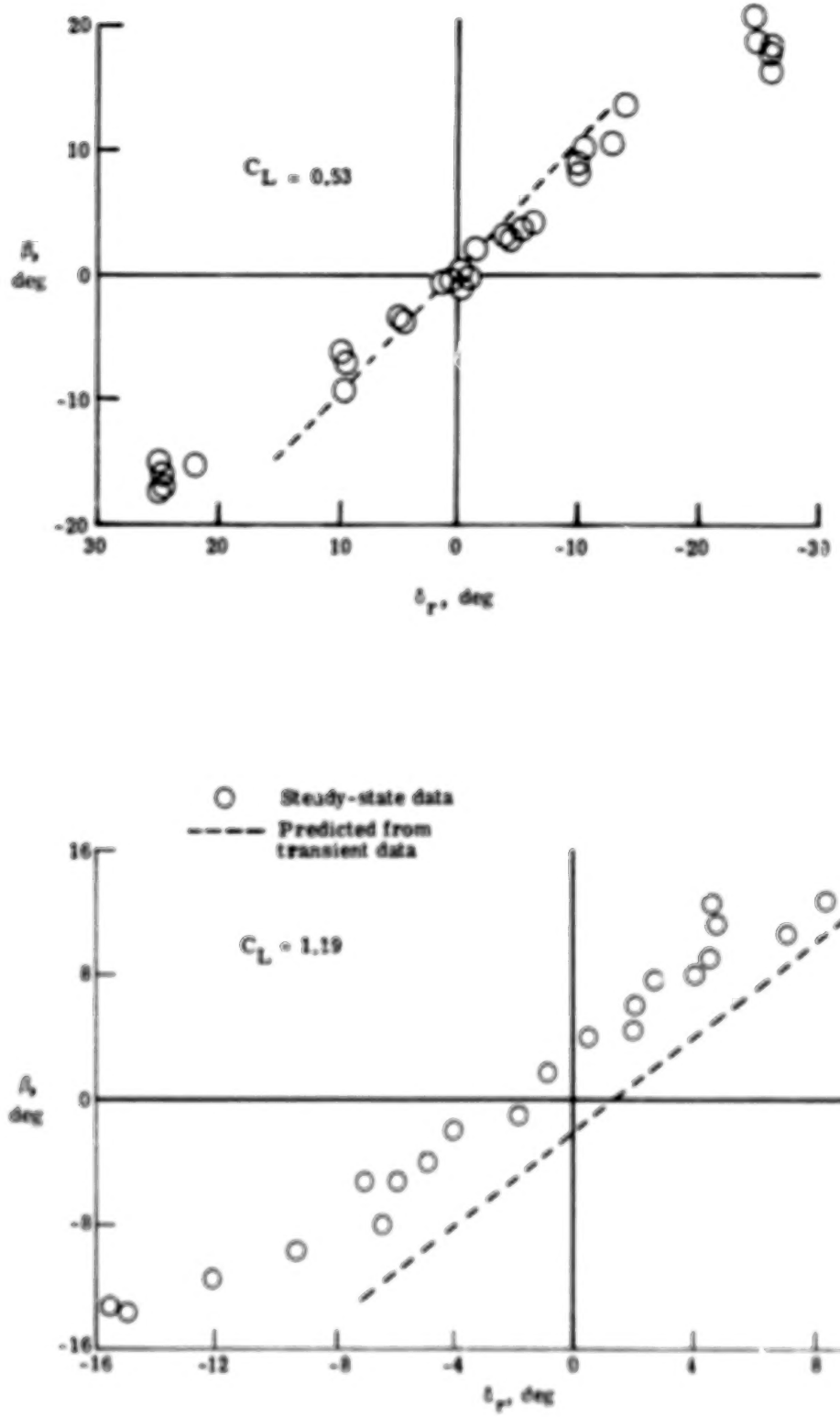

Figure 29.- Measured and predicted sideslip angle plotted against rudder deflection in nonsymmetric steady-state flights.

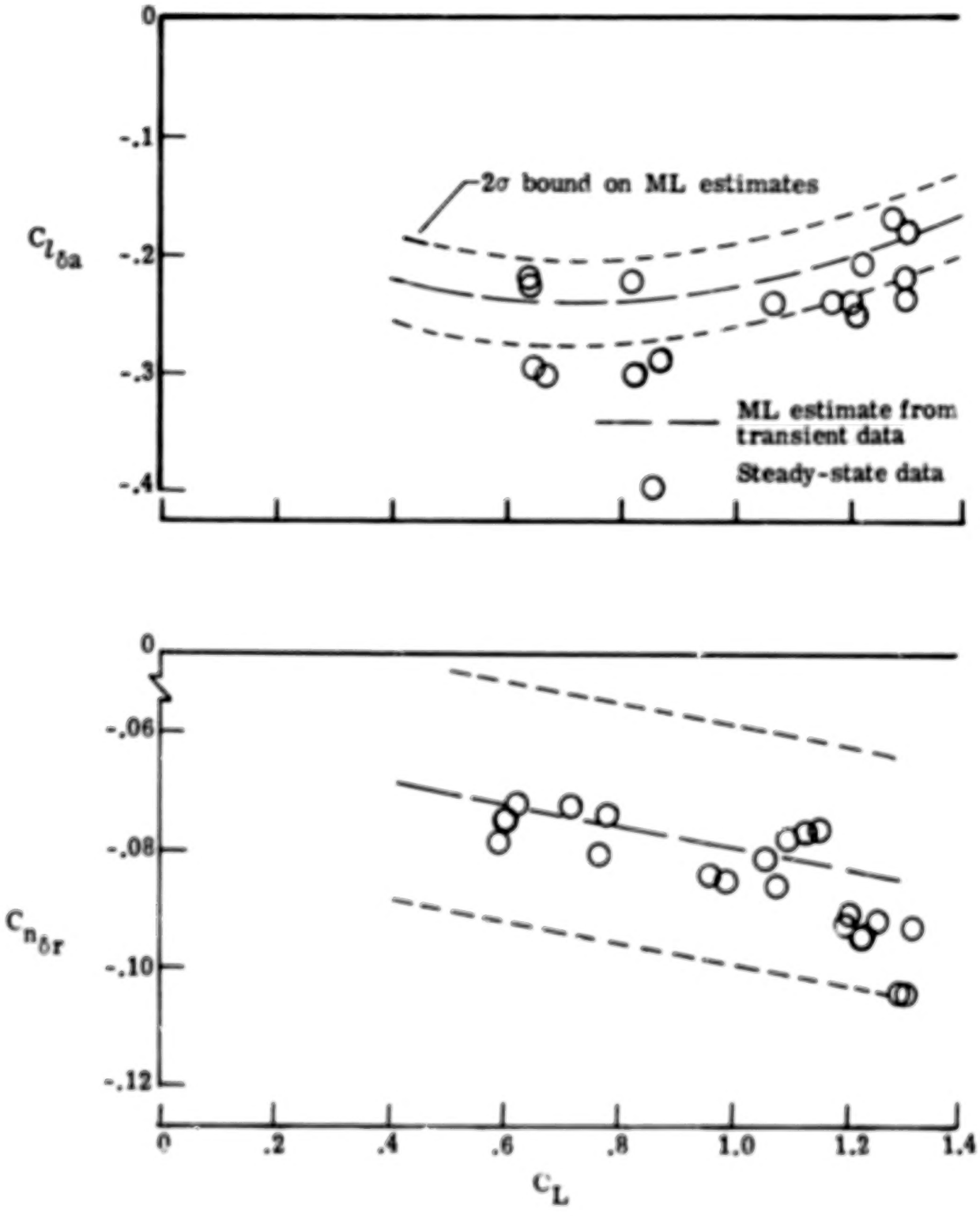

Figure 30.- Aileron and rudder effectiveness estimated from steady-state and transient flight data.

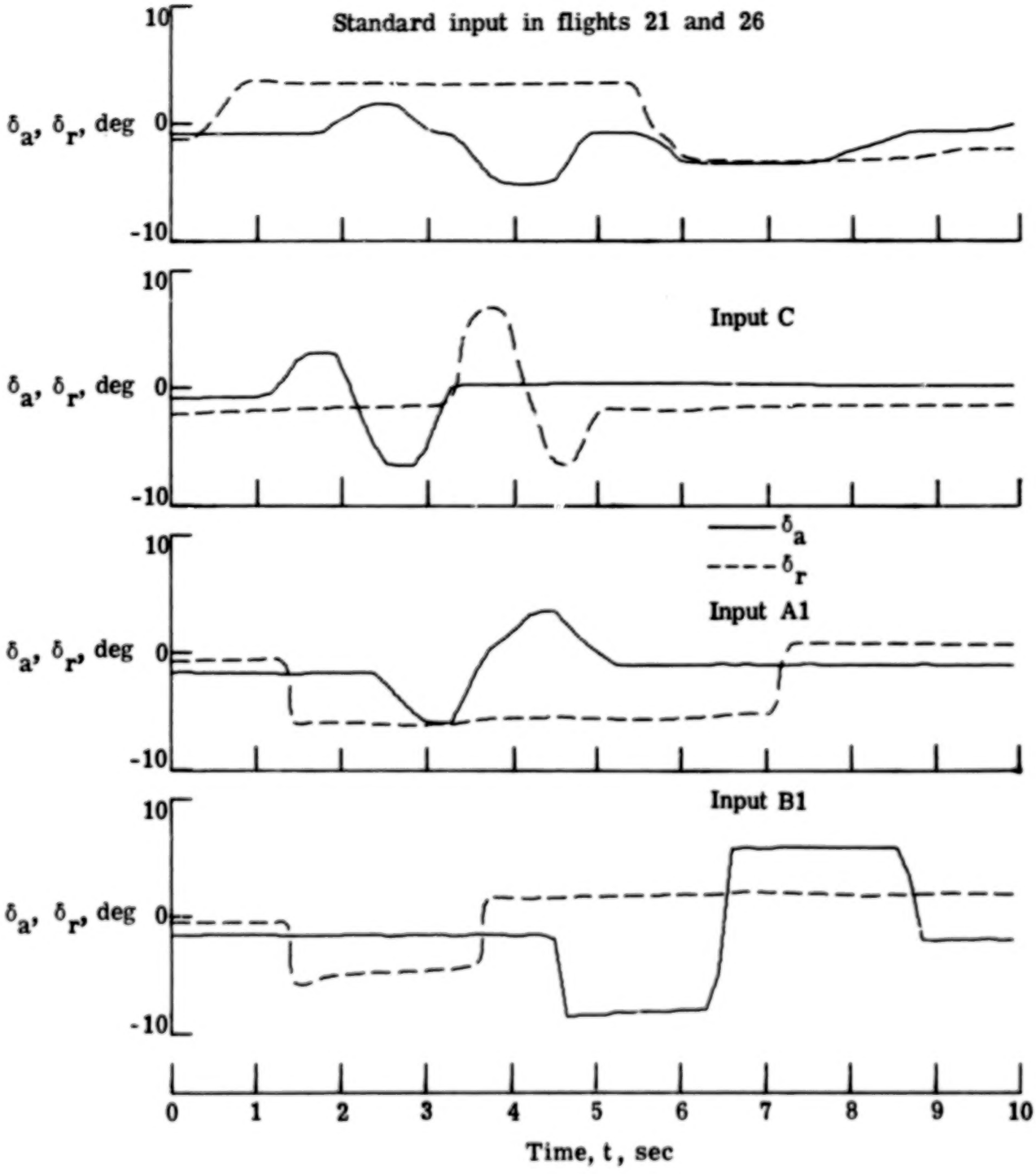

Figure 31.- Different aileron and rudder deflections used in test.

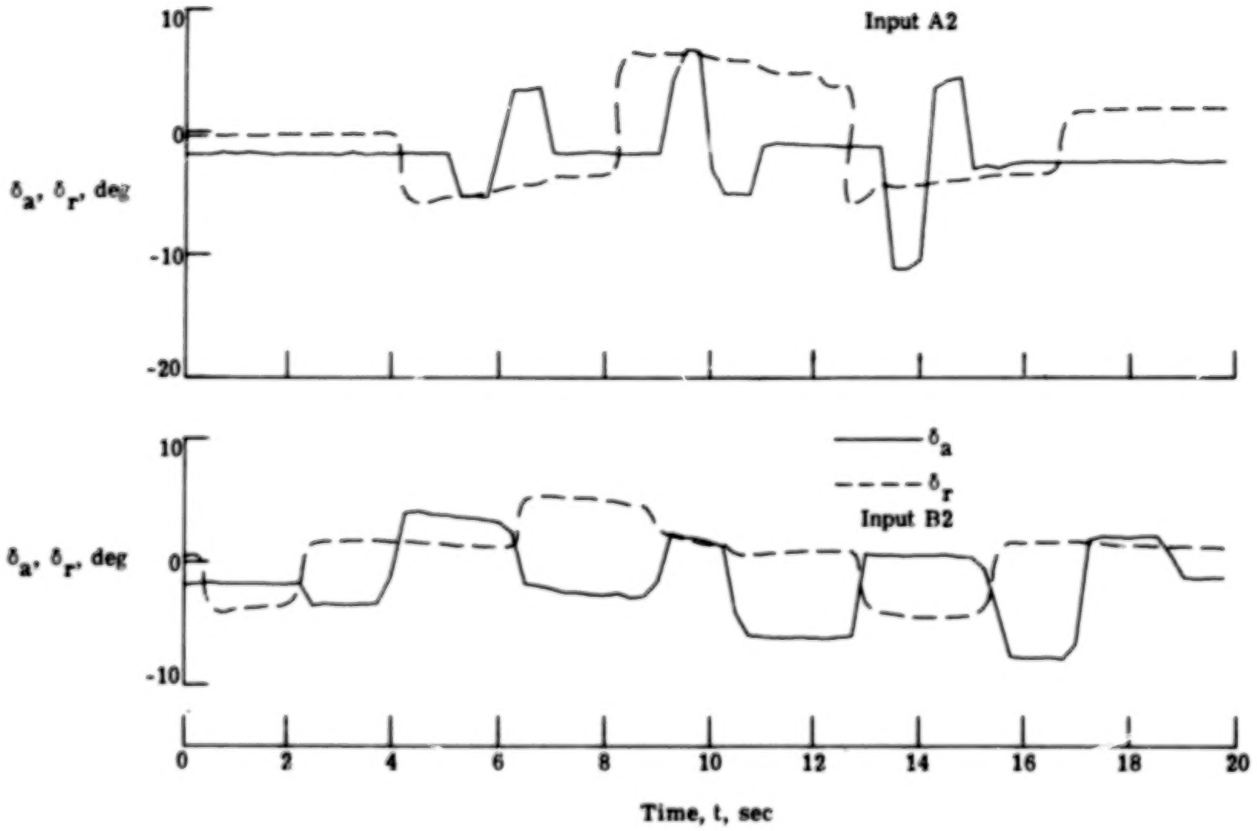

Figure 31.- Concluded.

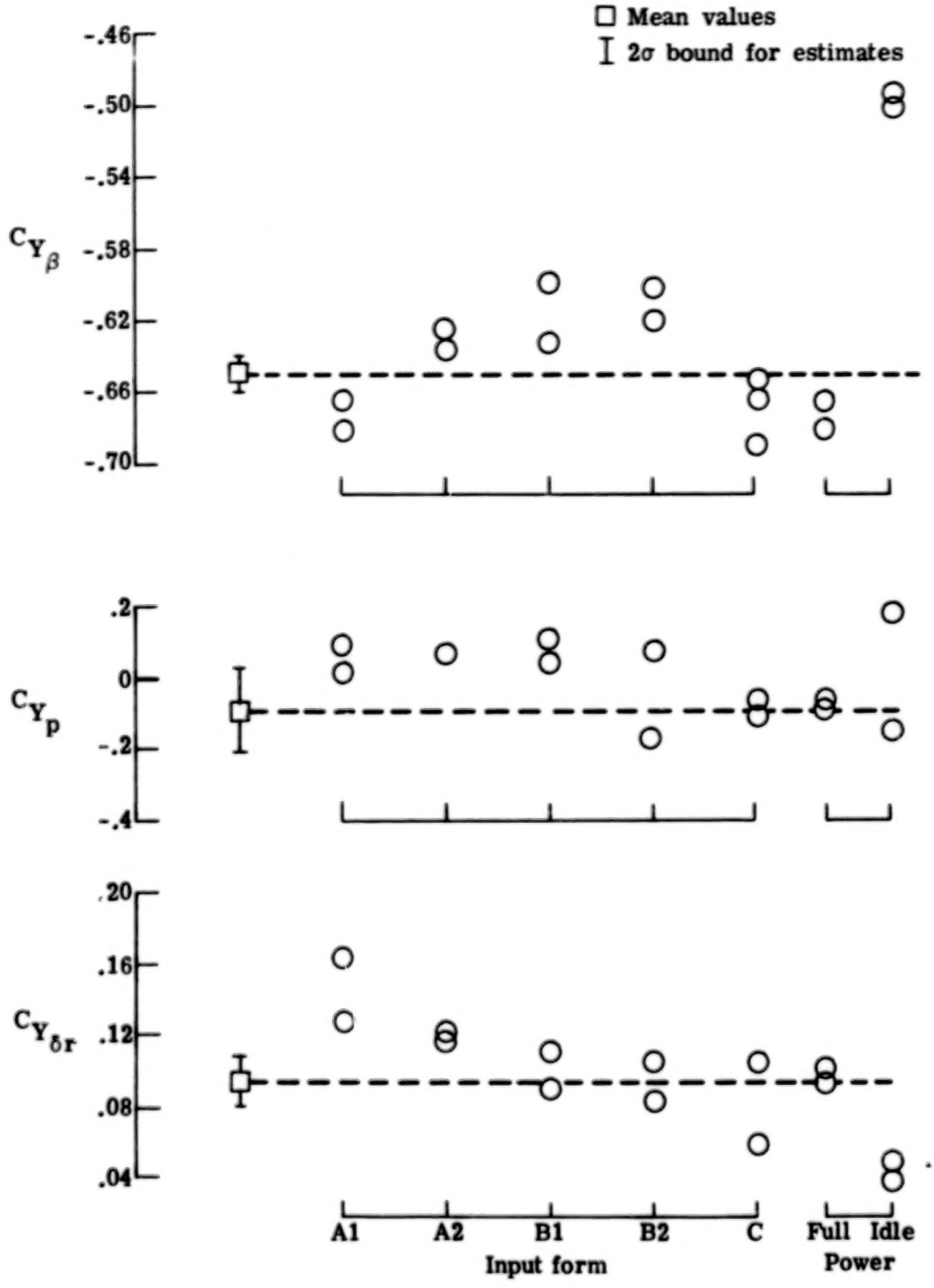

Figure 32.- Effect of different input forms and power settings on estimated lateral parameters. Maximum likelihood method.

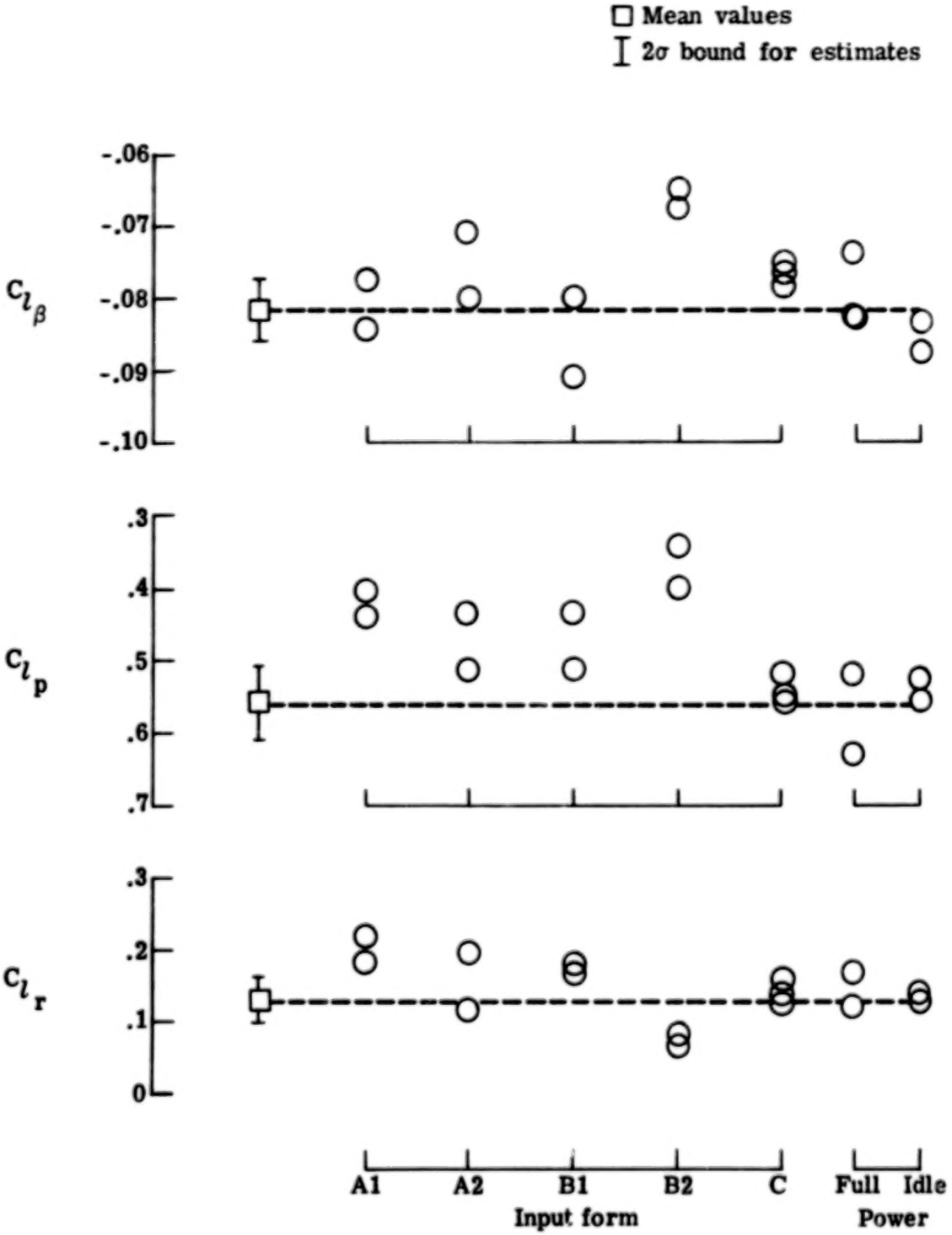

Figure 32.- Continued.

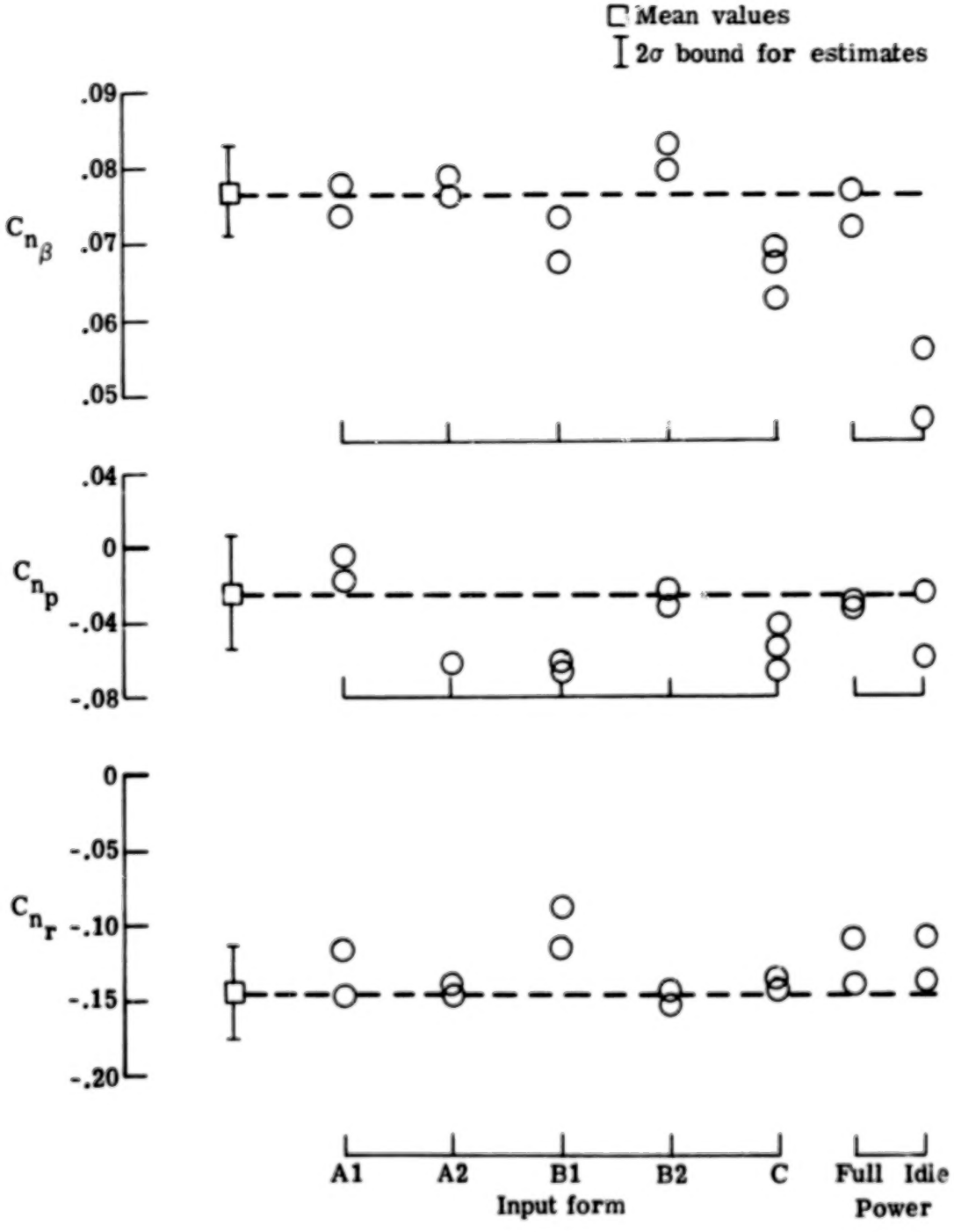

Figure 32.- Continued.

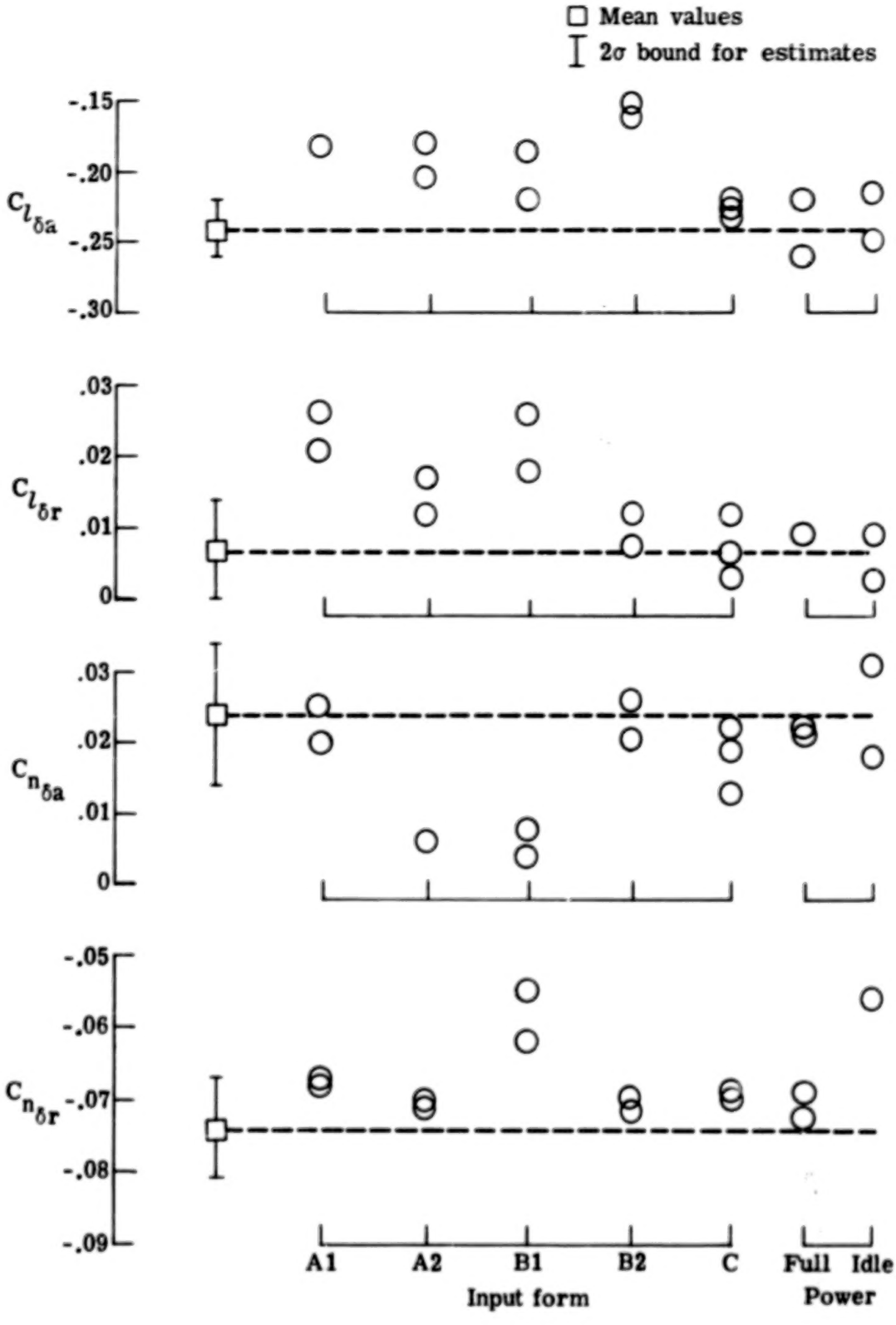

Figure 32.- Concluded.

1. Report No.	2. Government Accession No.	3. Recipient's Catalog No.
NASA TP-1306		

4. Title and Subtitle	5. Report Date
DETERMINATION OF STABILITY AND CONTROL PARAMETERS OF A LIGHT AIRPLANE FROM DATA USING TWO ESTIMATION METHODS	March 1979
	6. Performing Organization Code
7. Author(s)	8. Performing Organization Report No.
Vladislav Klein	L-12291
	10. Work Unit No.
9. Performing Organization Name and Address	505-06-63-02
NASA Langley Research Center Hampton, VA 23665	11. Contract or Grant No.
	13. Type of Report and Period Covered
12. Sponsoring Agency Name and Address	Technical Paper
National Aeronautics and Space Administration Washington, DC 20546	14. Sponsoring Agency Code

15. Supplementary Notes

Vladislav Klein: The George Washington University, Joint Institute for Advancement of Flight Sciences, Langley Research Center, Hampton, Virginia.

16. Abstract

Two identification methods, the equation error method and the output error method, are used to estimate stability and control parameter values from flight data for a low-wing, single-engine, general aviation airplane. The estimated parameters from both methods are in very good agreement primarily because of sufficient accuracy of measured data. The estimated static parameters also agree with the results from steady flights. The effect of power and different input forms are demonstrated. Examination of all results available gives the best values of estimated parameters and specifies their accuracies.

17. Key Words (Suggested by Author(s))	18. Distribution Statement
Aerodynamic parameters Parameter estimation Equation error method Maximum likelihood method	Unclassified - Unlimited Subject Category 02

19. Security Classif. (of this report)	20. Security Classif. (of this page)	21. No. of Pages	22. Price*
Unclassified	Unclassified	99	$6.00

* For sale by the National Technical Information Service, Springfield, Virginia 22161

NASA-Langley, 1979

END

APR 30 1979